Emerging pollutants in water: innovative approaches of study and treatment

Davide Magrì

PhD supervisors: *Dr. Despina Fragouli*
Dr. Athanassia Athanassiou

A thesis submitted for the degree of
Doctor of Philosophy

Ph.D. course in Bioengineering and Robotics
Curriculum: Bionanotechnology
XXXI Cycle (2015-2018)

Nanophysic dpt., Istituto Italiano di Tecnologia, Genova, Italy
DIBRIS, Università degli studi di Genova, Genova, Italy

to my family
to my love
to my friends

…let the horses think because they have a bigger head
L. Pesce

Declaration

I hereby declare that except where specific reference is made to the work of others, the contents of this dissertation are original and have not been submitted in whole or in part for consideration for any other degree or qualification in this, or any other university. This dissertation is my own work and contains nothing which is the outcome of work done in collaboration with others, except as specified in the text and Acknowledgements. This dissertation contains fewer than 65,000 words including appendices, bibliography, footnotes, tables and equations and has fewer than 150 figures.

Davide Magrì
December 2018

Acknowledgments

The realization of this thesis is the result of countless collaborations and would not have been possible without the contribution of many people. First, I have to thank the Fondazione Istituto Italiano di Tecnologia and my supervisors Athanassia Athanassiou and Despina Fragouli for the possibility and for the support they offered me.

I want to thank Gianvito Caputo, Paola Sánchez-Moreno and Marina Veronesi for teaching me so much and for having supported me scientifically and humanly in the difficulties of every day.

In the same way I thank the technicians who are the pillar on which the research carried out in IIT is based. In particular, I thank Lara Marini, Giorgio Mancini, Marco Scotto, Alice Scarpellini, Simone Lauciello, Doriana De Bellis, Giammarino Pugliese, Simone Nitti, Sergio Marras and Riccardo Carzino for taking care of me.

I thank all the scientists and professionals of the various collaborations: Pier Paolo Pompa, Nicola Tirelli, Marti Duocastella, Alberto Diaspro, Tiziano Bandiera, Stefania Girotto, Benedetto Grimaldi, Claudia De Mei, Clarissa Braccia, Andrea Armirotti, Francesco De Angelis, Mattia Bramini, Mario Miscuglio, Paco Palazon, Mirko Prato, Javier Pinto Sanz, Suset Barroso, Roberto Marotta, Giuseppe Vicidomini, Davide Morselli.

I also thank friends and PhD who more than anyone have taught me the value of working together. As first the two more brilliant persons I met Cataldo Pignatelli and Luca Pesce, but also Tiziano Catelani, Fabrizio Scoponi, Roberto Donno, Arianna Gennari, Andrea Castelli, Alexander Devis, Chiara Setti, Laura Campagnolo, Adriano Savoca, Francesca Gatto, Simonluca Piazza, Sara Accornero, Giorgio Tortarolo, Marco Castello, Giacomo Tedeschi, Daniele Bonventre and all the SMART guys.

Abstract

Water quality is one of the major challenges that humanity has to face. Tackling the problem of pollution needs the use of all the resources and expertise available to fill the lack of knowledge and technology. Concern is growing over the many emerging contaminants, including heavy metals ions and plastics, which are omnipresent and poorly managed.

In this contest, the presence of micro- and nanoplastics in the marine environment is raising strong concerns. The lack of appropriate methodologies to collect the nano-

plastics from water systems imposes the use of engineered model nanoparticles to explore their main characteristics and behaviour. In order to develop a nanoplastic model more reliable and realistic compared to the common polystyrene nanospheres, in this thesis, laser ablation has been applied to induce the formation of plastic nanoparticles in water starting from a bulk polymer film. The process was performed on Polyethylene Terephthalate, a commercial polymer used to produce beverage bottles, widespread in the environment. PET nanoparticles with an average size <100 nm, were carefully characterized in terms of chemical/physical properties. Size, shape, surface chemistry and colloidal stability were analyzed and compared with what expected from a real sample. As the oral route has been defined as the main route for human exposure to nanoplastics, their biological interactions and the effects on single intestinal epithelial cells and on a model of intestinal barrier have been assessed.

The aquatic environment exposes the nanoplastics to a great variety of substances and contaminants. The nano-

plastics can therefore act as carriers for many toxic substances with risks for aquatic organisms but also for humans. The nanoplastic model was studied in presence of three model contaminants a pesticide, a drug and a heavy metal ion (glyphosate, levofloxacin and Hg^{2+} respectively). The binding capacity toward these contaminants, was demonstrated and characterized quantitatively and qualitatively. The synergic biological effect of the contaminant-nanoplastic complexes was investigated *in vitro* on macrophages and intestinal epithelial cells. The conventional toxicological assays have been implemented with a preliminary metabolomic analysis.

Concerning heavy metal ions pollution, considerable attention is being devoted to the development of low-cost and environmentally safe materials for their removal from polluted waters. Several strategies have been applied to solve the problem of toxic metal ions contamination in water, where the development of nanotechnology, and in particular of novel metal oxide nano-sorbents provides a promising and efficient alternative. The application of these technologies is however limited by the difficult management of nanomaterials in the environment.

Therefore, the use of a bionanocomposite made of titanate nanosheets embedded in a silk fibroin matrix was proposed as eco-friendly approach for water treatment applications. The nanocomposite has been characterized and its ion exchange performances have been analysed under various conditions. The nanocomposites capacity to efficiently retain and adsorbed ions, with no release of titanate nanosheets has been proved. By modifying the nanocomposite formulation, it was also possible to enhance the materials selectivity towards the lead ions.

Table of contents

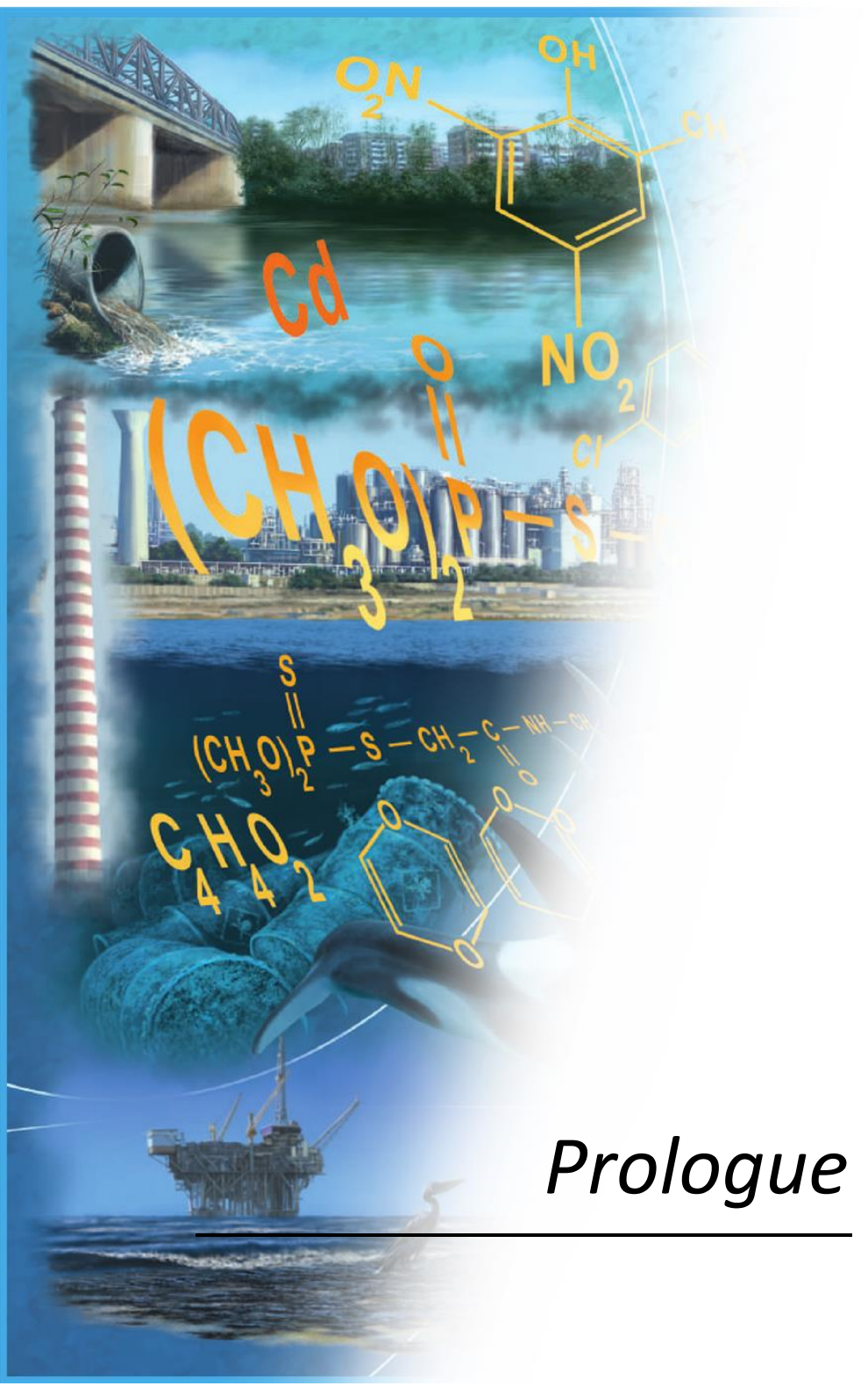

Prologue

Research Design and Introduction

Motivation background

Climate changes and population growth in the twenty-first century raise the problem of quantity and quality of water, forcing humanity to face one of the major challenges ever.[1] The alteration of the water cycle,[2] attributed to the higher temperatures, may increase floods and droughts[3] with severe impact on human health due

to the lack of safe drinking water and improved sanitation, which currently affects more than 30% of the world's population. Human activities such as agriculture, industry and municipalities (domestic purposes) exploit one third of Earth's accessible renewable freshwater generating together an enormous amount of wastewaters containing numerous chemical compounds.[4–6] To date a global strategy to fight water pollution barely exists, indeed still exist highly contaminated water environments, while current solutions for their remediation in most cases are not efficient for many classes of pollutants.[5,7] The term "chemical pollutants" refers to all those organic or inorganic compounds harmful to the ecosystem. It is possible to distinguish two classes of pollutants on the base of their origins:

- Substances directly emitted to the environment by different resources, the so-called primary pollutants.
- The products of metabolic transformations or chemical and photochemical degradations and reactions, defined as secondary pollutants.

Considering that to date the number of described substances exceed 127 million,[8] and that all these diverse substances may undergo numerous interactions and modifications in the environment, the management and the qualitative/quantitative assessment of secondary pollutants is usually a more challenging task and requires a broad interdisciplinary approach.[5,9]

Table 1. Examples of the main ubiquitous water pollutants.[4,5,10–12]

Source	Class	Illustrative Examples	Main problems
Industry	Solvents, intermediates, petrochemicals, additives, lubricants, flame retardants, heavy metals ions, plastic	Tetrachloromethane, methyl-t-butylether, benzene, toluene, xylene, phthalates, polychlorinated biphenyls (PCBs), polybrominated diphenylethers, chromium, mercury, lead	Persistence, drinking-water contamination, biomagnification in food chain, long-range transport, diverse health effects
Agriculture	Pesticides, salts, nutrients, pharmaceuticals, hormones, plastic	Dichlorodiphenyltrichloroethane (DDT), atrazine, glyphosate, tributyltin (TBT), ions of sodium, chloride, potassium, magnesium, sulphate, calcium and bicarbonate, nitrogen and phosphorus, ivermectin, quinolones, somatotropin	Persistence, contamination of ground and surfaces water with biological active chemicals, bacterial resistance, accidental poisoning, biomagnification, diverse health effects
Municipalities	Pharmaceuticals, hormones, microorganisms and viruses, plastic	Diclofenac, Ibuprofen, cocaine, quinolones, ethinyl estradiol, Cholera, Escherichia Coli, Hepatitis A, Dengue	Ecotoxicological effects, inhibition of enzymatic activity, bacterial resistance, fish feminization, human health
Natural, geogenic and biogenic contaminants	Inorganic contaminants, cyanotoxins, taste and odour compounds	Arsenic, selenium, fluoride, uranium, lead, cadmium, mercury, microcystins, geosmin, methylisoborneol	Persistence, cancer, fluorosis, aesthetic (taste and odour)
Mining	Acids, leaching agents, heavy metals ions	Sulfuric acid, cyanide, mercury, copper	Long-term contamination of water resources, metal remobilization, acute and chronic toxicity

Table 1 gives an overview of the main sources and classes of water pollutants of environmental and toxicological concern. The current systems of control and treatment of wastewater are effective for only a small part of the well-known classes of macropollutants such as salts, nutrients, natural organic matter, and acids, occurring at µg/l to mg/l concentrations.[13] It is far more difficult to establish effective treatment strategies and assessing the presence in the aquatic environment of the thousands of trace contaminants, defined as micropollutants, that are present in water at very low concentrations (pg/L to ng/L).[5,14,15] Many of these micropollutants do not dissolve in water, and therefore settle and accumulate in the sediment. When organisms are exposed to these contaminants they are retained and they bind to their tissues (particularly fatty tissues) with their concentration to continuously increase (bioaccumulation). By biomagnification, the concentration of contaminants bioaccumulated in the single organisms further increases, progressively, in the higher levels of the food chain up to the top predators, such as humans.[16] Due to a quite long half-life in the environment, a significant feature that increases the risk factor

of many of these compounds is their persistence. Persisting more than decades, contaminants such as heavy metal ions end pesticides mainly cause long-term effects to the human health and environmental quality, and therefore such type of compounds are classified as legacy pollutants.[17] The impact of legacy contaminants on the food web strictly depends on their behaviour in complex aqueous media, in presence of salinity and temperature, in the sediments or in animal tissues. The several health effects related to pollutants depend on:

- level of exposure
- route of exposure (inhalation, ingestion, manual handling)
- time of exposure

Contrary to short term effects induced by acute toxicity, only a few long-term monitoring studies have addressed the consequences of environmental pollutants to the human health.[17,18] Some of the pollutants present in water are well known contaminants with known effects, and their use is currently strictly regulated. For example, chronic exposure to heavy metal ions can cause cancer,

neurotoxicity, genetic mutations, and endocrine disruption.[17,19] For many others, such as nanomaterials, glyphosate, many drugs, micro and nanoplastics, the so-called "emerging pollutants" (EPs) or "contaminants of emerging concerns" (CECs), basic studies for the effects to the humans, are lacking although they are considered a potential threat to the ecosystem and to human safety and health.[20]

A proper assessment of any environmental and in particular water pollutant relies on:

- Knowledge of the type and origin of the pollutants.
- Access to models of appropriate complexity to understand the transport processes and the fate of the pollutants and to predict future scenarios.
- Availability of analytical methods for temporal and spatial quantification of the contaminants.
- Availability of methods to quantify the adverse effects of the pollutants on environment and human health.

The same points are crucial for the design and application of technologies for the removal of the pollutants and for

the in situ remediation.[5] As mentioned above, in many cases these indispensable tools are lacking, and it is this necessity that motivated this research work, which is based on the study and development of new models and technologies in order to discover the best strategies to deal with various pollution scenarios.

Objectives and experimental approach

The research described in this doctoral thesis is evolved on two complementary fronts, basic and applied research, focusing on the study of two different types of pollutants: nanoplastics, an emerging type of pollutant, and heavy metal ions, well known persistent and bioaccumulative pollutants.

There is a growing interest in the problem of plastic pollution and the resulting degradation derivatives. Plastics dispersed in aquatic systems are in the form of macroplastics, microplastics and nanoplastics. Much of the researches on the effects on the living organisms and the human health are focused on microplastics while little is known about nanoplastics. In fact, most of the studies

concerning nanoplastics are based on the use of engineered nanospheres of polystyrene, a limited model which extremely differs from nanoplastics deriving from environmental degradation of the macro and microplastics. Therefore, part of the studies of the present thesis was carried out with the aim of developing and studying a model of nanoplastics to be used as a reference for the investigation of the effects to biological systems of this new group of emerging pollutants. It was used a top-down approach, in contrast to that of the colloidal synthesis of engineered polymer nanoparticles used so far, aimed at the degradation of solid plastic targets by laser ablation rather than the production of nanoparticles by polymerization, according to the real pathway of environmental formation of these pollutants. It was decided to focus on the formation of polyethylene terephthalate (PET), a kind of plastic widely spread in the environment and already found in food, therefore of interest to human health.[21] The strategy followed for the PET nanoplastics formation had the scope to minimize any chemical interferents, such as surfactants or precursors, to better assess the behaviour of nanoplastics in the various media

and the interaction with other environmental contaminants. Toxicological evaluations, performed considering the oral route as the main route of human exposure, required an “omic” approach for a deeper understanding of the biological impact of the PET nanoplastics.

The specific objectives of the project were the following:

- To develop a versatile nanoplastics synthesis process applicable to diverse types of polymers different from the widely used Polystyrene.
- To produce a “realistic model” of nanoplastics characterizing their physicochemical features.
- To understand the nanoplastics behaviour in the aqueous media.
- To evaluate the interaction of nanoplastics with different types of contaminants.
- To assess the impact of nanoplastics on *in vitro* human cells.

While for emerging pollutants the development of monitoring and removal strategies is premature or in the embryonic phase, and still requires a great effort in research, for the most known categories of contaminants there is a

continuous evolution of the technologies for their detection and removal from the environment. In this contest many approaches have been used for heavy metal ions remediation. Several conventional chemical, physical and biological strategies have been applied to solve the problem of toxic metal ions contamination in water, and the development of nanotechnology provides a promising alternative to develop innovative materials with enhanced remediation performance. Despite the high adsorption capability and removal efficiency of nanomaterials, their application is still limited by the difficulties of their large-scale application and the little knowledge of environmental and health risks deriving from their diffusion. For this reason, part of the research presented in this thesis was dedicated to the development of a solid composite system, allowing to exploit the properties of nanomaterials maximizing safety and usability. The strategy applied followed an eco-friendly approach based on the use of a polymeric support made of regenerated silk fibroin combined with titanates, a class of metal oxide nanomaterials largely applied in water treatment applications.

The Specific objectives of this part of the project were the

following:

- To synthetize a water stable composite for the removal of heavy metal ions from water.
- To find the most effective configuration to combine the properties of both fibroin matrix and titanate nanofillers.
- To assess the functionality of the embedded titanates and the retention efficiency of silk fibroin.
- To characterize the specificity of the sorbents in complex aqueous solutions towards heavy metal ions.

I had a core coordination function at all stages of this research work, and I was actively involved in all the experiments and results produced. Nevertheless, this work is the result of a synergistic collaboration between various groups, mainly from the Instituto Italiano di Tecnologia:

- Nanobiointeractions and Nanodiagnostics group (IIT) for the study of toxicological effects and for the characterization of the nanoplastic behaviour.
- D3 PharmaChemistry group (IIT) for the development and execution of NMR and metabolomics experiments.

- Electron Microscopy facility (IIT) for the high-resolution imaging and the STEM-EDX analysis.
- Nanomaterials Engineering Group (University of Padova) for the synthesis of titanates.

Outline of the thesis

The thesis is structured in two main sections. The first one is composed of two chapters devoted to the nanoplastics model development and characterization and the second one dedicated to the development of the fibroin-titanates composite for the removal of heavy metal ions from water.

Each chapter consists of an introduction that collects the state of the art and the main concepts inherent to the research developed, the description of the experimental procedures, and as last the obtained results are presented and discussed.

In chapter 1 is presented the development of the model of PET nanoplastics. The details of the application of the laser ablation technique in water for the synthesis of polymeric nanoparticles and the physicochemical

characteristics of the obtained nanoplastics are described. The chapter concludes with the toxicological evaluations of the nanoplastics carried out on single cells and on a Caco2 barrier.

Chapter 2 opens with the assessment of interactions of nanoplastics with other aquatic contaminants. The biological effect of the pollutants is related to the synergistic effect obtained in the presence of nanoplastics through *in vitro* studies. The metabolic impact of treatment on Caco2 cells and on macrophages has been studied in order to predict possible long-term effects.

Chapter 3 presents a new strategy to overcome the limits and risks related to the use of nanomaterials for water treatment applications. The chapter illustrates the synthesis of the nanocomposite system composed of a dispersion of nanostructures based on titanium oxide embedded in a fibroin matrix. Particular attention is given to the mechanisms of ion exchange, the selectivity and the behaviour of the composite in complex aqueous media.

Chapter I

Nanoplastics: model development and assessment

State of the art

Plastic in the aquatic environment

Since 1907, with the invention of Bakelite, humans have developed an unquenchable addiction to the use of plastics in everyday life. This dependence on plastics, associated with strong consumerism and poor recycling, is leaving its mark on our environment to the point of irreversibly influencing the planet's geology, welcoming the dawn of the so-called Plasticene era.[22–24] The rise of plastic production is the concrete demonstration of the

global expansion of this, today, indispensable material. From 1950 to today, global plastic production has exceeded 380 Mt, increasing by around 190 times (Figure 1).[24–26]

The more than 5 billion tons of plastic produced till now are enough to envelope the Earth in a layer of plastic wrap,[24] and according to future prospects, maintaining this rate of production, in 2050 the amount of plastics will reach 40 billion tons.[27] Most of the global plastics that have been produced are still present in the environment. Particularly, the rise of disposable products has critically

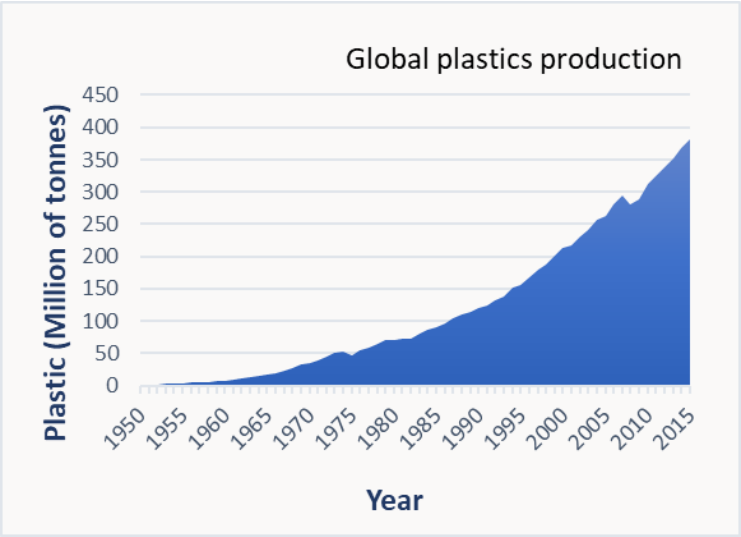

Figure 1. Annual global plastic production measured in million of tonnes per year.[24]

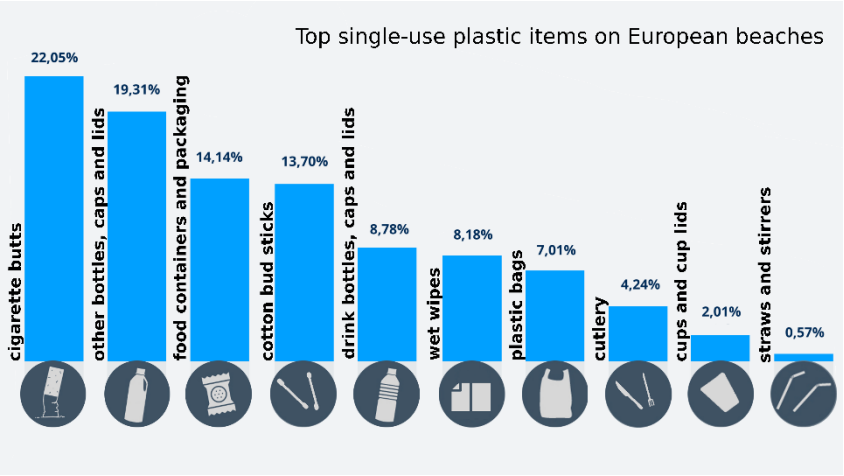

Figure 2. List and percentage of the top single-use plastic items founded on European beaches in 2016.[28]

increased the production of plastic litter. Due to the last decades increasing evidence of plastic contamination, world governments started considering this issue an important health and environmental hazard. The European Parliament approved measures to ban the main disposable plastic items by 2021 (Figure 2), which represent the largest fraction of plastic debris on our beaches.[28,29] And in fact, up to 4.6% of the total plastic waste generated in costal countries reach ocean, which constitute the 70% of all the litter in the sea.[22,30] Plastic is now a ubiquitarian element in the environment but sea and ocean represent a particularly dynamic ecosystem

therefore quantifying plastic pollution choking the seas and knowing its fate are arduous tasks. This is particularly true for the smaller size plastic fraction. Researchers reported the presence of plastic debris in the surface water and the sediment of rivers and lakes, while from '90s is known the accumulation of plastic debris floating in the ocean, as well as it is known the pollution of plastic in deep sea, estuaries, coral reefs, sea ice and many others aquatic habitats.[31–43] Eriksen and his team studied the floating plastic distribution in world's oceans comparing all sizes items.[32] Plastic pollution is moved throughout the world's oceans by the winds and currents converging in accumulation zones such as the five subtropical gyres (North Pacific, North Atlantic, South Pacific, South Atlantic, Indian Ocean), enclosed seas such as Mediterranean Sea and extensive coastal regions. Estimates show a minimum of 5.25 trillion particles, weighing 268.940 tons, floating in the marine environment.[32] The data suggested that during fragmentation plastics are lost from the sea surface. Although pathways and mechanisms related to the loss of plastic debris in marine environment are unknown, the

phenomenon could be related to the sinking, the degradation and the ingestion of plastic by the marine fauna.

Types of plastics

Plastics are a family of hundreds of different materials with a wide variety of properties designed to meet the needs of each application. Although plastics can also be of semisynthetic origin based on biological organic polymers, most of these materials are derived from fossil raw materials. The plastic manufacture consumes approximately the 8% of global oil extraction, but only 4% is applied as source material, the rest is spent to produce energy useful for the synthesis processes.[24] Due to the modification of the chemical synthesis processes, such as polyaddition, cross-linking and condensation, and to the additives used, more than 15 new classes of polymers have been developed in the last 50 years.[26] In 1988 the Society of the Plastics Industry (SPI) introduced a numerical classification system to allow consumers to identify different types of plastic:

1. Polyethylene Terephthalate (PET)
2. High-Density Polyethylene
3. Polyvinyl Chloride
4. Low-Density Polyethylene
5. Polypropylene
6. Polystyrene
7. Polymethyl methacrylate (PMMA), Polycarbonate (PC), Nylon (NY), Polylactic acid (PLA), etc.

The demands and consumption of the different types of plastic is strictly related to their application (Table 2).

Table 2. Main plastic materials, demand and field of application.[11]

Polymer	European demand	Application
PS, PS-E	6.7%	Eyeglasses frames, plastic cups, egg trays (PS); packaging, building insulation (PS-E), etc.
PET	7.4%	Bottles for water, soft drinks, juices, cleaners, etc.
PUR	7.5%	Building insulation, pillows and mattresses, insulating foams for fridges, etc.
PVC	10%	Window frames, profiles, floor and wall covering, pipes, cable insulation, garden hoses, inflatable pools, etc.
PE-HD, PE-MD	12.3%	Toys, (PE-HD, PEMD), milk bottles, shampoo bottles, pipes, houseware (PE-HD), etc.
PE-LD, PE-LLD	17.5%	Reusable bags, trays and containers, agricultural film (PE-LD), food packaging film (PE-LLD), etc.
PP	19.3%	Food packaging, sweet and snack wrappers, hinged caps, microwave - proof containers, pipes, automotive parts, bank notes, etc.
OTHERS	19.3%	Hub caps (ABS); optical fibres (PBT); eyeglasses lenses, roofing sheets (PC); Touch screens (PMMA); cable coating in telecommunications (PTFE); and many others in aerospace, medical implants, surgical devices, membranes, valves & seals, protective coatings, etc.

In this dissertation the focus was on Polyethylene Terephthalate due to its high production volume, large presence in marine environment and its peculiar application in food and beverage packaging.

Polyethylene terephthalate (PET)

PET is a semicrystalline, thermoplastic polyester also known with many commercial names such as Arnitel, Mylar, Rynite.[44–47] PET is chemically and thermally stable, strong, durable and low permeable to gas. The presence of a large aromatic ring (Figure 3) in the repeating units of

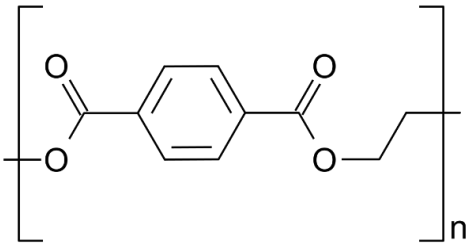

Figure 3. PET molecular structure.

this polyester gives the polymer notable stiffness and strength, especially when under stretching the polymer

chains are aligned. The unique combination of intrinsic properties (Table 3) of this material make it easily processable, manageable and suitable for a wide range of application.[44,47]

Table 3. Intrinsic properties of PET polymers.[44]

Property	Value
Average molecular weight	30,000–80,000 g mol−1
Density	1.41 g cm−3
Melting temperature	255–265 °C
Glass transition temperature	69–115 °C
Young's modulus	1700 MPa
Water absorption	(24 h) 0.5%

As shown in Table 2 due to its properties PET is one of the most requested and produced plastic and its global consumption has been reported to exceed $17 billion per year.[11,44] PET is used in several shapes as fibres, sheets and films, while more than 50% of synthetic fibres globally produced consist of PET. It is largely used in food and beverage packaging, but also in automotive, in electronics, to produce X-ray sheets and many others everyday items.[44,47–49]

PET synthesis can be performed starting from two different chemical reactions:

- esterification of ethylene glycol and terephthalic acid performed at 240–260 °C and 300–500 kPa.[50]

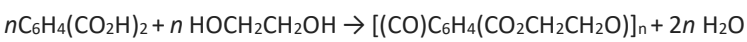

- transesterification between dimethyl terephthalate (DMT) and ethylene glycol (in excess) performed at 140–220 °C and 100 kPa, with methanol as a by-product; second transesterification step proceeds at 270-280 °C, with continuous distillation of ethylene glycol.[47,50]

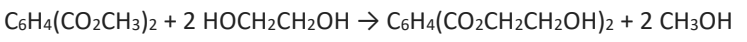

Polymerization proceed through polycondensation of the monomers with water as the by-product.[44,50]

The raw polymer can then be easily processed through extrusion, injection or blow moulding. This last procedure is used to produce bottles, which due to their shape easily diffuse in the environment.

Degradation of plastic

Durability and resistance to degradation make the plastic very versatile but at the same time a material with a serious environmental impact due to the inability of nature to assimilate it in a short time.[51] The degradation time of some plastics in the environment is estimated to range between hundreds and thousands of years and can be influenced by several factors, such as temperature and oxygen concentration.[52,53] The main environmental processes involved in plastic degradation are, mechanical/physical degradation, thermo-oxidative degradation, photodegradation, hydrolysis and biodegradation.[54–56] Generally abiotic degradation precedes biotic processes.[55] In nature, light provides the activation energy to trigger the first photodegradation mechanisms which leads to the polymer oxidation; this makes the plastic brittle, causing its breakdown in small fragments.[44,54] Thermo-oxidative degradation is an oxidative breakdown phenomenon which, together with the sunlight induced photodegradation process, mainly happens to plastics

present in shorelines. Its efficiency is significantly affected by the low temperature of the seawater and the location of the plastic in the water column.[53] Mechanical/physical degradation, caused by wind, sand and waves action, is important in aquatic environments. Furthermore the water may contribute through hydrolysis to the marine debris degradation with the polymer bond-breaking.[56] Fragmented plastic can be further depolymerized due to the attack of some species of marine microorganisms, such as bacteria or fungi, on its surface.[55,57] As many other polymers, PET breakdown phenomena are mainly driven by photo-oxidation reactions induced by the UV-light in presence of oxygen.[44,55,58] Under marine environmental conditions, photo-oxidation induces mainly the cleavage of the ester bond and the formation of vinyl and carboxylic acid end groups, exposed on the polymer surface.[44,55,58] PET in water can also undergo thermo-oxidative degradation and hydrolysis, even if extremely slow due to low temperatures, exposing carboxylic acid and alcohol functional groups and reducing its molecular weight.[55] The compact structure of PET makes it very resistant to biodegradation and natural enzymes

with significant efficacy are still being sought.[57,59,60] The visual effect of PET degradation processes is the yellowing of the polymer, while the recent discovery of PET microplastics in the sea confirms that such material can degrade and reduce in size when exposed to the environment.[61] In fact, even if slowly, the degradation processes will produce a progressive plastic fragmentation and the constitution of particles of all sizes.[62] The macro- and Microplastics (MPs) have been largely investigated in the last decades, however only recently the research started to focus on the nanometric fraction, broadly described in next section.[63]

Nanoplastics

The fact that the quantities of plastic found in the oceans are by far lower than the estimates, is partly answered by the phenomena of plastic debris fragmentation.[62] Initial studies concerning plastic pollution were focused on the detection of macroplastics, with a size >5 mm, and subsequently MPs, with dimensions ranging between 5 mm

and few tenths of microns, in biota and ecosystems.[32,54,64–67] Although the numerous research findings of the presence and effects of MPs in the hydrosphere, due to the lack of appropriate methodology to detect and characterize nanomaterials in the environment, there are rare empirical information about the abundance and behavior of the so-called Nanoplastics (NPs).[54,63,68]

European commission defined NPs all those plastic objects having at least one of their dimension <100 nm, according to the common definition of nanomaterial, nevertheless some authors set the upper size limit at 1000 nm (Figure 4).[65,69–71] As for MPs, based on their origin the NPs can be divided into two groups:

- Primary NPs are plastics originally manufactured

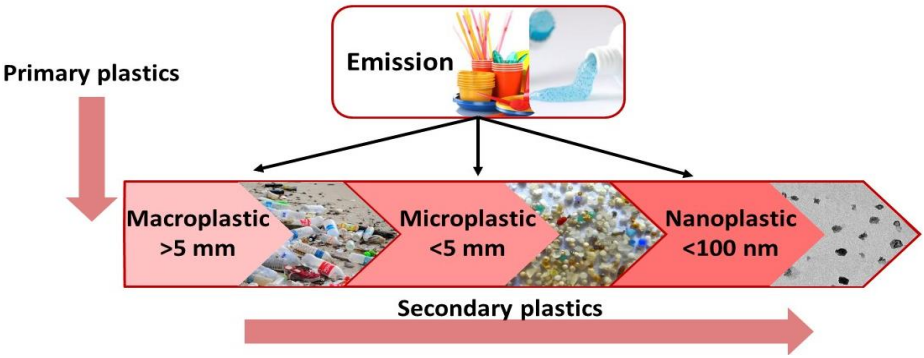

Figure 4. Scheme of the size- and origin-based definition of plastics pollutants.

with the specific size, and their environmental release is often related to the product application.[65,70] Primary NPs are present in exfoliants used in personal care products, industrial scrubbers, paints, adhesives, coatings, redispersible lattices, biomedical products, drug delivery, electronics, magnetics and optoelectronics, and can be also released during thermal treatment processes such as 3D printing or foam cutting.[65,71–74]

- Secondary NPs are the unintentional products of plastic degradation in the environment and, as for MPs, may have irregular shapes and an altered chemical structure.[63,75] Secondary NPs can derive from the rolling of the tires, from the degradation of agricultural plastic mulch, microfibers from textiles, and many other plastics items in the ocean such as plastic bottles.[65,74]

Although measuring NPs in the environmental matrixes presents several technical challenges that have not yet been met, their occurrence due to solar light degradation of weathered MPs collected from marine waters was

demonstrated in laboratory under controlled and environmentally representative conditions.[63,76] Into the environment, NPs may experience various changes such as homo- and hetero-aggregation due to water pH, ionic strength and interactions with the natural organic matter, or with microorganisms and macromolecules (e.g. formation of an ecocorona).[77,78] NPs can rapidly form aggregates in the aqueous environment, as in the case of nanopolystyrene, speeding up their sedimentation rate of the aggregates due to the density higher than that of the dispersed nanoparticles.[65,79] This behaviour varies according to the type of polymer, the surface chemistry and the environmental conditions, such as the currents that through their mechanical action facilitate the NPs dispersion in the water, and slow down their precipitation towards the ocean floor.[80] Nevertheless, as observed for some polymers denser than water, at the nanoscale the Brownian motion is predominant, and the NPs collisions with water molecules and other present ionic species may prevent the NPs from sedimentation.[81,82]

The sub-micrometric fraction deriving from the plastic degradation may penetrate in the marine food chain

through the diet with effects at all trophic levels.[64,83,84] In fact, traces of such pollutants have been found in protists and zooplankton up to mollusks, fishes, birds and cetaceans.[83] Their presence in the food chain may have an impact on humans, and for this reason, numerous studies are underway to investigate their biological effects and define an effective risk assessment.[70,85] According to the current knowledge, the ingestion of these sub-micrometric particles may elicit negative outcomes on behavior, fertility, hepatic function, immune response, and gene expression pattern,[86–91] while lethal effects have been reported only at much higher concentrations compared to the environmental ones.[77] As widely described in chapter 2, the high surface/volume ratio of the smallest plastic debris makes the NPs ideal candidates to interact and transfer many hazardous contaminants (polychlorinated biphenyls, organochlorine pesticides, polyaromatic hydrocarbons, etc.) to living organisms, increasing their impact and toxicity.[92–94] Compared to the microplastics, the smaller size of NPs (comparable to that of biological components and proteins), associated with their surface characteristics (i.e. surface chemistry and surface energy),

may alter their interactions with the surrounding substances and their biological impact.[56,95,96] In fact, as already observed for diverse types of organic and inorganic particles, the smaller size favors their passage through the intestinal barrier.[97,98] The numerous data deficiencies related to the limitations of using models, described in the following section, prohibits a comprehensive understanding of the risks posed by these pollutants.

Models of Nanoplastics

Given the enormous complexity of the ecosystem, a properly detailed characterization of a micropollutant results impossible. The main relevant process and characteristics of NPs must be described at limited level of complexity in controlled laboratory condition, in order to assess the fate and the biological and environmental effects of these pollutants.[4] Under laboratory condition it is possible to study NPs, adapting several methods applied to other nanomaterials such as UV-Vis spectrometry, electron microscopy, dynamic light scattering (DLS), field flow

fractionation (FFF) *etc*.[65] However, to date, the lack of method of detection and collection of NPs from the environment imposes the use of artificial models. The studies related to this class of pollutants have been mainly based on the use of monodispersed polystyrene (PS) nanospheres, synthesized by colloidal chemistry, following bottom-up approaches (table 4).[52,69,97,106,111,112]

Table 4. Major used model of NPs in terms of material and size

Material	PS	PS	PS	PS	PS	PS	PS	PC	PMMA
Size (nm)	20	30	40	50	70	90	100	158	86-125
Ref.	99–101	79,102	52,103,104	97,105,106	69,90,107	108	109	52	110

Such protocols typically produce plastic nanostructures with few defects and homogenous chemical composition, substantially different from the NPs dispersed in the environment, which have irregular shapes, similar to a fractal structure, and complex surface chemistry, due to the degradation experienced.[63] To obtain models closer to reality, it is necessary to reproduce the weathering of the plastic artificially using a top down approach such as accelerated weathering tester or laser ablation in water.[63,113,114]

Laser ablation

Despite accelerated weathering testers which reproduces the damage caused by sunlight, rain and dew are a suitable way to reproduce plastic weathering and breakdown, a quicker and more effective alternative to mimic NPs formation in water is pulsed laser ablation (PLA) (Figure 5).[63,113,114] PLA technique consists of the removal of material from a substrate by direct absorption of laser energy. Lasers allow to provide accurately large amounts of energy into defined regions of space and time. During the PLA process the photons absorbed by the solid target give rise to the high temperature plasma that produces a shockwave and the plume expands in a

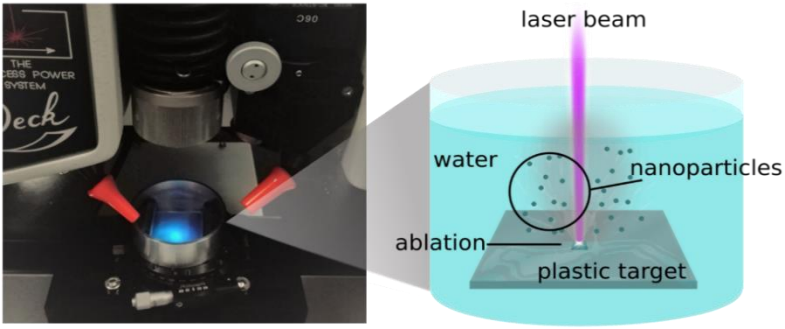

Figure 5. Experimental set-up of pulsed laser ablation in water.

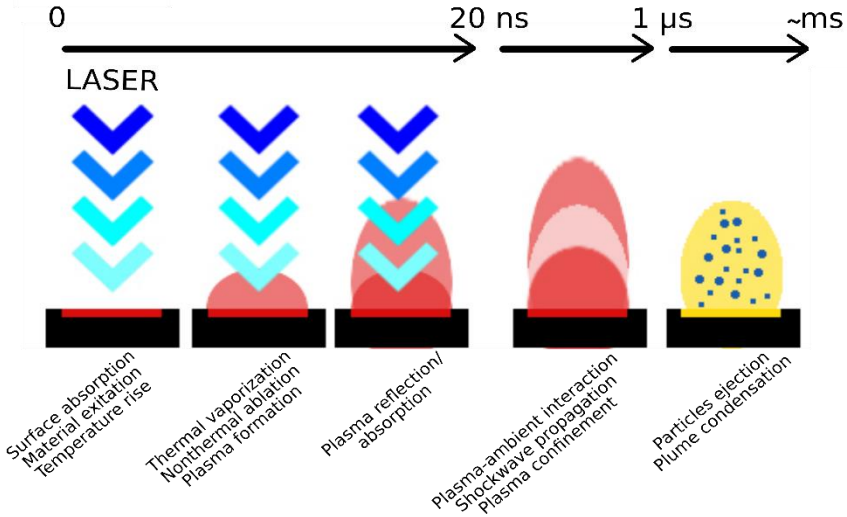

Figure 6. Approximate timeline of ns energy absorption and laser ablation along with the various processes occurring during and after the laser pulse are given.

cavitation bubble. In the last stage plasma collapses and the nanoparticles are released in surrounding liquid; during the bubble collapse the nanoparticles mix with water where can undergo coalescence/aggregation processes (Figure 6).[115,116] The ablation occurs above a specific threshold fluence that is the energy per unit area [J/cm^2] on the target surface. Typical threshold fluences in air are between 1 and 10 J/cm^2 for metal targets while for inorganic insulators and organic material are between 0.1 and 2 J/cm^2.[117] Above the ablation threshold the material removal typically shows a logarithmic increase

with the irradiation fluence in accordance with Beer–Lambert law.[115] The pulse duration is an important parameter: when the pulse length is shortened energy is more rapidly projected into the target leading to a faster material ejection.[115] In some cases, such as for polymers irradiated with pulsed UV laser light, the excitation energy induced by the laser irradiation can be enough to initiate the photochemical process and directly break bonds (photo-decomposition). Even in these cases although limited in water, thermal modifications can occur due to the excited states of lattice phonons, and the entire mechanism is known as photophysical.[115,118,119] Due to the possibility to control size and polydispersity of the produced samples, as a function of the irradiation fluence, wavelength, and pulses number, PLA has been largely applied for the synthesis of inorganic nanomaterials (e.g. metals, semiconductors and ceramics), it has been recently proposed for the fabrication of several kinds of polymeric nanoparticles.[119–122] The PLA process in water, as already demonstrated in previous studies, favors the heat exchange between the ejected material and the

surrounding aqueous medium, decreasing the thermal effect on the polymer.[119,120] The cooling of the ablation plume in water associated to high fluences allows high production yields limiting the burst of the material.[120] Therefore, PLA in water is a green fabrication technique which offers the possibility to produce nanoparticles without impurities, chemical precursors, and their byproducts.[114,123,124] All these features make the PLA technique in water, suitable for the development of a model of NPs and allow to limit the variables favoring, thus, a more controlled study of the system.

Materials and methods

Synthesis of PET NPs.

A top-down physical approach was applied for the formation of the NPs. In detail, laser ablation of commercial PET films (Goodfellow Cambridge Ltd.) was performed by exposing the samples to a pulsed UV laser irradiation in Milli-Q water, using a KrF excimer laser (irradiation wavelength 248 nm, pulse duration of 20 ns, repetition rate of 20 Hz, Coherent-CompexPro 110) coupled with a micromachining apparatus (Optec-MicroMaster). The ablation was carried out with an

irradiation fluence of 4.5 J/cm^2, by shooting 50 pulses on a 4 cm^2 area. To obtain NPs concentration up to 300 µg/mL, a low temperature (45 °C) rotavapor treatment was performed. In order to remove the big, micrometric sized, particles, the obtained dispersions were filtered (Cellulose Acetate, Ø = 0.22 µm, Millipore) before performing all the studies and the characterizations.

PET NPs quantification.

To evaluate the amount of PET NPs produced, in terms of mg/mL, the weight of nanoparticles in a stock colloidal sample was quantified by means of thermogravimetric analysis (TGA) (Q500, TA Instruments). Measurements were performed adding drop by drop (50 µl) the PET NPs suspension. The water was evaporated under an inert N_2 atmosphere with a flow rate of 50 mL/min at a temperature of 50°C. A calibration curve was constructed by measuring UV-Visible absorption spectra (Cary 6000i, Varian) of NPs at a wavelength of 238 nm using a quartz cuvette with a path-length of 1 cm.

High-Resolution Scanning Electron Microscopy (HRSEM)

A first morphological characterization of NPs was performed by HRSEM microscopy using a JEOL JSM-7500LA equipped with a cold field emission gun (FEG), operating at 10 kV acceleration voltage. The suspension of NPs was drop casted on silicon substrates and dried in vacuum at room temperature. The samples were coated with a very thin layer (2 nm) of gold/palladium by a sputter coater (Cressington 208HR).

Transmission Electron Microscopy (TEM)

The transmission electron microscope (JEOL JEM 1011) was used to characterize the morphology and the size of the NPs. The images were collected operating at an acceleration voltage of 100 kV and recorded with an 11 Mp fiber optical charge-coupled device (CCD) camera (Gatan Orius SC-1000). The suspension of NPs was drop

casted on ultrathin carbon layered Cu grids (CF300-CU-UL, Electron Microscopy Science) and dried in vacuum. The NPs size distribution was determined using the ImageJ software.

Asymmetric flow field-flow fraction (AF4)

AF4 system (AF2000 MF Mid Temperature, Postnova Analytics GmbH, Germany), provided with Multi-Angle Light Scattering MALS (PN3609) detectors and Refractive Index RI (PN3150) detector, yielded information concerning the PET NPs size distribution. The flat separation channel was equipped with a spacer of 350 µm and with a 10 kDa molecular weight cut-off regenerated cellulose membrane (Postnova Analytics) at the accumulation wall. The carrier liquid consisted of a 0.9 %w/v NaCl solution. Data from the MALS detector were processed using the Postnova AF2000 Control software (version 1.1.0.31), exploiting the spherical model to obtain the radius of gyration values. The measurement conditions adopted are: an injection flow of 0.2 mL/min, a power type elution step with a cross flow

of 3.0 mL/min, a transition time of 1 min and a detector flow of 0.5 mL/min.

Dynamic Light Scattering (DLS) and Zeta Potential (Z-Pot)

Hydrodynamic diameter (DH) and Z-Pot of PET NPs as a function of pH were performed using a Zetasizer Nano S (Malvern Instruments) spectrometer. DLS was studied in Milli-Q water, while for the evaluation of their stability in biological media, DLS was also performed on NPs in Dulbecco's modified Eagle's medium (DMEM) supplemented with 10% of non-heat inactivated HyClone™ Fetal Bovine Serum (FBS, GE Healthcare Life Science). Z-Pot was measured after pouring 10 µl of the NPs stock (300µg/mL) into 1 mL of a low salinity solution (0.002 M) containing the desired buffer.

X-ray Photoelectron Spectroscopy (XPS)

XPS analysis was performed using a SPECS-Lab

spectrometer with Al Kα source (hv= 1486.6 eV) operated at 15 kV with an emission current of 10 mA. Charge neutralizer consisting of low-energy (ca. 7 eV) electrons was applied and energy scale calibration was performed by setting the C-C/C-H component of C1s spectrum at 284.8 eV. NP samples were prepared by drop casting the suspension on a gold substrate dried in vacuum at room temperature.

Monodimensional Proton Nuclear Magnetic Resonance (1D ^{1}H NMR)

NMR experiments were performed, in collaboration with D3 Pharma Chemistry group, to evaluate the products of degradation of ablated PET. The experiments were recorded at 25°C with a Bruker FT NMR Avance III 600-MHz spectrometer equipped with a 5-mm CryoProbe™ QCI ^{1}H/^{19}F-^{13}C/^{15}N-D quadruple resonance, a shielded z-gradient coil, and the automatic sample changer SampleJet™ NMR system. The analyzed aqueous medium was collected precipitating the NPs through 15 min of

centrifugation at 20000g; a final concentration of 10% D_2O (Sigma-Aldrich) and 0.4mM of 3-(trimethylsilyl) propanoic acid (TSP) (Sigma-Aldrich) were added to the supernatant for the lock signal and ^1H chemical shift reference respectively. ^1H NMR experiments were recorded with the one-dimensional (1D) version of the NOESY (nuclear Overhauser effect spectroscopy) pulse sequence and with H_2O signal presaturation. A total of 256 scans were recorded for each spectrum, with a mixing time of 10 ms and a relaxation delay of 30 s. The data were multiplied with an exponential window function with 0.1 Hz line broadening prior to Fourier transformation.

Colloidal stability

The critical coagulation concentration (CCC) and the critical stabilization concentration (CSC), two important parameters in colloidal stability studies, were assessed.[125] CCC is the minimum salt concentration at which the most rapid NP aggregation is observed and gives information

on the surface charge density of the particles. CSC is defined as the minimum salt concentration at which the system begins to re-stabilize when the salinity is increased and is related with the surface hydrophilicity. PET NPs were dispersed in simple saline media at different concentrations of NaCl (from 0.002 to 2M). The NPs aggregation kinetics studies were performed spectrophotometrically by monitoring the variation of the optical absorbance (Abs) at λ= 570 nm over time. The Abs versus time was plotted at every salt concentration, and the slopes of these curves (∂Abs/∂t) enabled the determination of the Fuchs factor (W) defined by the following equation:

$$W = \frac{k_f}{k_s} = \frac{d(Abs/dt)_f}{d(Abs/dt)_s} \qquad \text{Eq.1}$$

where "k_f" refers to the fastest aggregation-kinetics rate constant, and "k_s" is the rate constant for the slower coagulation regime.

Protein corona

Protein corona complex formation is the first step to

understand the NPs behavior in biological media. Therefore 100 µl of PET NPs (300 µg/mL) were incubated in 1 mL of DMEM supplemented with 10% of FBS for 1 h at 37 °C. The samples were then centrifuged (15 min at 20000g) to pellet the particle−soft-corona complexes. Pellets were re-suspended in 1 mL of Milli-Q water and this procedure was repeated three times to remove proteins with low affinity for the NPs surface. Particle-protein complexes were characterized by DLS, Z-Pot and polyacrylamide gel (SDS–PAGE). The corona complexes were separated of the NPs and denatured by boiling for 5 minutes in blue loading buffer (3 parts sample diluted with 1 part Laemmli buffer with 2-mercaptoethanol at a final concentration of 355 mM). Samples were separated by size in a 12% polyacrylamide gel. After running the electrophoresis under constant voltage of 130 V for about 45 minutes the gel was stained with the 2D-SILVER STAIN-II kit (Cosmo Bio).

Experimental conditions for cell studies

Since oral appears to be the main route of exposure to

NPs, all the toxicological studies described below have been performed, in collaboration with the Nanobiointeractions and Nanodiagnostics group, on Caco-2 human epithelial colorectal adenocarcinoma cells (gently provided by Dr. Isabella De Angelis, Istituto Superiore di Sanità (ISS), Rome, Italy) were cultured with DMEM supplemented with 10% non-heat inactivated HyClone™ FBS, 1% penicillin-streptomycin (Sigma-Aldrich), and 1% non-essential amino acids (Invitrogen) and incubated in a humidified atmosphere with 5% CO2 at 37 °C. Cryopreserved stocks were sub-cultured twice before the experiments.

Cell viability assay

The effect of PET NPs on Caco-2 cell viability was studied by measuring the cell metabolic activity using an MTS (3-(4,5-dimethylthiazol-2-yl)-5-(3-carboxymethoxyphenyl)-2-(4-sulfophenyl)-2H-tetrazolium, inner salt) assay (CellTiter 96® AQueous One Solution Cell Proliferation Assay from Promega). Briefly, Caco-2 cells were seeded in

96-well plates at a concentration of 1 x 10^4 cells/well. Following 3 days of culture, the cells were exposed to a concentration of 1, 5, 15 and 30 µg/mL of PET NPs. Benzalkonium Chloride (BC) at a concentration of 50µg/mL was used as positive control. Cell viability was studied at 24, 48 and 96 hours by adding 20 µl of CellTiter 96® AQueous One Solution Reagent per well and incubating for 3h at 37 °C. Finally, the absorbance of each well was measured at 490 nm using a microplate reader (Synergy HT, Biotek).

Lactate dehydrogenase release assay

The impact of PET NPs on Caco-2 cell membrane was assessed by using a lactate dehydrogenase (LDH) assay (CytoTox-ONE™ Homogeneous Membrane Integrity Assay from Promega). As for the cell viability assay, cells were seeded in 96-well plates at a concentration of 1 x 10^4 cells/well and after 3 days of culture, NPs were added. The effect on LDH release was studied after 24, 48 and 96 hours. To determine the maximum LDH release (positive

control), 2 µl of Lysis Solution were added to positive control wells 10 min before the assay was performed. A volume of CytoTox-ONE™ Reagent equal to the volume of cell culture medium present in each well was added and plates were incubated for 10 min at 22 °C. Finally, 50 µl of Stop Solution (per 100 µL of CytoTox-ONE™ Reagent added) were added to each well to stop the reaction and fluorescence was recorded in a microplate reader with an excitation wavelength of λ_{ex}=560nm, and an emission wavelength of λ_{em}=590nm. The fluorescence of the culture medium background was measured and subtracted from the experimental values.

Apoptosis detection by staining with annexin V-FITC and propidium iodide

The Annexin V-FITC Apoptosis Detection kit (Miltenyi Biotec) was used to detect apoptosis and necrosis by flow cytometry. Caco-2 cells (2 x 10^5 cells/well) were seeded in 12–well plates and incubated with 1, 5, 15 and 30 µg/mL

of PET NPs for 96 hours. Dimethyl sulfoxide (DMSO) at 5% (v/v) incubated for 48 h was used as positive control. After incubation, cells were harvested with TrypLE™ Select Enzyme (1X) (Thermo Fisher Scientific) and pelleted by centrifugation at 300g for 5 min. They were then washed and redispersed in 100 µl of 1x Binding buffer, and 10 µl Annexin V-FITC were added in each sample. Cells were incubated for 15 min in the dark at room temperature following the manufacturer instructions. After incubation, cells were washed and resuspended in 500 µl of Binding buffer. 5 µl of propidium iodide (PI) solution were added prior to analysis by flow cytometry using a MACSQuant® Analyzer Flow Cytometer.

Measurement of intracellular Reactive Oxygen Species (ROS)

Intracellular ROS generation of Caco-2 cells after incubation with NPs was measured by using 2',7'-dichlorofluorescin diacetate (DCFDA) (Invitrogen), a

molecule which can penetrate cellular membranes and can be oxidized by ROS giving a fluorescent compound (λ_{ex}=485, λ_{em}=535 nm). Briefly, Caco-2 cells pre-incubated for 30 min with a solution of 10 µM DCFDA in HBSS were seeded at a concentration of 2 x 10^4 cells/well in 96-well plates. After 96 hours of incubation with 1, 5, 15 and 30 µg/mL of NPs, the fluorescence intensity of the DCFDA oxidized product, DCF, was measured. The percentage of ROS was normalized to the negative control cells (100%). *Tert*-butyl hydroperoxide (TBHP) to a final concentration of 100 µM was used as positive control.

Uptake of PET NPs

In order to follow the NPs in the in vitro test of uptake and transport, they were fluorescently labelled with 5-Aminofluorescein (Fluoresceinamine, isomer I) (Sigma-Aldrich). The acid groups of the NPs surface were activated with 1-ethyl-3-(3-dimethylaminopropyl)-carbodiimide hydrochloride (EDC) (Thermo Scientific) (20 mM), and then fluorescein amine (50 µg/mL) was

covalently coupled. After 2 hours of reaction the NPs were dialyzed against Milli-Q water, overnight, using a dialysis membrane (molecular weight cut-off of 3500, 1.15 mL/cm, Fisherbrand). Uptake of fluorescein-PET NPs by Caco-2 single cells was assessed by flow cytometry and confocal microscopy. Cells were seeded in 12 well plates at a density of $15x10^4$ cells per well one day before treatment. Then, they were treated with 30 µg/mL of NPs for 30 min, 1, 3, 6, 19 and 24 hours and the fluorescence intensity were measured by flow cytometry. Caco-2 cells (5×10^4) grown on glass coverslips of 12mm diameter and incubated for 96 hours with NPs, were fixed with 4% paraformaldehyde for 15 min at room temperature, permeabilized with 0.01% Triton X100 for 5 min and blocked with 0.5% bovine serum albumin in PBS for 20 min. They were then stained with 0.1 nM Alexa FluorTM 594 Phalloidin for 30 min and Hoechst 33342 (Thermo Fisher Scientific) at a concentration of 5 µg/mL for 5 min, to localize actin microfilaments and cell nuclei, respectively.

Intracellular trafficking of NPs

To investigate the subcellular localization, living single Caco-2 cells exposed to fluorescein-PET NPs (30 μg/mL) for 24, 72 and 96 hours where incubated for 1 hour at 37 °C with LysoTracker™ Red DND-99 (Thermo Fisher Scientific) in DMEM at a concentration of 75nM. The cells where then washed with PBS and incubated with Hoechst 33342 at a concentration of 5 μg/mL for 5 min to localize their nuclei. Image acquisition was performed using a confocal microscope (Leica TCS-SP5) using a 40x oil objective, with λ_{ex} of 405, 488 and 561 nm and a resolution of 1024 × 1024 pixels. Image analysis was performed using ImageJ software.

NPs characterization in lysosomal-like fluid

NPs (30 μg/mL) were dispersed in a 0.1M citrate buffer (Sigma-Aldrich) presenting a pH of 4.5. The incubation was performed at 37° C and the DH was monitored through DLS analysis at several time points up to 2

months.

Intestinal layer formation

Caco-2 cells were seeded in 12 well/plates onto porous Millicell Hanging Cell Culture Inserts (diameter (d): 12mm; surface (A): 1.12 cm^2; pore size: 0.1 µm) in 0.5 mL of DMEM at a seeding density of 17 x 104 cells/insert in the apical (Ap) side. 1.5 mL of the medium was poured into the basolateral (Bl) compartment. Cells were grown for 21 days and the culture medium was changed every two days to allow the formation of tight junctions and microvilli.40 After 21 days confluent and differentiated cell monolayers were formed, and the integrity of the epithelia was confirmed by measuring the Trans-epithelial Electrical resistance (TEER) (methods in supporting information file).

Trans-epithelial Electrical resistance

Trans-epithelial Electrical resistance (TEER) of Caco-2

barrier was measured with chopstick electrodes using a Millicell-ERS-2 Volt-Ohm Meter (Merck Millipore) maintaining a constant temperature of 37 °C. TEER values were expressed as Ohms (Ω) x cm^2 and calculated according to the following equation:

$$TEER = [\Omega_{\text{cell monolayer}} - \Omega_{\text{cell-free filter}}] \times \text{filter area} \quad \text{Eq.2}$$

The differentiated Caco-2 monolayers were incubated with 5, 15 and 30 µg/mL of PET refreshing the apical medium every two days in order to keep the concentrations of NPs stable. The integrity of the layers was assessed by determining the TEER values after 1, 5 and 9 days in order to mimic an acute and a chronic intestinal exposure.

Lucifer yellow assay

The impact of PET NPs on epithelium integrity was studied by assessing any difference in the transport of the paracellular marker Lucifer Yellow (LY, Sigma Aldrich) from the Ap to the Bl compartment between treated (5,

15 and 30 µg/mL of PET NPs) and untreated inserts. After 1, 5 and 9 days of treatment, the medium was collected, and intestinal layers were washed twice with Hanks' Balanced Salt Solution (HBSS, Thermo Fisher Scientific). Afterwards, 0.5 mL of 0.4 mg/mL LY solution in HBSS and 1.5 mL of HBSS were added to the Ap and the basolateral Bl compartment respectively. Cells were incubated for 2 h at 37 °C and 100 µl of the Bl HBSS of each insert were then collected and poured into a black 96-well plate. Finally, fluorescent intensity of LY was determined using a spectrofluorometer (λ_{ex}=428 nm, λ_{em}=536 nm). The percentage of LY passage from the Ap to the Bl side of intestinal layers treated with PET NPs was compared to untreated inserts.

Transport of fluorescein-PET NPs through intestinal epithelia

Caco-2 monolayers were incubated with 7 and 30 µg/mL of fluorescein functionalized PET NPs dispersed in phenol red-free 10% FBS supplemented DMEM (Thermo Fisher

Scientific). In order to maintain the concentration of NPs in contact with cells stable, the medium was changed every 2 days up to 9 days. The transport of NPs through the intestinal epithelium from the Ap to the Bl compartment was quantified after 1, 5 and 9 days of exposure. The fluorescein-NPs were quantified using a spectrofluorometer (FluoroMax-4, Horiba). The sample solutions, placed in a quartz cuvette with a path-length of 1 cm, were excited at a λ_{ex} of 495 nm. The construction of the calibration line and the measurements were done referring to the peak of emission at a λ_{em} of 516 nm.

Caco-2 barrier fixation

For the TEM characterization of Caco-2 barrier, samples were fixed through a 2 h incubation in 1.5% glutaraldehyde (Electron Microscopy Science) in 0.09 M Sodium Cacodylate (Sigma-Aldrich) buffer (pH 7.4) before the analysis, post fixed in 1% osmium tetroxide (Electron Microscopy Science) in the same buffer and stained overnight with 1% uranyl acetate (Electron Microscopy

Science) aqueous solution. Cells were then dehydrated in a graded ethanol series, infiltrated with propylene oxide and embedded in epoxy resin (Epon 812, TAAB). Semi-thin and thin sections of the embedded cell monolayer were cut with an ultramicrotome (UC6, Leica) equipped with a diamond knife (Diatome).

Cytokine release

Inflammatory cytokine release (IL-8, MCP-1) in the Ap and Bl compartment from the intestinal epithelia and from Caco-2 single cells was assessed after 1, 5 and 9 days of exposure to PET NPs with a Bio-Plex MAGPIX Multiplex Reader (Bio-Rad), according to the manufacturer's procedure. Cells were stimulated with Interferon-gamma (IFN-γ; 50 ng/mL) and Interleukin-1 beta (IL-1β; 10 ng/mL) as positive control.

Results and discussion

Morphological characterization of NPs

Given the absorption characteristics of the polymer chosen for the development of the NPs model, PET, it was decided to use a KrF excimer laser emitting at a wavelength of 248 nm.[119,121] In fact, although the PLA technique is extremely versatile and applicable on various materials, the ablation of polymers such as polyethylene and polypropylene, which absorb at wavelengths below 200 nm (Figure 7), requires the use of high energy photons or

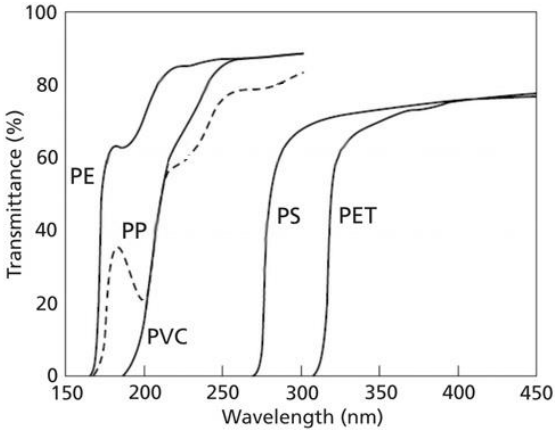

Figure 7. UV Transmittance spectra of polyethylene terephtalate (PET), Polystyrene (PS), Polyvynil chloride (PVC), Polypropylene (PP), Polyethylene (PE). [124]

a multiphoton approach.[119,126] The first essential information to evaluate if the PLA in water is an efficient technique for the synthesis of a model of NPs, is the morphology of the obtained product. For this reason, the entire product of ablation has been analyzed by HRSEM (Figure 8). In accordance with what is observed for the degradation of bulk polymers in accelerated weathering testers,[63] the plastic fragments produced, upon the interaction of the laser beam with the polymer target surface and the generation of the shock wave, have an irregular morphology and a broad size distribution, between tens of nanometers and microns. Following the aim of the thesis

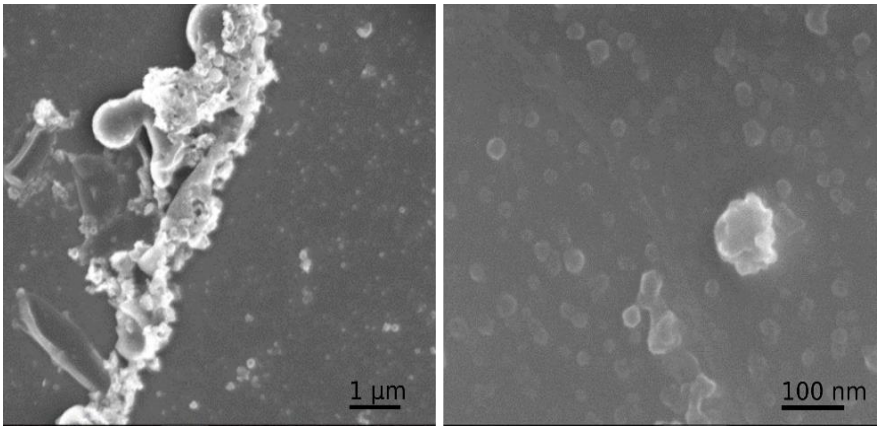

Figure 8. HRSEM micrograph of PET NPs. On the left side clusters produced during ablation, on the right the detailed NP morphology.

and the definition of NPs, the selection of the nanometric fraction of the ablated material was carried out by filtration using a filter with a cutoff of 200 nm. Although the filtration causes the loss of about 45% of the product, it allows a substantial improvement in the polydispersity of the NPs size (figure 9). After the filtration, each ablation

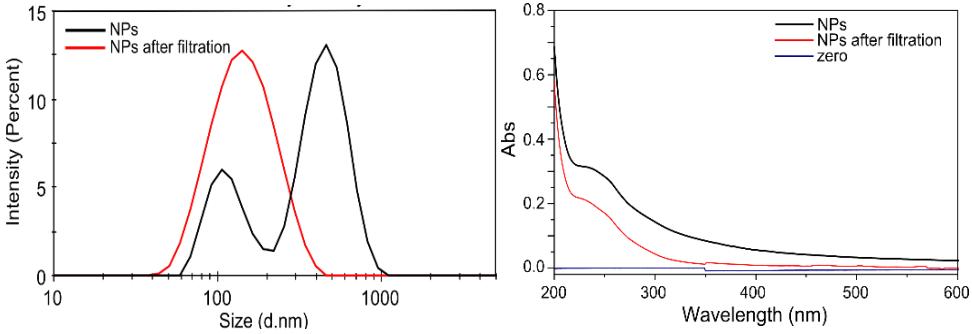

Figure 9. DLS analysis and UV-vis quantification of NPs before (black) and after (red) filtration.

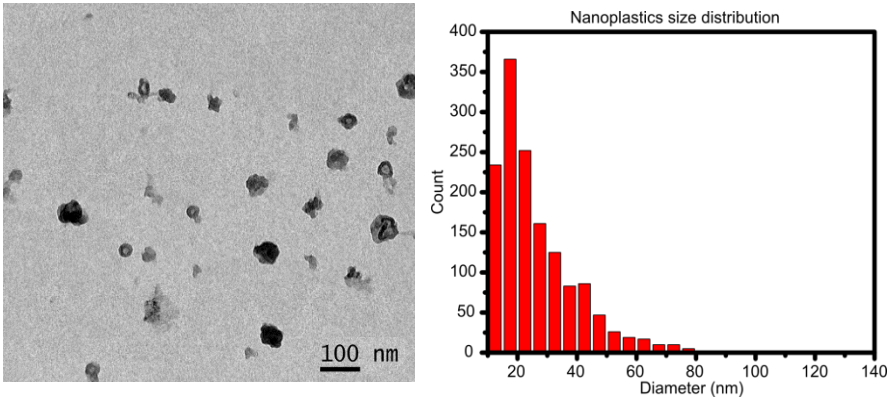

Figure 10. TEM image (left) and size distribution (right) of PET NPs.

cycle had a yield of ~10 µg/mL of NPs. The rotavapor treatment allowed to concentrate the NPs up to 300 µg/mL. As visible by the TEM analysis of the filtered samples (Figure 10), although the presence of some clusters, typical of real NP samples, were observed, the particles are well dispersed with an "approximatively" spherical shape.[63] The analysis of the NPs size distribution indicated

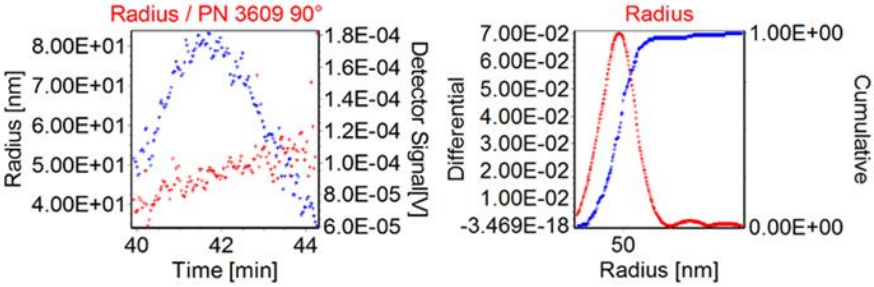

Figure 11. AF4 resulting PNP gyration radius: (left) AF4 chromatogram, (right) normalized size distribution

a principal population with a mean diameter of 26.7±14.2 nm (Figure 10). To define the dimensions of the NPs in wet media, DLS and AF4 measurements were carried out in the aqueous medium. The obtained results showed a hydrodynamic (D_H) and gyration radius (R_g), obtained by DLS and AF4 respectively, greater than the geometric one, ranging between few tens to about 100 nm. This is due to the presence of fragments and long polymeric chains, formed in the liquid as a result of the degradation induced by UV light, which cover the surface of the nano-particles. In particular, concerning DLS, the D_H laid at 109.5±13.3 nm (Figure 8), strictly comparable with the R_g of 47.1 nm resulting from AF4 analysis (Figure 11), ob-tained through a sphere model fitting.

Chemical characterization of NPs

The surface chemistry of a material is a fundamental parameter necessary for the evaluation of its environmental and biological fate. In order to

characterize the surface chemistry of the NPs XPS analysis was performed, and the results were compared with the XPS data obtained by analyzing the pristine polymer. The relative O/C ratio, determined by the elemental concentration analysis, increase from 12.3% for the pristine PET to 32.1% for PET NPs. This gives a first indication about the higher degree of oxidation for the NPs. This is confirmed by the C1s and O1s high resolution

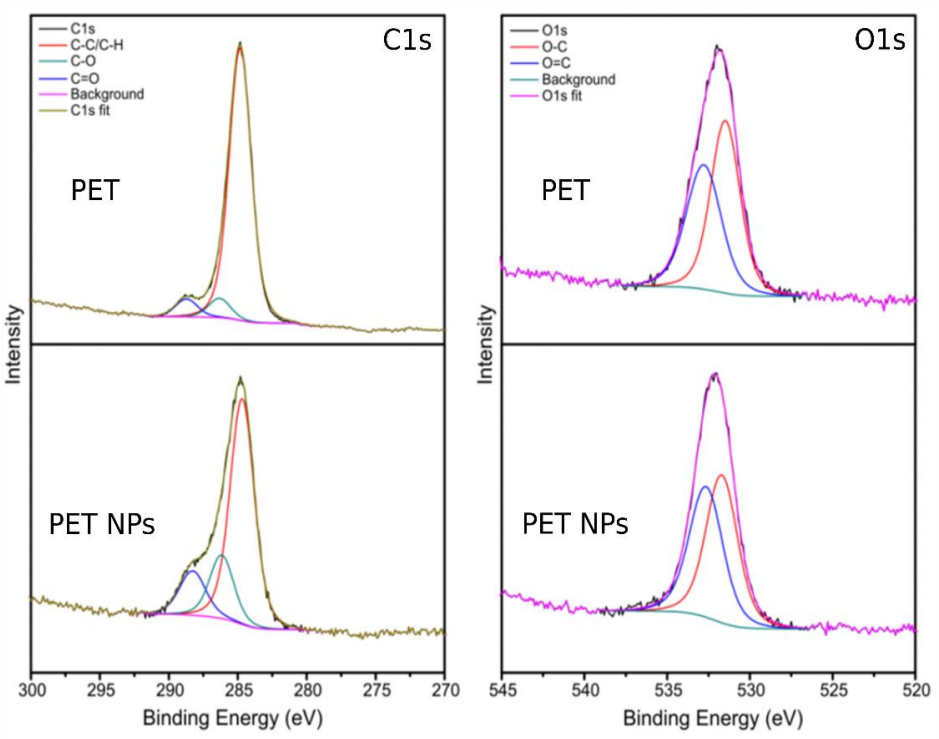

Figure 12. XPS C1s (left) and O1s (right) high-resolution spectra of the pristine PET and of the as-synthesized PET NPs.

spectra as shown in Figure 12 where the spectra of the untreated PET film and of the NPs are shown. Three different contributions were fitted in the C1s spectra at 284.8 eV corresponding to C-C and C=C of the phenyl ring (C-C, C=C) at 286.3 and 288.7 eV concerning C-O and O-C=O bonds, respectively.[127,128] Two components attributed to O-C ester group at 531.5 eV and O=C carboxyl oxygen at 532.8 eV were present in the O1s spectra.[129] As shown in Table 5 the quantities of C-O and O-C=O bonds components are double on the NPs compared to the pristine PET.[120,130,131]

Table 5. Species percentage calculated on the C1s and O1s XPS spectra of untreated PET and PET NPs.

Element	Species	PET	PET NPs
C1s	C-C/C=C	88.0±0.1%	70.7±0.1%
	C-O	6.2±0.1%	15.3±0.1%
	C=O	5.8±0.1%	14.0±0.1%
O1s	O-C	53.6±0.1%	51.5±0.1%
	O=C	46.4±0.1%	48.5±0.1%

These findings may indicate the exposure of new carboxyl end-groups groups on the material surface, a typical sign of PET photodegradation promoted by thermo-oxidative and photo-oxidative pathways.[55,120,130,132]

The production of acidic residues was further corroborated by the alteration of the pH of the ablation medium. Performing the synthesis in phosphate buffer 0.1 mM, the pH drops from the initial value of 7.05±0.2 to the final value of 5.65±0.2. Such pH modification could be related to the hydrolysis of PET, one of the processes involved in its degradation in water, which boosted by laser ablation induce the formation of carboxylic acid and alcohol functional groups and is fostered at pH values different from neutrality, in a sort of autocatalytic reaction.[55,133–135]

The ^{1}H NMR analysis performed in D_2O evidences the predominant presence of two organic acids in the medium of ablation after the synthesis of NPs. Apparently, no aromatic signal related to the monomer unit was detected. The more concentrated organic acids have been identified spotting different organic acids in supernatant solutions accordingly with the assignment reported in literature.[136] The predominant peaks at 8.45 ppm and 1.94 ppm have been therefore assigned to the Formic and Acetic acid respectively (Figure 13). The

quantities measured for these two principal substances are in the order of 270 µM for formic acid and of 180 µM for acetic acid. The measurement carried out on the same medium after the rotavapor treatment, at low temperature, showed that the concentrations of acetic and formic acids formed in the medium during laser ablation are both reduced reaching sub-micromolar and

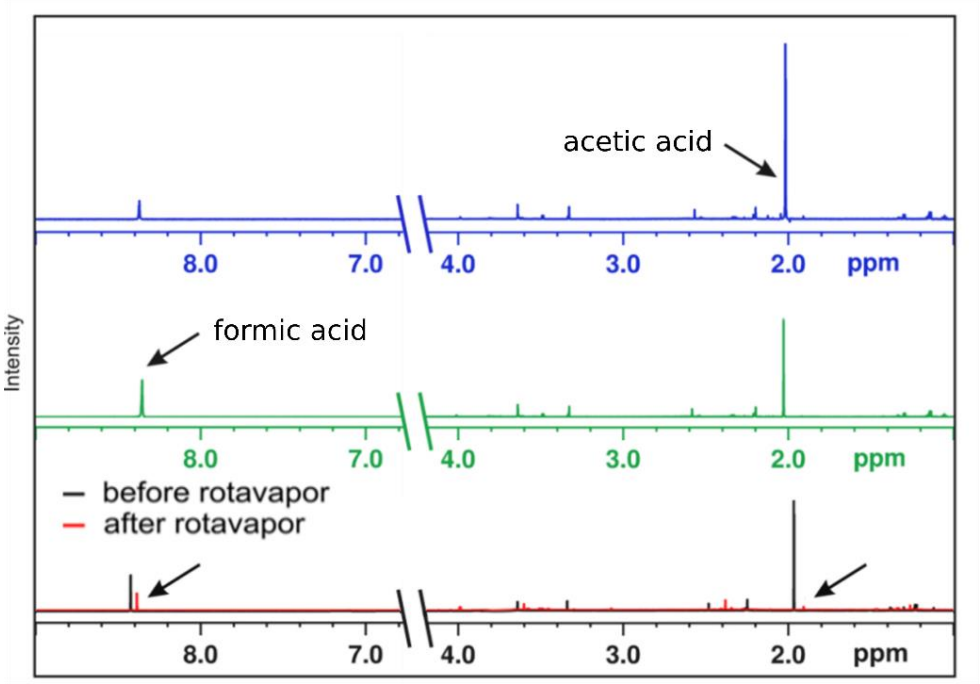

Figure 13. ^{1}H 1D NMR spectra of the ablation medium: the starting sample (black), sample after the concentration of NPs in rotavapor at 45 °C (red), sample plus formic acid standard (green), sample plus acetic acid standard (blue).

lower than 5 µM values respectively. Other very low signals related to small amounts of alcohols and other organic contaminants are considered negligible. These results facilitate the study of the biological impact of PET NPs allowing to exclude effects linked to any contaminants derived from the synthesis process.

The analysis of the surface charge of the NPs dispersed in buffer media with different pH values by Z-Pot, have corroborated the presence of carboxylic acid groups on the NP surface. As shown in Figure 14, NPs are negatively charged and show a behavior typically observed in colloidal systems with weak acid groups on their surface.

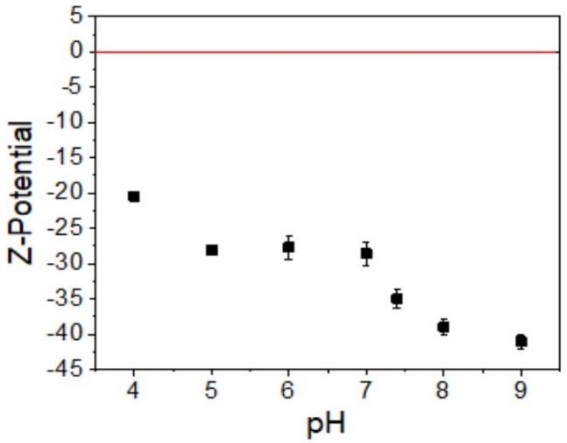

Figure 14. Z-Pot of PET PNPs as a function of pH

In particular, as shown, the absolute values Z-Pot are lower at acidic pH compared to those of basic pH.[125]

Characterization of NP behavior in aqueous media

In nature, NPs are exposed to environments of high variability, with conditions that can cause alterations in their colloidal stability, affecting their fate. Although, as it is observed, the NPs are stable in MilliQ water for up to 6 months, it is essential to evaluate the effect of the pH and

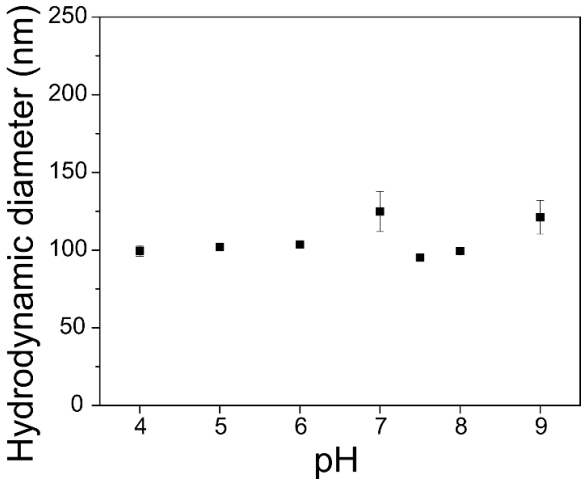

Figure 15. Effect of different pH on the hydrodynamic diameter distribution of NPs.

saline concentration of the liquids where they are dispersed, on their stability. DLS analysis showed that the NPs maintain their original D_H within a wide pH range, from 4 to 9, indicating good stability in such conditions (Figure 15).

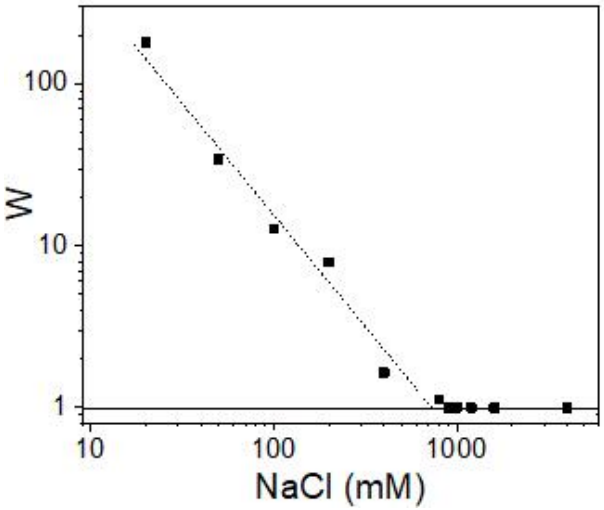

Figure 16. Fuchs factor (W) versus NaCl concentration. The dashed line, that fits with the points at low aggregation regime, helps to locate the CCC value

On the other hand, the coagulation kinetics at different NaCl concentrations was studied to evaluate the effect of the salinity on the colloidal stability. Calculation of the stability (Fuchs) factor W and, thus, the CCC (critical coagulation concentration) and CSC (critical stabilization con-

centration) give also information about the surface characteristics of the NPs. W is related to the coagulation probability and is included in a range between 1, for completely unstable system and ∞ for a totally stable one. As shown in Figure 16, W decreases gradually with increasing the salt concentration until the CCC value is reached, at circa 700 mM a value associated with a very stable system. The high stability of the colloid is supplied by the strong repulsive forces among NPs, due to the high surface charge density. Over the CCC point, the NPs are unstable and start to aggregate quickly. This lack of re-stabilization given by the so-called hydration forces in high ionic-strength media is a clear indication of the hydrophobic nature of the PET NP surface.[137,138]

Characterization of NP behavior in cellular media and protein corona formation

In an environment as well as in biological media, NPs interact with macromolecules such as proteins that can

affect their colloidal behaviour altering their stability. Knowing that saline concentrations close to those of cellular media (154 mM) cause NPs coagulation (Figure 16), the influence of serum proteins on particle behaviour has been studied. The D_H is a parameter indicative of NP stability, thus DLS measurements have been performed on NPs dispersed in a serum-free cell culture medium (SF-DMEM) and DMEM supplemented with 10% FBS (c-DMEM). The size distribution of NPs was measured after 2.5 hours of incubation in the different media (Figure 17). The high salt concentration of SF-DMEM destabilizes NPs

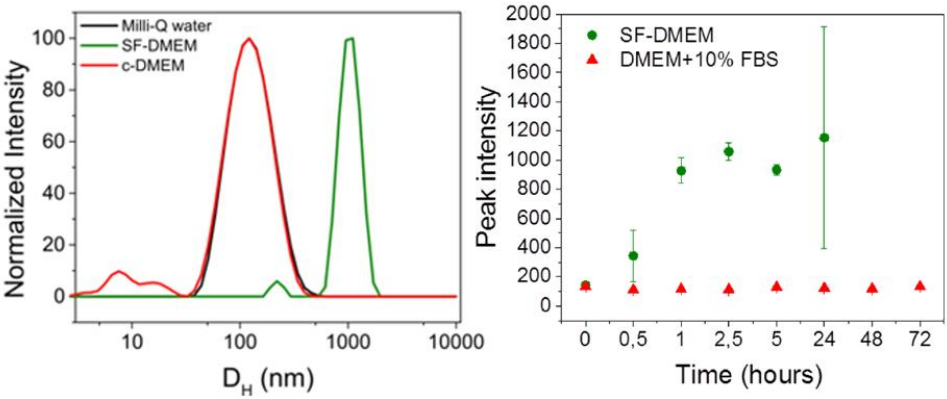

Figure 17. Hydrodynamic diameter (D_H) distribution of NPs in Milli-Q water (black) after incubation for 2.5 h in serum-free Dulbecco's modified Eagle's medium (DMEM) (SF-DMEM; green) and in DMEM supplemented with 10% fetal bovine serum (FBS) (cDMEM; red) (left). Aggregation kinetics of NPs when dispersed in serum free DMEM (SF-DMEM; green circles) and DMEM supplemented with 10% of FBS (c-DMEM; red triangles) (right).

inducing the formation of large aggregates, up to micron size. This destabilization does not occur in c-DMEM, in the presence of serum proteins. The aggregation kinetics shown in Figure 17 demonstrate that NP interaction with proteins improves their stability and prevents their aggregation. NPs in c-DMEM stably maintained their size in the timescale of the experiment (up to 72 hours). Contrarily, in SF-DMEM the D_H of NPs increase with respect to NPs in water already at the first time points studied, indicating a fast aggregation kinetics. This means that the formation of a protein layer around the NPs, also

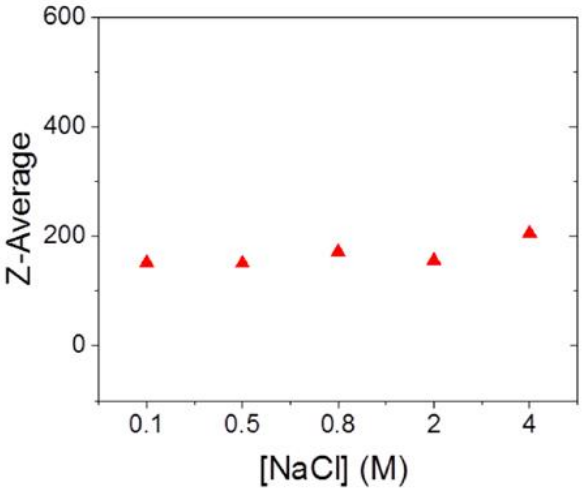

Figure 18. Z-Average of particle−soft-corona complexes (NPs incubated for 1 h with 10% FBS) dispersed in different concentrations of NaCl solutions.

known as “protein corona”, increases their colloidal stability even at high NaCl concentrations. It is well established that protein surfaces tend to be very hydrated and, thus, additional stability is provided by creating a steric hindrance based on structured water molecules strongly bonded to proteins.[139] In fact, unlike bare NPs, presenting a rapid aggregation regime over 700 mM, NPs-protein complexes were stable up to 4M (Figure 18).

The formation of a protein corona was further confirmed by the change in surface charge of the NPs before and

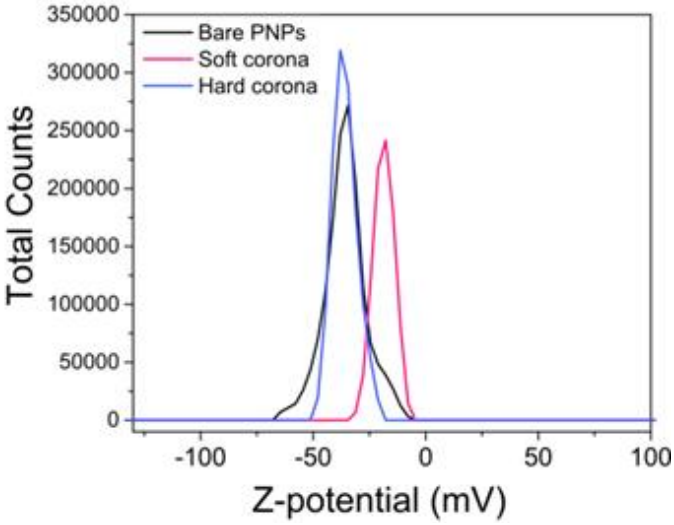

Figure 19. Z-Pot of PET NPs before (black) and after incubation with 10% of FBS: soft corona (red) and hard corona (blue).

after incubation with proteins (Figure 19).[140] The method of "pelleting" has been applied,[141] before the Z-Pot measurement. In particular, after one hour of incubation with 10% FBS, NPs were centrifuged to pellet the particle-soft-corona complexes, and the surface charge was measured before and after washing three times the NPs. This method allows to discriminate if the interactions between proteins and NPs are strong and stable (hard corona) or labile and proteins are loosely associated to the NPs and in rapid dynamic exchange with the medium (soft corona). Before the wash, surface charge decreased from -35.0±1.2 mV to -16.0±1.3 mV (value for the bare NPs) in presence of proteins, while returned at ≃-36 mV

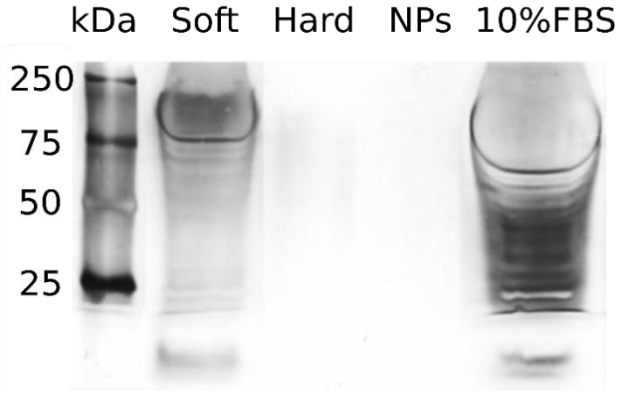

Figure 20. SDS-PAGE of the soft and hard protein corona on the PET NPs after 1 hour of incubation in DMEM completed with 10% FBS. PNPs and the completed medium (10% FBS) were used as negative and positive control respectively.

after the wash suggesting the absence of proteins strongly adsorbed (hard corona) on the NPs surface. A further confirmation comes from the SDS-PAGE analysis of the same samples showing the amount of protein adsorbed on NPs in terms of band intensity (Figure 20). Although this protein layer is poorly associated to NP surface, soft corona confers them a new biological identity that will determine their interaction with cells.[140]

Uptake, intracellular localization and cytotoxicology of PET NPs

The combination of characteristics such as size, surface charge, hydrophobicity and colloidal stability revealed by the analysis of this NPs model reinforce the idea that this type of pollutants can interact with living organisms and be a risk to humans. As shown by different studies oral route may be the main way of exposure to NPs (through the food chain).[70,142] Therefore, a preliminary *in vitro*

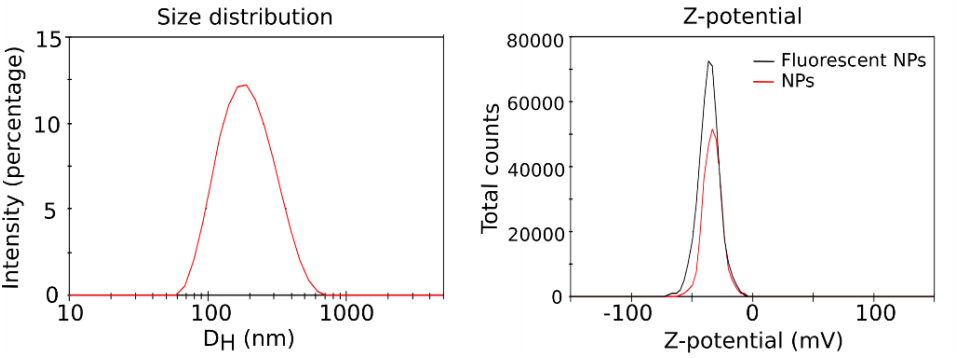

Figure 21 Size distribution of fluorescent NPs (left) and Z-potential of NPs (red line) and fluorescent NPs (black line)

evaluation of the cytotoxic effect of PET NPs was performed on the Caco-2 cell line, widely applied in toxicity studies for oral exposure scenarios.[143] To follow the internalization of NPs, fluoresceinamine was conjugated to the carboxylic groups of the NP surface by means of a carbodiimide (EDC) method. The NPs tag did not alter their characteristics of D_H and Z-Pot (Figure 21). The actual internalization of NPs has been verified through confocal microscopy. The cytoskeleton was labeled with phalloidin to define the entire cell volume and allow to evaluate the internal presence of NPs labeled with the fluorophore. The analysis shown in Figure 22 confirms expectations and demonstrated the

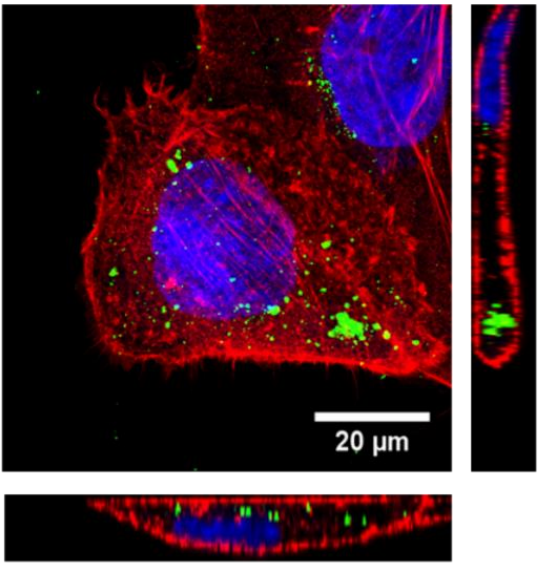

Figure 22. Confocal microscopy of Caco-2 cells incubated for 24 h with fluorescent NPs. Hoechst/nuclei (blue), Phalloidin/actin (red), NPs (green). Lateral boxes represent z-stack projections along x-z and y-z axes.

effective cellular uptake of NPs. Subsequently, Caco-2 cells were exposed to 30 µg/mL of NPs for 24 hours and the kinetic profile of NP uptake have been obtained by flow cytometry (Figure 23). The analysis showed the mean intracellular fluorescence values from flow cytometry distributions of ≥100,000 cells treated at different time points. The cell fluorescence intensity increased linearly without reaching the saturation due to the splitting of nanoparticles between cells following cell division.[144] After the demonstration of the cellular

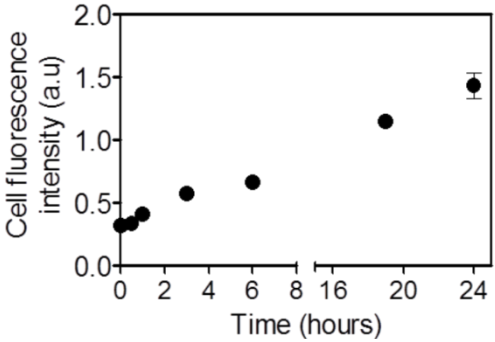

Figure 23. Cellular uptake kinetics of fluorescent NPs by flow cytometry.

capacity to internalize the NPs it is crucial to investigate the uptake mechanism, to better understand their fate. Using a pH-responsive endosomal tracer, confocal

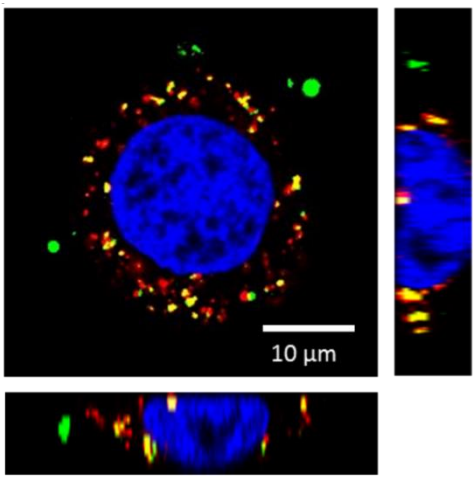

Figure 24. Confocal microscopy of Caco-2 cells incubated for 24 h with fluorescent NPs. NPs co-localized with Lysotracker positive organelles of Caco-2 cells. Hoechst 33342/nuclei (blue), Lysotracker (red), NPs (green). Lateral boxes represent z-stack projections along x-z and y-z axes.

microscopy showed the colocalization of fluorescence signals of NPs in correspondence with lysosomes after 24 hours of treatment (Figure 24), suggesting that the endocytic pathway is the mechanism used by the NPs to enter the cells, in accordance with previous studies on diverse types of nanoparticles, such as polystyrene and poly(DL-lactide-co-glycolide).[145,146]

Depending on the polymeric composition of the NPs, the acidity of the lysosomal environment could affect their integrity and induce their degradation or leave them intact favoring the intracellular accumulation of the pollutants. The biodurability or biopersistence may influence the long-term toxicity of the NPs after chronic exposure. Given the technical impossibility to follow the degradation of NPs in living cells for long periods, the lysosomal environment was reproduced in vitro by utilizing a simplified cell-free assay that mimics the lysosomal fluid. In particular, the NPs were dispersed in citrate buffer (pH 4.5) and incubated at 37 °C, up to 2 months. As shown in Figure 25, the D_H value of the NPs remained stable and was comparable to that of as-

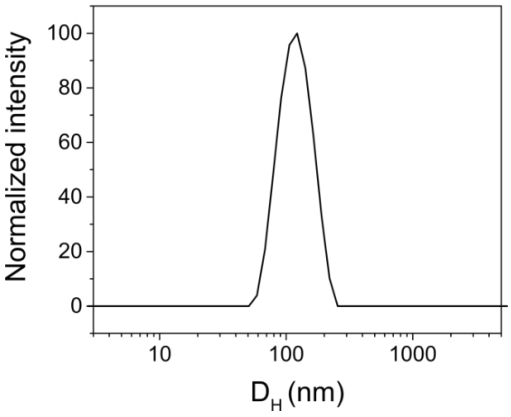

Figure 25. Normalized size distribution of PET PNPs incubated for 2 months in 0.1M citrate buffer (pH 4.5) at 37°C.

synthesized NPs stored in water, suggesting that the lysosomal environment (at least in terms of acidic and temperature conditions) is not enough to induce NP degradation.

The acute toxicological assessment of NPs was performed by studying cell viability, integrity of cell membrane, ROS generation, apoptosis and necrosis, and inflammatory response. Caco-2 cells were incubated with 1, 5, 15 and 30 μg/mL of PET NPs and the toxicological assays were performed after 24, 72 and 96 hours of treatment. The cell viability was evaluated by an MTS assay (Figure 26) and the effect of NPs on the cell membrane integrity was determined by LDH assay (Figure 27). No evidence of

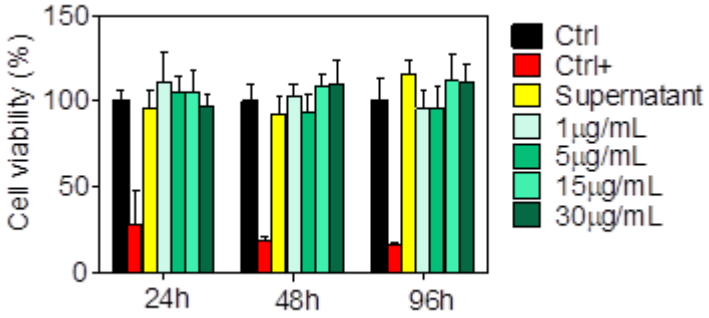

Figure 26. Viability of Caco-2 cells exposed to different concentrations of NPs for 24, 48 and 96 h. Cell viability of the solution where the NPs were synthesized was also studied after pelleting the particles (supernatant). Benzalkonium Chloride (Ctrl+) (50 µg/mL) was used as positive control.

acute toxicity related to treatment emerged from the cell viability and membrane integrity data. Moreover, NP treated cells did not show any significant change in apoptosis and necrosis compared to the control group (Figures 28), in qualitative agreement with previously

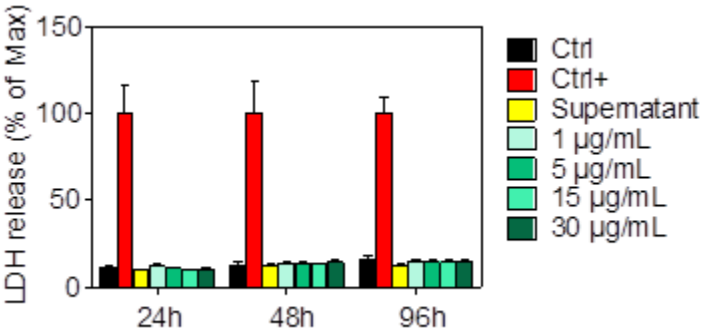

Figure 27. Lactate dehydrogenase (LDH) release in cell supernatant after 24, 48 and 96 h treatment with NPs. Cell lysis solution was used to obtain the maximum LDH release (Positive control).

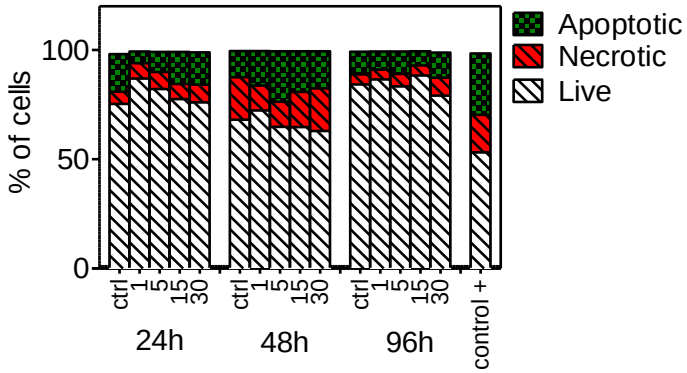

Figure 28. Apoptotic, necrotic and live Caco-2 cells after 24, 48 and 96 h of treatment with different concentrations of PET NPs. DMSO (5%) was used as positive control.

reported data with 50 nm polystyrene NPs applied on the same cell line.[147] Fullerene, metal and metal oxide nanoparticles have been suggested as nanomaterials with reactive oxygen species (ROS) scavenging ability,[148,149] but the presence of nanoparticles inside cells could also result in disturbances in cell metabolism that

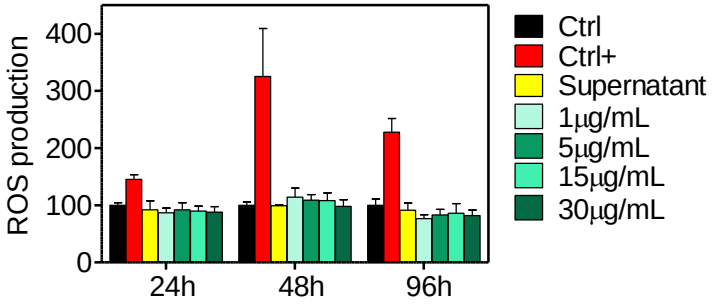

Figure 29. ROS production by Caco-2 cells after 24, 48 and 96 h of incubation with NPs. *Tert*-butyl hydroperoxide (TBHP) (100 µM) was used as positive control.

could increase the ROS production.[150–153]As shown in Figure 29, cells treated with NPs did not increase ROS generation.

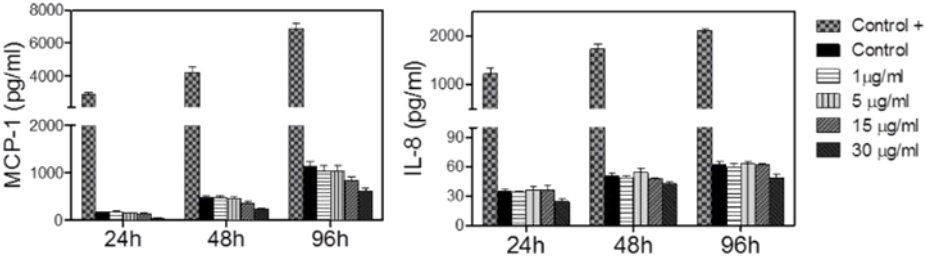

Figure 30. Inflammatory response of Caco-2 cells upon exposure to NPs. Release of MCP-1 (left), IL-8 (right).

The absence of inflammatory effects is corroborated by the analysis the Caco-2 production profile of pro-inflammatory cytokine proteins IL-8 and MCP-1 (Figure 30) which seems to maintain its basal level in accordance with published results on the same cell type.[154–156] Using the same cell line it is possible to structure a simplified *in vitro* model of intestinal epithelium, useful to investigate the transport of PET NPs upon ingestion. In order to establish the intestinal barrier model, this was produced by seeding Caco-2 cells on porous filters, and after 21 days of culture, polarized differentiated cell monolayers were obtained.[157,158] TEM images showed the formation of the typical tight junctions and microvilli (Figure 31). The

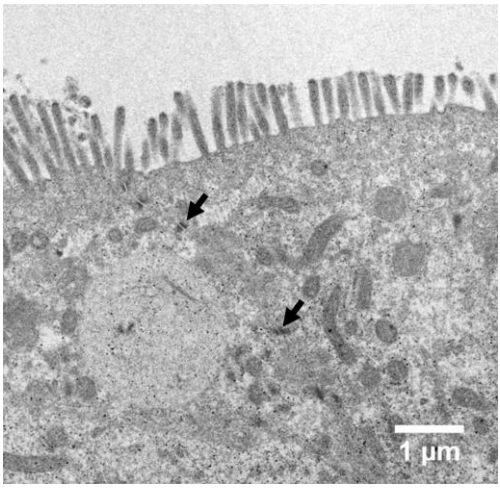

Figure 31. Transmission electron microscopy image of differentiated Caco-2 cells presenting the typical tight junctions and microvilli on the apical surface.

integrity and confluence of the layers were confirmed by a TEER value of 339 ± 24 Ω cm^2.[159] As shown in Figure 32, TEER values, that as reported in other studies decreases up to 80% at the earlier time points in case of cellular

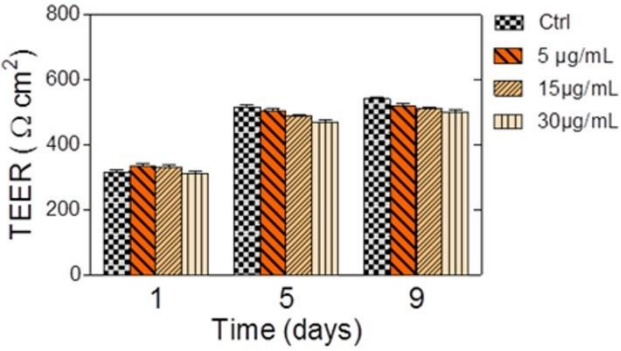

Figure 32. TEER measurements of non-treated inserts (Ctrl) and intestinal layers incubated with different concentrations of NPs after 1, 5 and 9 days of exposure.

layer damages, with NPs were not significantly decreased upon chronic incubation.[97,160,161] Cell barrier integrity after exposure to PET NPs was additionally assessed by translocation studies using Lucifer Yellow (LY), a marker of paracellular transport. Inserts were incubated with a solution of LY in the Ap side for 2 hours and the transport to the Bl side was fluorescently quantified. In accordance with TEER results, upon chronic exposure to NPs, transport of LY across the membrane was not significantly changed and was maintained below 0.2% (Figure 33), in contrast to published data in which after 24 hours of treatment with nanomaterials, LY translocation was increased until 25%.[162,163]

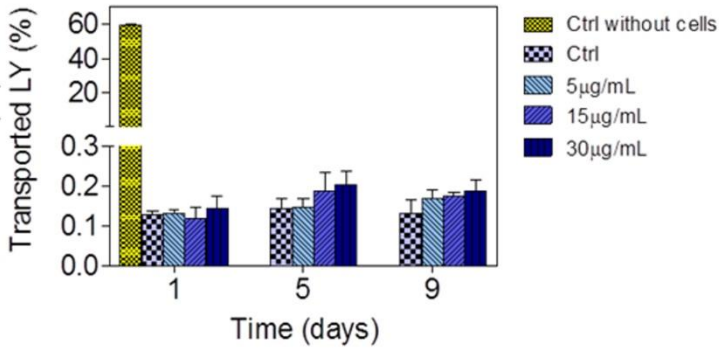

Figure 33. Percentage of transported Lucifer Yellow (LY) across the Caco-2 barrier after 1, 5 and 9 days of exposure to NPs compared to control layers and to the transwells without cells

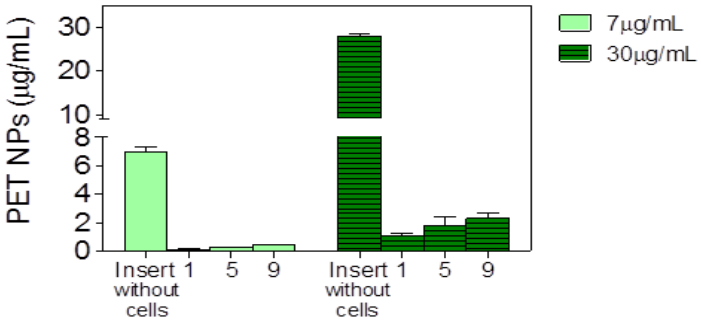

Figure 34. Comparison of the NP translocation through a filter without cells (1 day of incubation) respect to the Caco-2 barrier model (1, 5, 9 days of incubation).

Confirmed that NPs exposure did not alter the barrier integrity, the NP trans-monolayer transport kinetics have been assessed in terms of cumulative transport after 1, 5 and 9 days of treatment by administering two different concentrations (30 and 7 µg/mL) of NPs to the apical side (Ap) of the barrier (Figure 34). The number of transported NPs in the basal (Bl) increased with increasing incubation time. Both the concentration of 30 and 7 g/mL showed a very similar relative transport value. Confocal orthogonal cross sections showed the presence of NPs inside the differentiated enterocyte-like cells but also in the filter placed on the basal side (Figure 35). In the differentiates Caco-2 was observed a reduction of the NP uptake, compared to the undifferentiated status, as previously

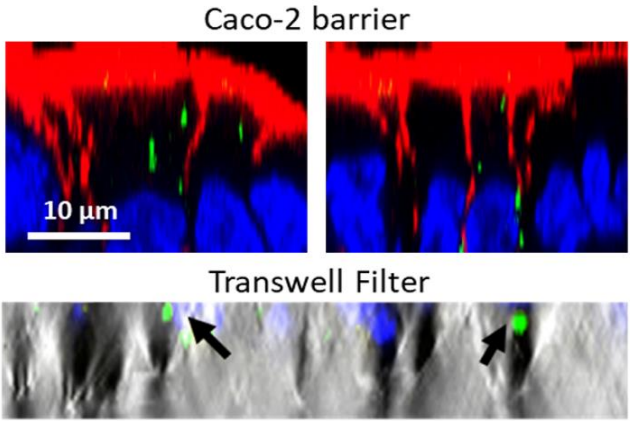

Figure 35. Confocal fluorescence cross-section images of Caco-2 barriers and their transwell filter exposed to NPs. The NPs are shown in green; actin and nuclei were stained with Phalloidin (red) and Hoechst 33342 (blue), respectively.

reported in literature with other organic and inorganic nanomaterials, due to the complex polarized nature of thick epithelial layers.[158,164] A concrete support

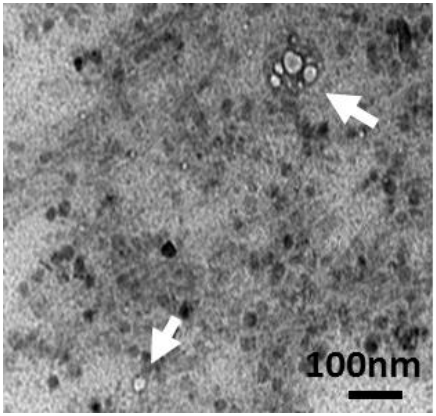

Figure 36 Transmission electron microscopy image of the basal medium of inserts chronically incubated (9 days) with NPs.

demonstrating the passage of NPs through the intestinal barrier model derived from the detection of NPs in the Bl medium by electron microscopy (Figure 36).

These results suggest that the transcytosis as the main mechanism of transport of NPs through the intestinal epithelium, and so that NPs were endocytosed via the apical membrane and exocytated from the basolateral one. Despite PET NPs did not produce short-term toxic effects on undifferentiated Caco-2 cells, the biodurability indicated by their stability in the lysosomal-like fluid also suggests their potential long-term effects. In addition, because of their ability to overcome the body barriers there is the risk that NPs can arrive to the blood stream accumulating into the organism.

Conclusions

The incessant development of technologies implies the emergence of unknown risks, as in the case of plastic pollution. The lack of knowledge of its destiny at the end of use, of the effects on the environment and on health, requires the focus of scientific efforts and the development of new experimental protocols. This need is further amplified in the case of NPs for which there are no technologies for detection and removal, nor is there any knowledge the effects to the human health. Designing the development of technologies to remove NPs from the aqueous environment requires a strong basic knowledge of the pollutant itself, and the first step

is the production of a realistic NPs model. In this regard as presented in this chapter, a model that faithfully mimics a real NPs sample has been developed through laser ablation in water, by choosing a top-down rather than a bottom-up approach, with the advantage of producing nanoparticles without impurities, chemical precursors, and their byproducts. Physicochemical analysis validated the PET NPs model, since, in accordance to what has been observed in UV degraded PET plastics in the environment, organic acid groups decorate the surface of laser ablated NPs. The size of the NPs assessed at the various synthesis steps, after filtration, remain in the order of 100 nm, as illustrated in table 6.

Table 6. Size of NPs (Z-average) at the main experimental steps.

Samples	Mean diameter
As synthesized NPs	571.6±79.1 nm
NPs after filtration	109.5±13.3 nm
NPs-soft corona complex	155.4±5.8 nm
Fluorescein-NPs complex	147.4±3.1 nm

Working in a controlled environment, it was possible to define which conditions interfere with the stability of the

NPs, fundamental information to be able to predict the fate of these pollutants. The NPs dispersion showed long-term stability in various biological media. The small size and the stability of the NPs are two important factors, which increase the possibility of living organism exposure. Although many studies of toxicity and uptake have been performed to a wide variety of polymeric nanoparticles, only polystyrene has been used to model NPs and to investigate the effects to biological systems. Published data on polystyrene NP uptake have shown high variability mainly depending on the particles size, surface properties, and on the *in vitro* models adopted.[70,97,146,147] In order to clarify the biological fate of NPs, it is necessary to consider the importance of the NP composition, therefore all the extrapolation based on only polystyrene nanoparticle models have to be taken with caution. Thus, this study improved the knowledge on NPs behavior in complex biological media and offered a preliminary concept about the biological interaction of PET made NPs. Although the results obtained *in vitro* did not show any lethal or short-term toxic effects, the biopersistence and accumulation of NPs in addition to

their ability to interact with other contaminants requires further studies in the long-term and the application of omics approaches, as will be explained in the following chapter.

Chapter II

Interactions of Nanoplastics with water contaminants and their impact on cells

State of the art

(Nano-)Plastic as contaminant source and vector

Plastic fate and the impact on the ecosystem strictly depend on factors such as long-haul transport composition and persistence.[165] Although the problem of plastic pollution has been known for years, little is known about the chemical hazards that it entails. It is established that plastics may contain numerous chemical substances

derived from their production processes such as Antimony (Sb), Bisphenol A, phthalates and flame retardants, or from the interactions with other water pollutant substances present in the environment.[74,166–170] Degradation and breakdown of pristine plastics increase their exposed active surface area, and therefore the possibility to interact with the surrounding pollutants. Nevertheless, to date, little is known about the capability of NPs to act as vectors of contaminants and the relation between the plastic properties and the nature of the contaminants.[171] For example, rubbery polymer such as PE shows a greater affinity for contaminants while, conversely, PET and PVC exhibit lower sorption capacities.[74] As for MPs, NPs due to their high surface to volume ratio, the surface hydrophobicity and the exposure of active moieties formed during degradation (e.g. carboxyl residues), may have a good chemical affinity with a great range of environmental legacy contaminants. There are several evidences, in particular for MPs, about their interactions with hydrophobic organic chemicals such as persistent organic pollutants (POPs), polychlorinated biphenyls (PCBs) and polycyclic

aromatic hydrocarbons (PAHs) but also with inorganic hazardous substances such as heavy metal ions.[172–177] As for other nanomaterials sorption of organic contaminants may occur through hydrophobic, π-π stacking, and/or hydrogen bonding interactions, while electrostatic interactions and surface complexation can lead to the sorption of heavy metal ions.[178]

The nanometric size scale of the NPs strongly influences the biological and environmental impacts of these pollutants since in addition to the higher possibility of the occurrence of interactions and uptake by cells and microorganisms, NPs have higher exchange rates of the contaminants adsorbed on their substrate, due to the short diffusion path length and the large surface area.[171,179]

Plastic-interacting contaminants

In oceans and near coastal areas has been estimated the presence of PCBs, PAHs and organochlorine pesticides,

with concentrations ranging from 0.1 to 10,000 ng/g.[92] Contaminants present in the seawater may be adsorbed on the plastic surface and concentrate up to the order of 10^6. Inorganic contaminants present in the aquatic environment, such as metal ions, can also be adsorbed to plastics.[167,180] The type of metal ions adsorbed to plastic depend significantly on the type of the aquatic environment e.g. freshwater or seawater and on the time the plastic is dispersed in the environment.[181] In fact, aged plastics, exposed to sun light, adsorb 30 times more metal ions such as copper and zinc from seawater compared to their virgin counterparts.[182]

The chemicals found in plastic marine litter can be classified in four categories of origin:

- Additives added during the plastic production process (flame retardants, plasticizers and pigments).
- Contaminants from manufacture processes (monomers, BPA, etc.).
- Organic chemicals adsorbed from environmental pollution.
- Inorganic chemicals adsorbed from environmental pollution.

While the first two classes are easily detectable in plastic items and therefore well known, there is a growing concern to the complex mixture of chemical substances present in the environmental matrices. Particularly legacy contaminants such as many pesticides, drugs and heavy metal ions are considered chemical stressors because of their long-term effect. Moreover, all metal ions, PCBs, and the lipophilic pesticides tend to bioaccumulate and biomagnify in organisms, as will be discussed in the next paragraph, entering in the food chain.[17]

In this thesis, three model pollutants, showing high persistence in the marine environment and of strong interest both from the environmental and health effects point of view, have been chosen: Glyphosate representative of the pesticide class, Levofloxacin as a model drug pollutant, and mercury ions representative of the class of the heavy metal ions.

Glyphosate, a phosphoric amino derivative of glycine (Figure 37), is the most used herbicide in the world. Entered in the global market during the 70s, Glyphosate rapidly spread due to its systemic and non-selective

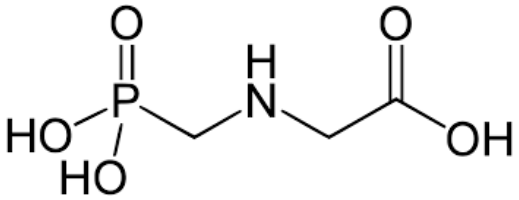

Figure 37. Glyphosate molecular structure

action against vegetable organisms and to the use of Glyphosate-resistant Genetically Modified Organism (GMO). Because of its widespread diffusion into the environment, it was at the centre of an important scientific debate about its adverse effects on health and environment. In fact, in 2015 the International Agency for Research on Cancer classified the substance as "likely carcinogenic" to humans. The degradation of Glyphosate in the environment is very limited and its half-life in water can last up to 91 days.[183,184] It is important to consider that in contact with water, Glyphosate quickly transforms into its main metabolite, aminophosphonic acid (AMPA), which maintains all the toxic characteristics of its precursor and is even more persistent, with a half-life of 240 days.[185] Glyphosate and AMPA were detected in 69% of water samples from aquatic ecosystems in the United States, while studies in Australia and Canada have shown

a concentration over 40 µg/L in the water systems.[186] Glyphosate can contaminate surface waters or may penetrate the soil reaching thus the groundwater, and therefore may significantly affect the quality of the drinking water.

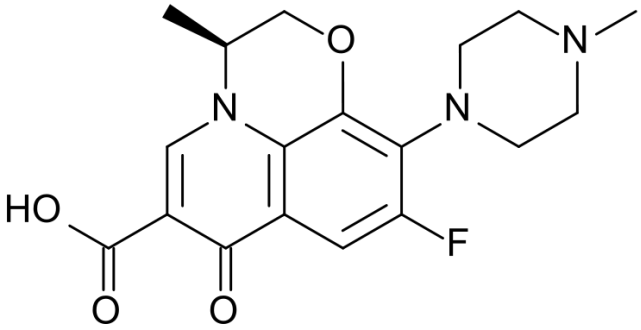

Figure 38. Levofloxacin molecular structure.

Levofloxacin or Levaquin, the S isomer of Ofloxacin, is an antibiotic belonging to the more recent generation of fluoroquinolones (Figure 38). It is widely used in human and veterinary therapies as an antibacterial agent with a broad spectrum of activity against gram-positive and gram-negative bacteria in and for respiratory diseases.[187,188] This newer class Quinolones displayed considerably improved activity against bacterial topoisomerase IV and DNA gyrase, greater penetration into Gram-positive organisms, and enhanced pharmacokinetics and

pharmacodynamics.[189] Levofloxacin, due to its stable carbostyril core structure, undergoes limited physical and metabolic changes after administration and is primarily excreted as unchanged drug in the urine.[188,190] After 48 hours of oral administration in humans, approximately 87% of the administered drug was recovered without any modification in the urine.[191] Excessive use of antibiotics in general and in veterinary medicine has resulted in the contamination of the natural environment. In fact, in veterinary medicine only 20% of fluoroquinolones are administered for the treatment of infections, about 80% is administered for preventive use.[192] Owing to its toxic effects on microbial activity, Levofloxacin is often poorly biodegradable in biological treatment systems, being detected as emerging contaminant in aqueous environments.[193] In Italy a level of 600 ng/L of Levofloxacin was detected in effluents of urban sewage treatment plants.[193]

Mercury (Hg) is a heavy metal belonging to the transition element series and is one of the ten most hazardous chemicals to the human health, according to the World's Health Organization (WHO) (Figure 39).[194] This

Figure 39. Mercury element properties, and an image of its liquid state.

environmental pollutant is known for its potent toxicity towards the living organisms. As it accumulates in the food chain, Hg directly threatens the public health via damaging the kidney, liver, brain, lungs, and the cardiovascular system. [195,196] It originates from several sources such as volcanic activities, industrial wastes, mining and combustion of fossil fuels.[197] Due to its volatile nature and long atmospheric persistence, Hg is ubiquitous and therefore a serious hazard for human society. In particular, the Hg^{2+} ion is one of the largest mercuric pollutant in environmental water. In oceanic waters, Hg mainly occurs as Hg^0, Hg^{2+}, MethylHg, and DimehyltHg.[198] Hg concentrations vary according to the type of water environment and is of a range of 1 ng/L in the groundwater, 10-100 ng/L in the drinking water in some European and American countries and 20300 ng/L

in waters around abandoned cinnabar mines. [196,199,200] The risk associated to Hg based pollutants is further increased by bacteria activity in lakes, streams, and ocean sediments which convert Hg from elemental into organic form compounds such as MethylHg. MethylHg is hazardous to organisms and human health as it is associated with the destruction of mitochondria and with nervous system failures.[196,201–203] Moreover a significant interaction between Hg and plastic fragments was found.[204]

Trophic transfer of plastic particles and biomagnification of pollutants

The importance of monitoring emerging contaminants even at low concentrations is due to their persistence. The affinity of contaminants for the biological components such as proteins and lipids, can trigger the so-called bioaccumulation phenomenon. The bioaccumulation of

polluting substances can take place directly from the environment through the respiratory and tegumentary surfaces (bioconcentration), and/or through the trophic transfer by the ingestion of other living organisms in (biomagnification). Biomagnification is considered a major mechanism for the accumulation of contaminants in organisms of higher trophic levels (Figure 40).[205] During this process the chemical concentration of a compound in an organism is higher than that taken directly by diet, due to

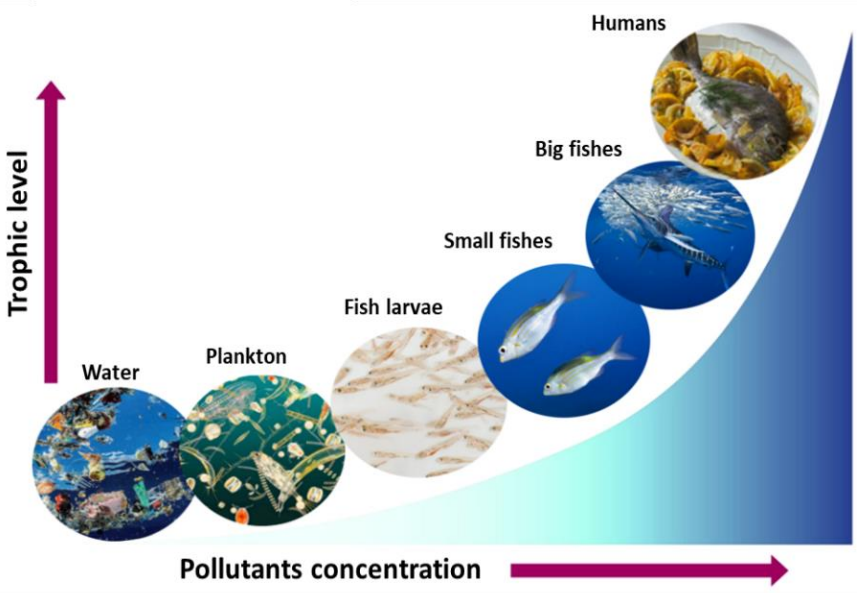

Figure 40. Trophic transfer and biomagnification of pollutants in a simplified marine food chain.

the dietary accumulation.[206] Plastics and the other contaminants species have been found at all trophic levels. The contaminants affect especially the zooplanktonic organisms at the bottom of the food chain, and they are biomagnified and accumulated through diet over the trophic chain. This process leads to an increase in concentration in living organisms up to even 1 million times than the surrounding media, leading to significant effects in top consumers such as humans.[165,207] Despite the lack of analytical detection methods that does not allow the detection of NPs in tissues and organs of organisms present in the environment, there are numerous data on the trophic transfer of plastic particles, which provide the evidence of the actual occurrence of this process of indirect ingestion of pollutants.[65,92] The transfer of MPs and NPs has been reported by studies in algae and zooplankton (lower trophic level organism) up to copepods, to pelagic shrimps, blue mussels, crabs and fishes.[102,208,209] In 2014, in a study of the NPs and MPs quantification in commercial products, Van Cauwenberghe and Janssen estimated the ingestion of about 11000 plastic fragments per person each year linked solely to the consumption of oysters

and farmed mussels.[210] In addition to the ingestion and the biomagnification of mere plastics in aquatic organisms, laboratory studies have demonstrated the risk of bioaccumulation of the substances adsorbed and transported on the plastic surface.[211,212] In fact, the environmental risk of plastic-related chemical contaminants is a consequence of aquatic organisms direct contact or ingestion of plastic particles with high concentrations of adsorbed chemicals, released from digestive tract into the tissues.[54] This risk is even higher for top predators, such as humans, and a correlation between consumption of MPs and accumulation of phthalates has been already observed in cetaceans.[165,213] As described previously the peculiar characteristics of NPs facilitate the mechanisms of transport of chemical contaminants and due to the predominance of Brownian motion which favours the colloidal stability improving the environmental dispersion and the availability to aquatic organisms, further increase the risks for exposed organisms health.[65,81,82] Thus, there is a growing concern to define an effective risk assessment of NPs and of their indirect impact as vector of other hazardous contaminants.[70,85]

Biological effects of NPs

According to the current knowledge, the ingestion of plastic may elicit negative outcomes on behaviour, fertility, hepatic function, immune response, and gene expression pattern, while lethal effects have been reported only at much higher concentrations compared to the environmental ones.[76,86–91] Severe developmental effects of NPs where observed in the early development of aquatic organism such as sea urchin embryos (Paracentrotus lividus) and medaka (Oryzias latipes).[65] Here NPs were adsorbed to the chorion of eggs and accumulated into the yolk and gallbladder during embryonic development but also in the gills, intestine, brain, testis, liver and blood, suggesting that NPs can pass the blood–brain barrier.[65] Studies on Daphnia using NPs as kairomones carriers suggested that NPs might interfere with the *chemical communication* among species, that causes behavioural disturbances in finding a mate or food, or in the avoidance of predators, indirectly affecting the food chain.[90] In the

studies of exposure and absorption of NPs by food (intestinal) route, highly variable uptakes of NPs, ranging from 1.5 to 10% of the total amount, have been reported. Results depending on various aspect such as the *in vitro* intestinal models, the size of NPs and their surface chemistry.[70] Compared to the MPs, the smaller size of NPs (comparable to that of biological components and proteins), associated with their surface characteristics (i.e., surface chemistry and surface energy), may favour their interactions with a wide range of molecules, such as proteins, lipids, carbohydrates, nucleic acids, ions, and water present in the gastro intestinal tract constituting complex corona and influencing the passage through cellular membrane.[56,70,95,96] *In vitro,* uptake and clearance seem to be the factors mainly influenced by the nanometric dimension. Interaction with lipid membranes, studied using coarse-grained molecular simulations, demonstrated that NPs may easily permeate into cellular membranes. Polymer chains may induce changes in the membrane structure, affecting cell physiology by alteration the molecular diffusion.[214] Perturbing cell membranes and endocytosis pathways, NPs could remain in the organism

longer than MPs.[214–216] This is reflected on clearance and on the uptake, indeed as observed in previous chapter and for diverse types of organic and inorganic particles, the smaller size favours the items passage through the intestinal barrier.[97,98] In a direct comparison of the movement of engineered carboxylated polystyrene NPs across a coculture of Caco-2 (enterocyte-like), HT29-MTX (goblet cell-like) and Raji B (M cell-like) cells, it was found that the transport of 50 nm particles was about two orders of magnitude faster than that of 200 nm particles.[97] In fact, contrarily to NPs, transport of MPs was temperature and M cells dependent.[97] In a real condition the intestinal lumen environment could greatly alter the nature of the NPs, and hence absorption may be affected. Human lung carcinoma cells (A549) uptake 40–50nm PS particles accumulating and concentrating those irreversible in the cytoplasm.[215] Other studies based on the use of polystyrene nanospheres have demonstrated possible acute toxicity, inflammation, up-regulation of IL-6 and IL-8 interleukins, up to lethal outcomes for macrophages (RAW 264.7) and epithelial cells (BEAS2B).[217,218] Given the unrealistic conditions and the high concentrations of NPs applied in

these *in vitro* studies, the results should be evaluated with accuracy even with respect to the observations found in this thesis on Caco-2 intestinal epithelium cells. Due to their limitations, conventional *in vitro* methods do not allow long-term assessments and chronical exposure evaluations, therefore, as described in the following paragraph, to answer this need it is possible to rely on omics tools.

Omics

'Omic' technologies adopt a holistic view of the molecules that translate into cell structures, functions, and dynamics of the organisms.[219] They are aimed primarily at the universal characterization and quantification of pools of genes (genomics), mRNA (transcriptomics), proteins (proteomics) and metabolites (metabolomics) in a specific biological sample impartially.[220] The set of data derived from this approach is integrated into the so-called systems biology (Figure 41).[219] The high-throughput of data

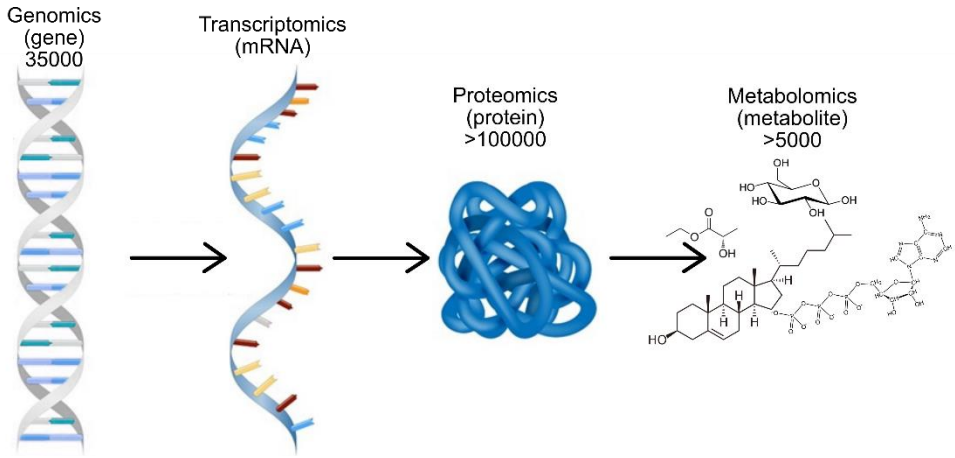

Figure 41. Flowchart of omic science and approximate amount of information at every step.

produced through the different types of omics studies allows to provide a huge volume of information about the molecular dynamics underlying a specific cellular behavior or process.[220] Proteomics and metabolomics are considered more dynamic fields than genomics as they can vary in response to environmental conditions.[221] Metabolomics has been increasingly applied to investigate prokaryotic and eukaryotic systems since the late 1990s, but producing a single analytical platform is a difficult task.[222] In fact, metabolites represent a more diverse set of chemical diversity than proteins (20 amino acids) or DNA (4 nucleotides) and therefore provide wide variations and

combinations in chemical and physical properties.[223] Although complete coverage of all cellular metabolites would require the use of various techniques, metabolomics, unlike genomics, effectively describe a phenotype within a given biological sample.[224] Proteomics also offers an accurate perspective on cell phenotype and response to stimuli. Such analysis allows to identify the expressed proteins, the interaction between group of proteins, their location and quantity, enabling a systematic overview of the expression profiles.[225] The main advantages are the high sensitivity and resolution but the accuracy of quantifications is still weak with respect to the common labeling-based methods.[226] Metabolomics and proteomics techniques are becoming an indispensable tool for short-term toxicology studies in vitro as they allow to appreciate the minimal variations in cell physiology and to predict chronic effects not obtainable with conventional methodologies.

Materials and methods

PET NPs interaction with contaminants

All the NPs used in this section, even the fluorescent ones, have been prepared and characterized (DLS, Z-Pot) as described in chapter 1. A final concentration of 300 µg/mL of PET NPs have been incubated for 48 hours under stirring condition at room temperature with aqueous solution of Levofloxacin 40 µg/mL (137µM) (Sigma-Aldrich) and Glyphosate 40 µg/mL (148µM) (Sigma-Aldrich) and of Hg^{2+} 25 µg/mL (ppm) ($HgCl_2$ 99.999%, Sigma-Aldrich) prepared in MilliQ water.

Isothermal Titration Calorimetry

The Isothermal Titration Calorimetry was used to study the interaction between the NPs and the mercury ions, the levofloxacin and the glyphosate. An Affinity-ITC instrument (TA instruments, Utah, US) was used to measure the binding thermodynamics. All the tests were done in MilliQ water in order to avoid any possible interference by the buffer. All solutions were degassed prior to the titrations. The solution of contaminant was loaded into the syringe and titrated into the sample cell, which contained 300 µl of NPs at a concentration of 100 µg/mL. At every step 2.5 µl of contaminants were injected: Levofloxacin [0.5 mM], Glyphosate [1 mM], Hg [0.1 mM]. In each titration, the reference cell contained water. The time delay between each injection was 200 sec to ensure the baseline returned to normal, and the RPM (rotations per minute) was set to 70. The blanks were done injecting the interactors in MilliQ water without NPs. Data analysis was

performed using the NanoAnalyze software (TA instruments, Utah, USA). The enthalpy of dilution of the different molecules were subtracted from the raw data.

Inductive Coupled Plasma-Optical Emission Spectroscopy.

Inductive Coupled Plasma-Optical Emission Spectroscopy (ICP-OES) was used to determine the Hg^{2+} concentration with an iCAP 6500 spectrometer (Thermo). 300 µg of NPs were collected a digested by a microwave digestion system (MARS Xpress, CEM) in 2.5 mL aqua regia ($1HNO_3$:3HCl) (Sigma-Aldrich). The solid degradation reaction was performed at 180° C for 15 minutes. Before the analysis, the samples were diluted with MilliQ water up to 25 mL and filtered through PTFE syringe filters (15 mm, pore size 0.45 µm, Sartorius).

Monodimensional Proton Nuclear

Magnetic Resonance (1D ^{1}H NMR)

All the NMR experiments were performed at 298 K on a Bruker Ultrashield Plus FT-NMR 600 MHz ADVANCE III equipped with a Cryoprobe^{TM} QCI 1H/19F–13C/15N–D and with a SampleJet^{TM} autosampler with temperature control. All the NMR experiments were conducted in collaboration with D3 Pharma Chemistry group.

NMR analysis of NPs-contaminants interaction

The samples in NMR tubes have been prepared by adding to 173 µl of NPs (345 µg/mL), 2 µl MetOH, and 5 µl of a specific pollutant: Levofloxacin (40 µg/mL) (Sigma-Aldrich) or Glyphosate (40 µg/mL) (Sigma-Aldrich). To analyze the sample, 20 µl of D_2O, for the lock signal, and 200 µM 3-(trimethylsilyl) propanoic acid (TSP) were added in 3 mm Bruker NMR tubes, up to a final volume of 200 µL. A 1D ^{1}H NMR spectrum was recorded for each sample just after preparation (t0), after 2 days (t1) and 4 days (t2) of mixing at 500 rpm at room temperature. The water suppression was obtained using the standard NOESY (nuclear Overhauser effect spectroscopy) presat

Bruker pulse sequence, with 64 k data points, a spectral width of 20 ppm, 2024 scans, an acquisition time of 2.7 s, a relaxation delay (d1) of 4 s and a mixing time of 100 µs. The data were multiplied with an exponential window function with 0.3 Hz line broadening prior to Fourier transformation. The ^{1}H NMR chemical shifts are referenced to the TSP signal.

Metabolomic NMR measurements of Media

2mL of the cell culture media previously collected from every treated sample (details in the next section) were thawed on ice, pelleted at 15000g and 4°C for 5 minutes; 400 µL of the supernatant were transferred into 5mm NMR Bruker tubes. To each tube were added 100 µL of 500 mM Phosphate buffer pH 7.4, 5 mM TSP and 0.2% SodiumAzide in D_2O, to a final concentration of 100 µM Phosphate buffer pH 7.4, 1 mM TSP and 0.04% SodiumAzide 10% D_2O. For each sample, the probe was automatically locked, tuned, matched, shimmed and the stability of samples temperature checked for 5 minutes before the acquisition. 1D ^{1}H spin−echo Carr−Purcell−Meiboom−Gill (CPMG) spectra were

acquired to suppress the water and the large NMR signals from macromolecules, such as proteins and other substances with short T_2 values.[227] We used a total echo time to 80 ms consisting of 128 repetitions with a τ_e time of 300 µs and a 180° pulse of approximately 27 µs. For each spectrum, a total of 256 scans were collected into 64k data points using an acquisition time of 2.7 s and a d1 of 4 s. Spectra were Fourier transformed and phase corrected, applying a line broadening of 0.3 Hz and zerofilling to 128 k points and were baseline corrected by applying a polynomial baseline correction.

Experimental conditions for cell culture and toxicity assessment

Caco-2 human intestinal epithelial cells and differentiated THP-1 cells were used as model to study their interaction with the NPs and the eventual cytotoxicity. The Caco-2 cells were cultured as described in the previous chapter.

THP-1 were grown in RPMI-1640 (Thermo Fisher Scientific) supplemented with 10% FBS (Thermo Fisher Scientific), 1% Penicillin-Streptomycin (Sigma-Aldrich) and 0.05 mM 2-Mercaptoethanol (Gibco-Thermo Fisher Scientific) in a 5% CO2 humidified atmosphere at 37 °C. THP-1 cells were differentiated in macrophages by exposure to 50 ng/mL phorbol-12-myristate 13-acetate (PMA, Sigma-Aldrich) for 3 days. Subsequently, the cells were re-feeded with fresh medium without PMA for 2 days to allow cell recovery. Cell differentiation was verified by evaluating cell adhesion and spreading under an optical microscope. Cryopreserved stocks were sub-cultured twice before the experiments. To test the toxicity of the NPs, cells were seeded in 96-well plates at a concentration of 1 x 10^4 cells/well. Following 3 days of culture, the cells were exposed to a concentration of 30 μg/mL of NPs, and studied after 24, 48 and 96 hours.

The effect of the NPs on Caco-2 Cell Viability was studied by MTS assay (CellTiter 96® AQueous One Solution Cell Proliferation Assay from Promega) while ROS production was measured by using DCFDA (Invitrogen). The methodologies followed for both cases are widely described in

chapter 1.

In order to perform metabolomic and proteomic studies cells were grown in 6 well plates at a concentration of 1 x 10^6 cells/well. After 2 days of exposure to the various treatments (NPs, contaminants, NPs-contaminants, control media) the media were removed and processed for the NMR analysis, while the cells have been frozen in liquid nitrogen and stored at -80°C for further studies of lipidomic and metabolomic of the intracellular metabolites.

Confocal microscopy

Caco-2 and THP-1 cells (5 x 10^4) grown on glass coverslips of 12mm diameter were incubated for 96 hours with NPs and then fixed with 4% paraformaldehyde for 15 min at room temperature, permeabilized with 0.01% Triton X100 for 5 min and blocked with 0.5% bovine serum albumin in PBS for 20 min. They were then stained with 0.1 nM Alexa FluorTM 594 Phalloidin for 30 min and Hoechst 33342 (Thermo Fisher Scientific) at a concentration of 5 µg/mL for 5 min, to localize actin microfilaments and cell

nuclei, respectively. To investigate the subcellular localization, living Caco-2 cells and macrophages exposed to fluorescein-NPs (10 μg/mL) for 96 hours were incubated for 1 hour at 37°C with LysoTracker™ Red DND-99 (Thermo Fisher Scientific) in DMEM or RPMI 1640 at a concentration of 75nM. Cells were then washed with HBSS and incubated with Hoechst 33342 (Thermo Fisher Scientific) at a concentration of 5 μg/mL for 5 minutes to localize cell nuclei. Image acquisition was performed using a confocal microscope (Leica TCS-SP5) at 60x magnification, with 405, 488 and 561 nm excitation laser wavelengths and a resolution of 1024×1024 pixels. Image analysis was performed using ImageJ software.

Metabolomic analysis

For the metabolomics analysis was used Workflow4Metabolomics W4M 3.0 release (http://workflow4metabolomics.org) an online free infrastructure for metabolomics built on the Galaxy environment which allows to build and run data analysis.

The workflows include spectra processing, alignment, bucketing and normalization; the statistical package include multivariate and univariate analysis.[228] A preliminary assignation of ^{1}H-NMR peaks was obtained using the NMR software SMA (Simple Mixtures Analysis) (http://mestrelab.com/software/mnova/sma) of Mestrelab and a library of about 50 common human metabolites.

Results and discussion

Characterization of NPs behavior in presence of contaminants

As discussed in the previous chapter, by associating the variations of D_H with the stability of the NPs it is possible to understand their behaviour even in complex media. Aggregation of nanoparticles is widely applied in chemical and biomolecular sensing as a sensitive and easy-to-visualize process to evaluate their interaction with other substances.[229] D_H changes with the coalescence and

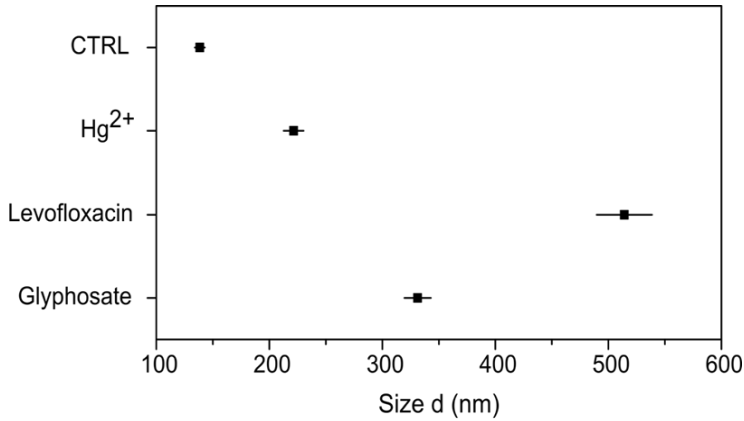

Figure 42. DLS analysis (performed in intensity) of PET NPs at pH 7 before and after incubation in Hg^{2+}, Levofloxacin and Glyphosate.

clusterization of the NPs and depends on the alteration in the repulsive forces which are regulating the colloidal stability. In order to characterize the effect of contaminants on PET NPs, 300 µg/mL of particles have been incubated in aqueous solution of Levofloxacin (40 µg/mL), Glyphosate (40 µg/mL) and of Hg^{2+} (25 µg/mL). After 48 hours of contact time, NPs were pelleted by centrifugation, washed twice, and resuspended in phosphate buffer 0.1 mM at pH 7. Subsequently the DLS analysis has been performed, and as shown in Figure 42, the D_H measured in intensity, is strongly affected by the presence of contaminants. Levofloxacin and Glyphosate induce the more evident alteration in the NP colloidal

stability, forming big clusters with sizes of 514±24 and 331±11 nm respectively. The presence of aromatic residues in the PET NP structure may be involved in the formation of interaction with the other organic compounds that induce the destabilization of the colloid and its consequent aggregation. Even Hg^{2+} with its positive charge induces the formation of NP clusters leading to D_H up to a size of 221±8 nm circa two times higher than that of the bare NPs (136±2 nm). As already reported for carboxylated PS, the colloids are destabilized by low concentrations of cations.[230]

Consistent with the DLS results, the Z-Pot measurements showed the change in the surface charge (Figure 43). In

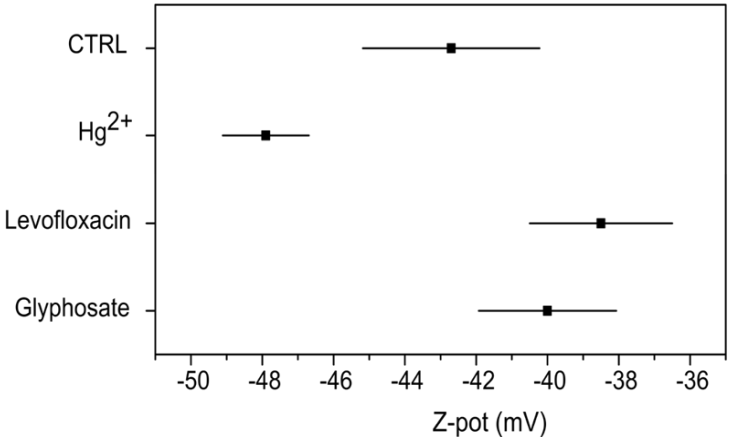

Figure 43. Z-Pot of PET NPs at pH 7 before and after incubation in Hg^{2+}, Levofloxacin and Glyphosate.

particular, the reduction of the Z-Pot in the NP sample pre-exposed to Hg^{2+} denotes an increase of the ionic concentration in the buffer. This may be due to the presence of the ions attached to the NP surface. In the case of Glyphosate and Levofloxacin the interaction of the NPs with the contaminants causes the shielding of the electrostatic charge on the surface of the NPs, with consequent reduction of the Z-Pot (in terms of absolute value). This induces the destabilization of the colloid and the formation of clusters observed by the increase in D_H.

Quantitative/qualitative characterization of contaminant-NP interactions

NPs are dynamic and complex objects whose behaviour is mainly influenced by the environment and external interactions. To understand such mechanisms, it is important to study NPs in their aqueous environment. Using NMR, it was possible to follow the evolution of NPs system in water, over time. After synthesis, NPs have been pelleted,

and resuspended in pure water. After the resuspension were immediately analysed by NMR in order to fix their status at the so-called time 0. As visible in Figure 44 the assignment of the peaks is a difficult task given the countless amount of signals present. Nevertheless, by simply comparing the spectra at various times, it is possible to glimpse important details. Observing the sample at time 0, many signals are large and defined, due to the limited mobility of the molecules attached to the surface of the NPs. Over time, after 2 days, the signals are more intense and defined. The organic fragments formed during the

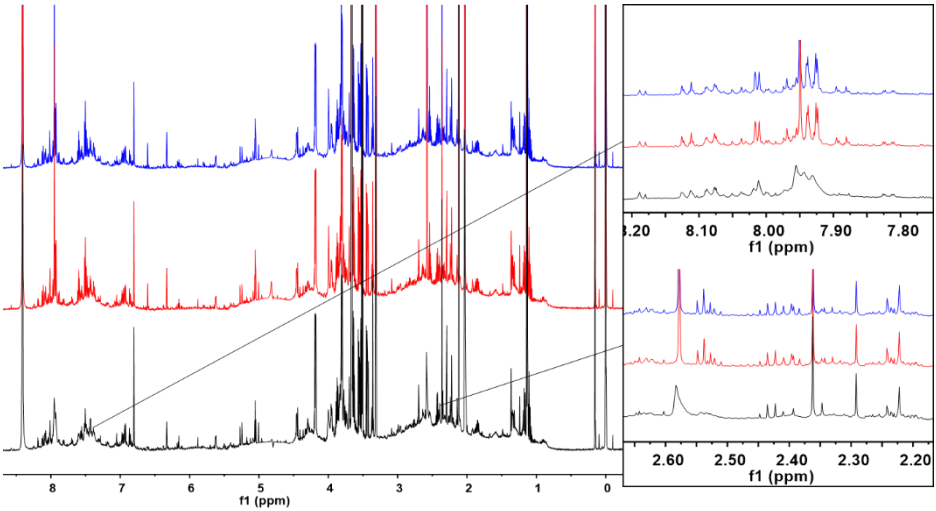

Figure 44. NMR analysis of pristine PET NPs in water at time 0 (black line) after 2 days (red line) and after 4 days (blue line). On the right some details showing the sharpening of the peaks, associated with the molecular mobility on the NP surface, during time.

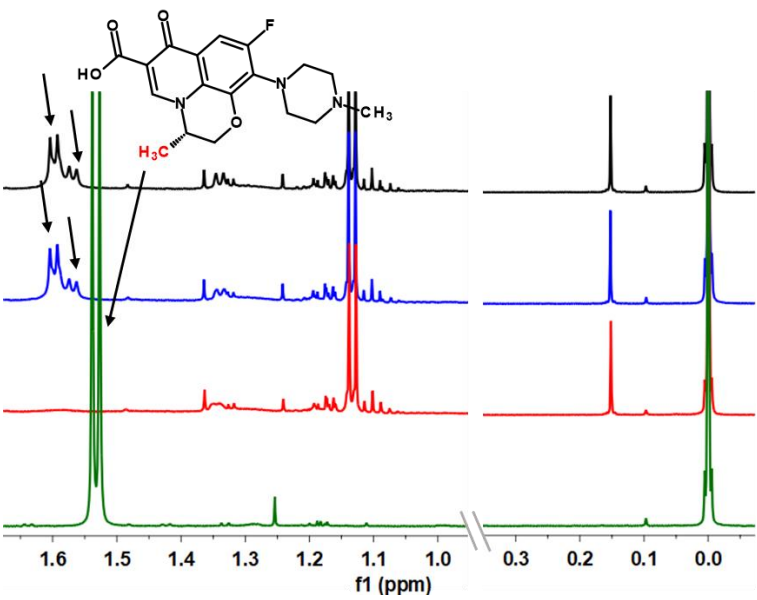

Figure 45. 1D ^{1}H noesy spectra expanded region of Levofloxacin (137 µM) in MilliQ (green), in presence of PET NPs at t0 (blue) and after 2 days of incubation (black). In red the spectrum of the bare PET NP. The arrow indicate the NMR signal assigned to Levofloxacin Methyl group.

ablation of the plastic that decorate the surface of the nanoparticles dissolve in solution and are freer to move and to respond to the magnetic stimulus of the NMR. After 4 days the situation does not change demonstrating the extreme stability of the MilliQ water NP system. Using the same approach, it was assessed and quantified the NP interaction with Levofloxacin and Glyphosate (Figure 45-46). By quantifying the full area of the peak referred to the only methyl group of Levofloxacin, a strong reduction

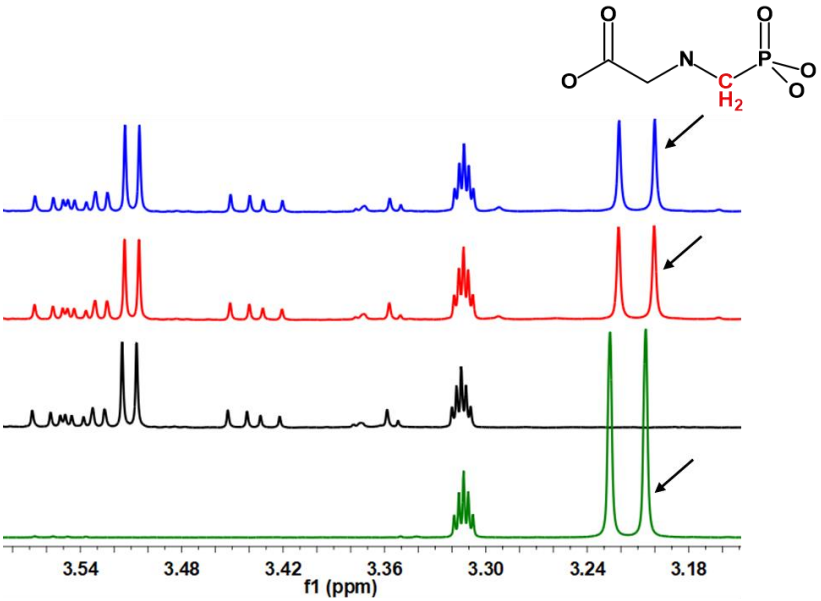

Figure 46. 1D ^{1}H noesy spectra expanded region of Glyphosate (148 µM) in MilliQ (green), in presence of PET NPs at t0 (red) and after 2 days of incubation (blue). In black the spectrum of the bare PET NP. The arrow indicate the NMR signal assigned to Glyphosate doublet of CH_2 group (J = 12.64 Hz).

in the concentration of the free molecule was observed compared to the incubation stock. This indicated a 0.036 g/g_{NP} binding of Levofloxacin. In addition to the observed decrease of the area, the strong line broadening and shift of the two doublets with respect to the reference, suggest that at least two further mild interactions are possible. Looking at Glyphosate spectra in presence of NPs it is observable the shift of the doublet and a strong decrease

of its intensity, confirming even in this case a binding among the molecule and the NPs. The amount of bound Glyphosate was evaluated to be 0.034 g/g_{NP}. Observing the temporal change of the spectra it emerges that the interaction of the NPs with the two contaminants is almost instantaneous. Both Glyphosate and Levofloxacin signals do not change prolonging the incubation time. Due to the technical limitations of NMR, Hg^{2+} was quantified by elemental analysis using ICP-OES. After eliminating the aspecific ligands, with three washing in MilliQ, the NPs were digested and analyzed. The results demonstrated that PET NPs can bind up to 0.014 g/g_{NP} of Hg^{2+} metal ions.

Established the effectiveness of PET NP binding of contaminants, ITC allowed to explore the type of mechanisms that regulates these interactions. ITC is a versatile and sensitive technique that allows the simultaneous determination of the thermodynamic parameters of an interaction.[231] Working with NPs there are some limitations mainly related to their concentration and colloidal stability which can influence the measurement of calorimetry.

The data presented were obtained by looking for the ideal condition, upon improving the signal to noise ratio. Given the great chemical variability of the surfaces of NPs, the possible interactions with the molecules of contaminants

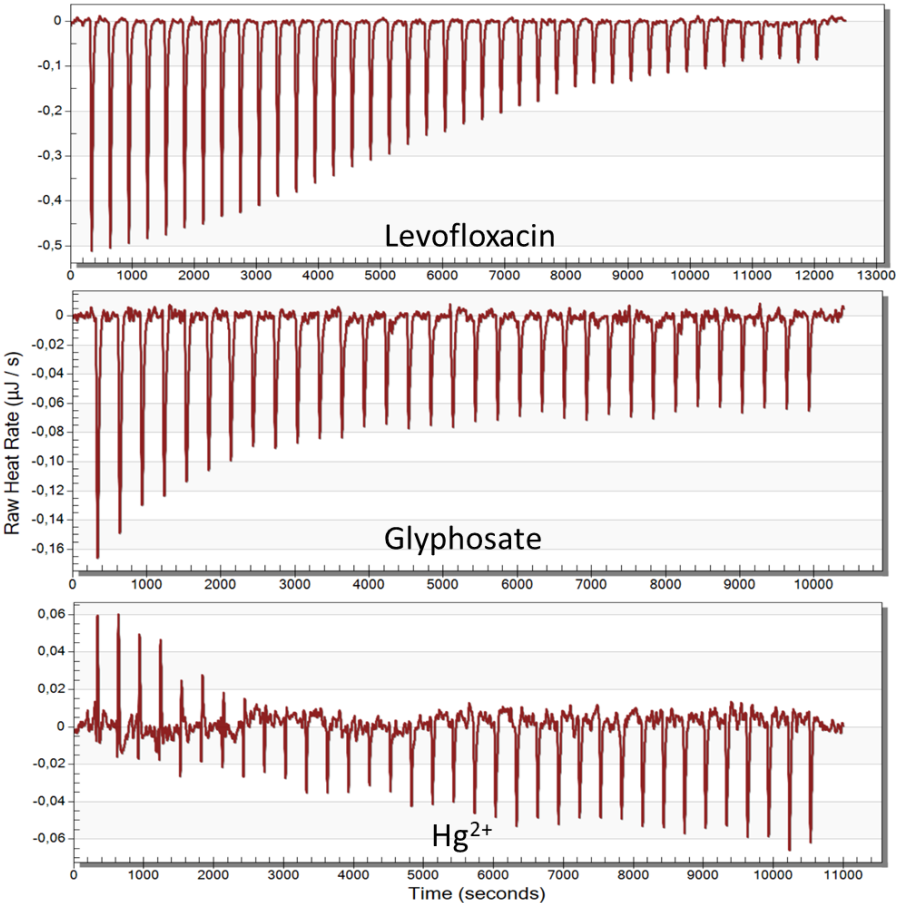

Figure 47. Thermogram showing the characteristic sequence of peaks corresponding to each ligand injection. Levofloxacin (0.5 mM), Glyphosate (1 mM) and Hg^{2+} (0.1) were injected in 100 µg/ml.

are not univocal. Therefore, the calculation of the thermodynamic parameters was obtained by fitting an independent site binding model. In Figure 47 are shown the ITC profiles in all cases. The curves for all three titrations had an exothermic peak profile. This indicates the establishment of interactions between the contaminants and NPs but could also be related to the homo-aggregation of the NPs themselves.[232] In this case, the results support what observed by NMR and ICP-OES, indeed the exothermic thermodynamic profile and the negative values of Gibbs free energy (ΔG) observed by the ITC measurements (Table 7, Figure 48) reveals that favourable interactions were established between the contaminants and the NPs in water. In particular, the resulting data demon-

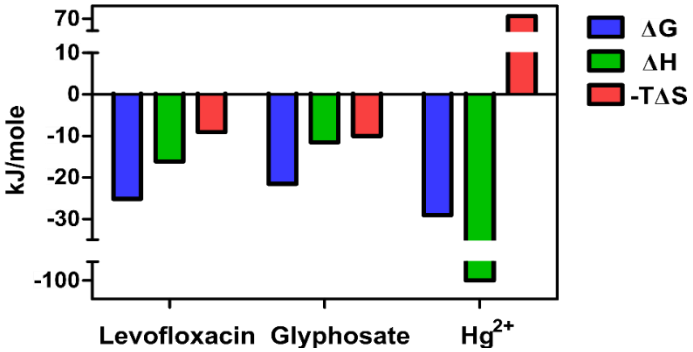

Figure 48. Thermodynamic binding profile for the contaminant-NPs interaction.

strated a favorable hydrogen and hydrophobic interaction for the two organic molecules. In the case of Hg^{2+}, although the negative value of Gibbs free energy indicates that the interactions are energetically favored, Entropy values higher than the Enthalpic ones cause a trend inversion. So high temperature, which means higher Entropy, decreases the binding of Hg^{2+}.

Table 7. ITC thermodynamic values of contaminants-NPs interaction.

	Levofloxacin	Glyphosate	Hg
ΔG (kJ/mol)	-25,13	-21,52	-29,05
ΔH (kJ/mol)	-16,10	-11,52	-100,00
-TΔS (kJ/mol)	-9,04	-10,00	70,95

Cytotoxicology of contaminants-NPs

In the chapter 1 the NP passage through the Caco-2 barrier was proved. This establishes the possibility that NPs can reach the bloodstream. Therefore, the study was also extended on macrophages (MF) that play the role of primary defence against external agents. First, as for Caco-

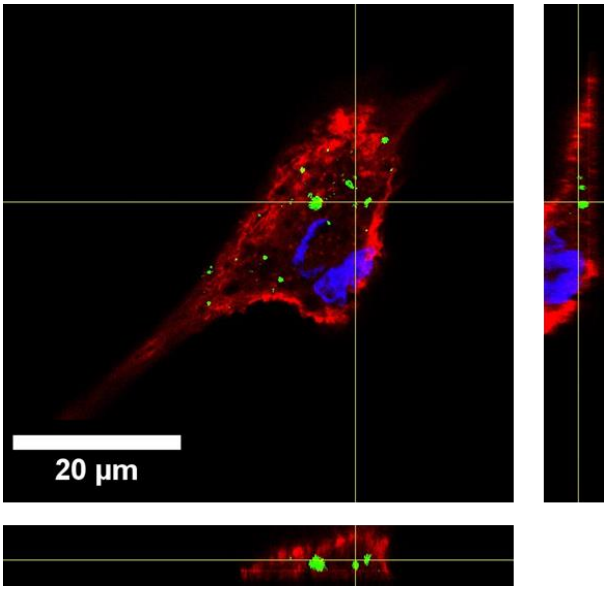

Figure 49. Confocal microscopy of MFs incubated for 24 h with fluorescent NPs. Hoechst/nuclei (blue), Phalloidin/actin (red), NPs (green). Lateral boxes represent z-stack projections along x-z and y-z axes.

2, it was evaluated the effective internalization of NPs. The MFs, differentiated from THP-1 cells, were treated with the NP functionalized with fluoresceinamine. After 24 hours, confocal microscopy has been performed as shown in Figure 49. The cytoskeleton staining allows to visualize the numerous pseudopodia typical of the MF and to define the intracellular space. As expected even in this case cells have internalized the NPs. Given their defensive role, MFs interact with particles through a wide

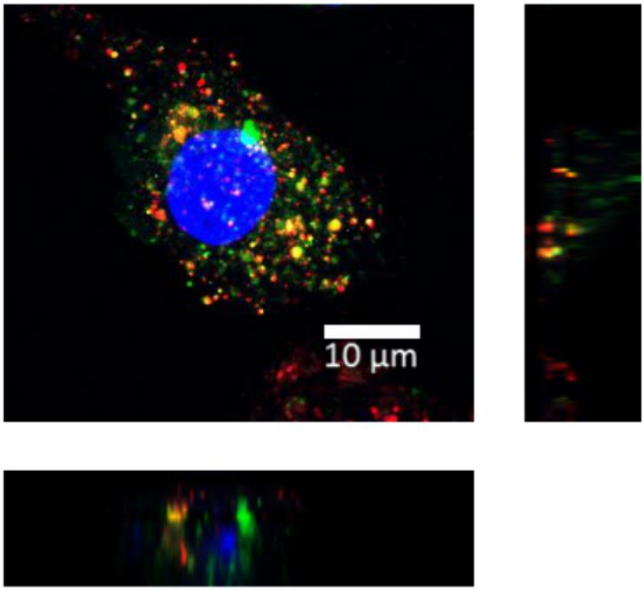

Figure 50. Confocal microscopy of MFs incubated for 24 h with fluorescent NPs. NPs co-localized with Lysotracker stained lysosomes. Hoechst 33342/nuclei (blue), Lysotracker (red), NPs (green). Lateral boxes represent z-stack projections along x-z and y-z axes.

variety of cell-surface receptors such as scavenger receptors, which facilitate phagocytosis that act as the main tool for the removal of external contaminants such as pathogenic microorganisms but also nanomaterials.[233] Using a pH-responsive endosomal tracer, the fluorescent NPs were colocalized with lysosomes as further confirm of NPs internalization and that endocytosis is the main cellular uptake pathway for NPs (Figure 50). Known the mechanisms of internalization of NPs are similar for MF

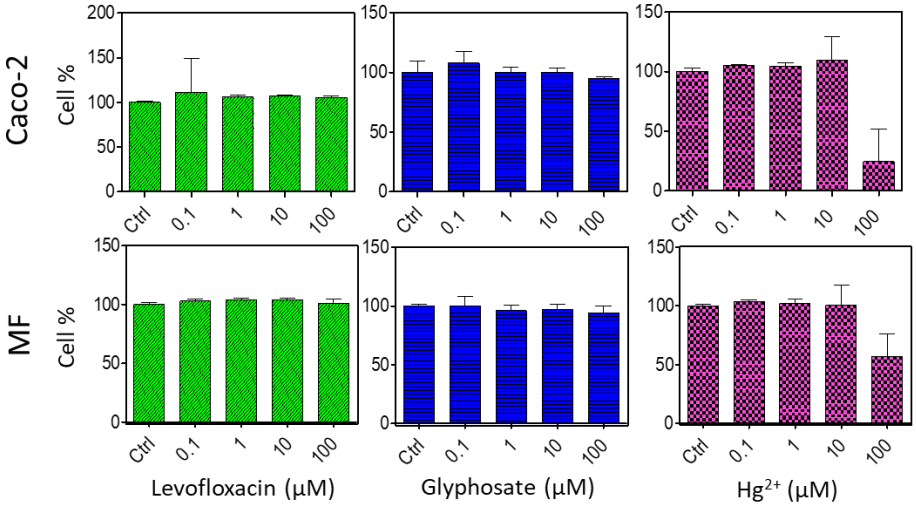

Figure 51. Viability of Caco-2 cells and MFs exposed to different concentrations of Levofloxacin, Glyphosate and Hg^{2+} for 96 h.

and Caco-2 cells, cytotoxic effect of pollutants have been characterized studying first the cell viability (Figure 51). The MTS assay showed a reduction of the cell viability only at high Hg^{2+} concentrations while no response was

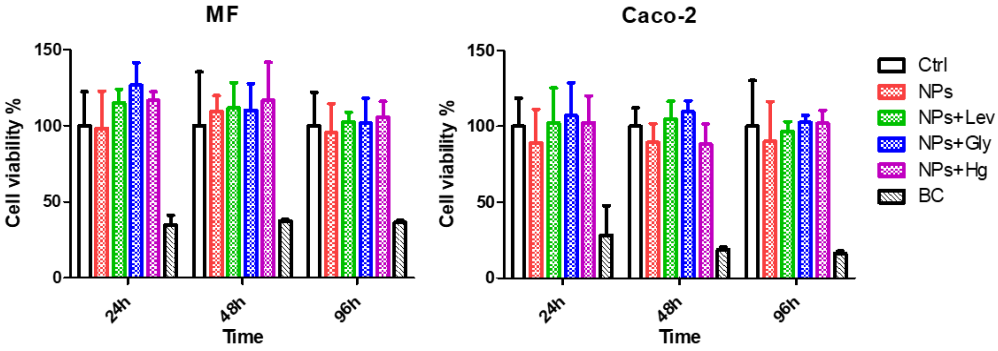

Figure 52. Viability of MFs and Caco-2 exposed up to 96 h to 30 µg/ml of NPs in combination with the three contaminants.

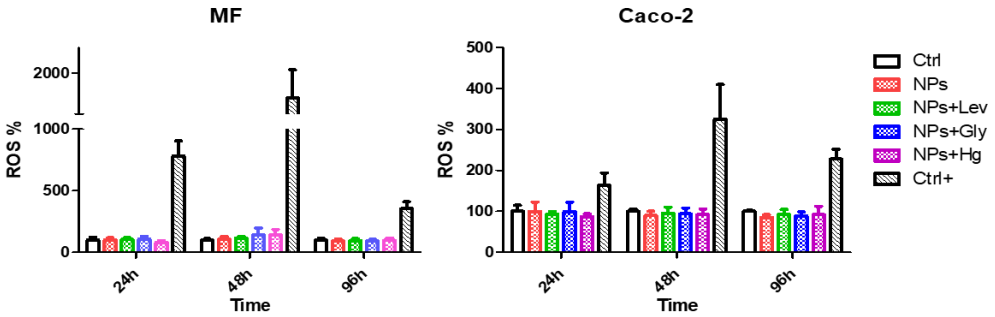

Figure 53. ROS production by MFs and Caco-2 exposed up to 96 h to 30 µg/ml of NPs in combination with the three contaminants. *Tert*-butyl hydroperoxide (TBHP) (100 µM) was used as positive control.

observed in presence of Levofloxacin and Glyphosate. The total absence of effects on cell viability was observed also treating cells with the contaminant-NP complexes (Figure 52). In the same way, the NPs, even in association with the contaminants, do not trigger oxidative events, keeping ROS levels close to the untreated control (Figure 53).

Metabolomic analysis

The use of conventional tests such as MTS and ROS did not show any significant response of the NPs treated

cells. In the absence of acute toxicity, *in vitro*, it is difficult to study the chronic effects triggered by stress. Nonetheless, the entrance of NPs in the endosomal cell pathway in addition to their biopersistence and accumulation must result in alterations, even small, of cell physiology and trophism. Metabolomics is the ideal strategy to address this toxicology task.[234] It represents a powerful tool for collecting several mechanistic information. As little variation of the basal cellular metabolism may induce long term effects, and this tool could be a good preliminary way *in vitro*, to preview the chronical impact of nanomaterials.[219,233]

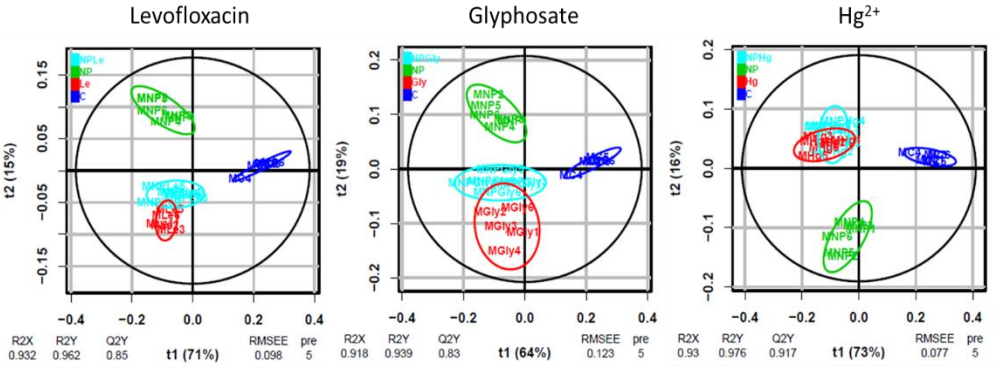

Figure 54. PLS-DA scores plots for Caco-2 control cells (blue), NPs (green) treated cells, contaminants (red) treated cells and contaminant-NPs (cyan) complex treated. The analysis was performed after 48 h of incubation time. The 95% confidence ellipses are displayed for each group.

Preliminary results of the analysis on the Caco-2 and MF culture media are shown in figure 54- 55. The Partial least-squares discriminant analysis (PLS-DA) of metabolomics data was performed on the four groups of treatment: the untreated control cells (blue), the cells treated with NPs (green), cells treated with the contaminants (red) and those treated with the complex contaminant-NPs (cyan). Interestingly, both in Caco-2 and in MF cells, a clear distinction of the treatment classes has been observed. A strong similarity between the classes treated with the contaminants and those treated with the contaminant-NPs complexes can be observed in Caco-2 cells. This is in line with expectations. In fact, as demonstrated

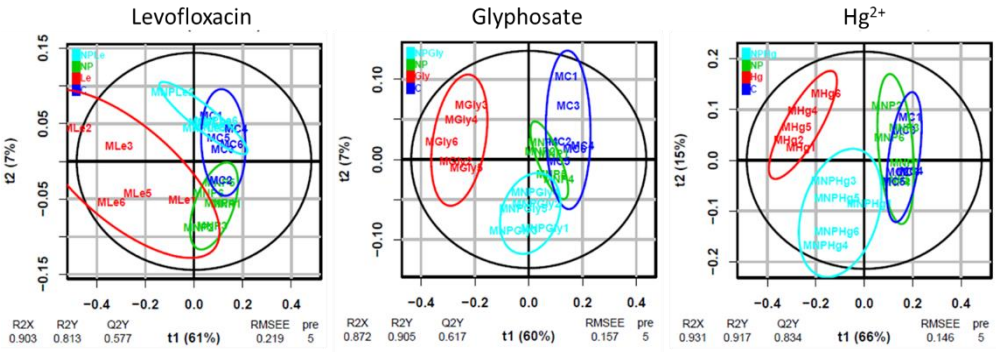

Figure 55. PLS-DA scores plots for MF control cells (blue), NPs (green) treated cells, contaminants (red) treated cells and contaminant-NPs (cyan) complex treated. The analysis was performed after 48 h of incubation time. The 95% confidence ellipses are displayed for each group.

by the presented interaction and binding studies, PET NPs are able to interact and therefore to transport other pollutants, modifying their chemical identity and therefore their impact on organisms.

Changing the cell model such evidence is not easily found. In fact, apparently, the metabolic response of MFs to the contaminant complexes-NPs differs from that to free contaminants, but the metabolic profile of untreated and NPs-treated cells appeared to differ less. The Levofloxacin treatment causes a high variability of responses with respect to the other groups, however it maintains its identity and remains well distinguishable. The major differences compared to Caco-2 are evidenced in the response to the contaminant-NP complexes. The PLS analysis confirms the diversity of the metabolic profile of the cells treated with the complex compared to the control groups, NPs and contaminants. This result could indicate a synergistic action given by the association of the contaminants to the PET NPs that act as carriers.

Associating the univariate analysis performed with

Workflow4Metabolomics W4M 3.0 to a SMA (Simple Mixtures Analysis) a preliminary peeks assignation and characterization was carried out. In table 8 the main buckets variations were associated to their specific metabolite

Table 8. Univariate analysis of Caco-2 (blue *) and MF (red *) significant metabolites.

Metabolite	Buckets	Hg/C	Hg/NP	Hg/NPHg	NPHg/C	NPHg/NP	NP/C	Le/C	Le/NP	Le/NPLe	NPLe/C	NPLe/NP	NP/C	Gly/C	Gly/NP	Gly/NPGly	NPGly/C	NPGly/NP	NP/C
Formate	8,46	* *			*	*	* *	*	*		* *	*	* *	*	*		*	*	* *
Phenylalanine	7,45	* *	*	*	*	*		* *	* *	*	* *			* *	*	*	*		
Tyrosine	7,177	* *	* *	*	*	*		*			*			* *	* *	* *			*
Histidine	6,9	* *	*		*	*		*			*			* *	* *		*		
Glucose	5,25	* *	*		* *	*	*	* *			*	*	*	* *	* *	*	*		*
Lactate	4,13	* *	*		* *	*	*	* *	*	*	*		*	* *	*	*	* *		*
Myoinositol	4,05	* *	*	*	*	*	*	* *	*	*	*		*				*		*
Creatine	3,9	* *	*		*		*	* *	*	*	*	*	*	* *	* *		*		*
Glycine	3,5	* *	*		* *	*	*	* *			*	*	*	* *			*		*
Taurine	3,41	* *	*	*	* *	*	*	* *	*	*	*		*	* *	*		*		*
Lysine	3.08-2.88	* *	*		*	*	*	* *	*		*		*	*	*		*		*
Methionine	2,64			*	*	*								*	*	*			
Succinate	2,39	*	*	* *	*			* *	* *	* *	*	*	*	* *		*	*		
Glutamate	2,35	* *			* *		* *	*			*		* *	*			*		* *
Alanine	1,47	* *	*	*	*		*	*	*	*	*		*	*	*	*	*		*
Valine	1,03	* *	*	*	*		*	*			*		*	*			*		*
Isoleucine	0,99	* *	* *		*		*	*	*		*		*	* *	*	*	*		*
Leucine	0,95	*	*		*	*		*	*	*	*		*	* *	*		*		

showing how different were the response of the two cell lines to the stress. The significance relation between cells treated with NPs and controls remained unchanged in all samples confirming the successful outcome of the analysis. Preliminary results of analysis on the culture media reported a slight change in the anaerobic metabolism with an overall increase in lactate amount respect to the controls. The increased level of lactate in Caco-2 cells may be a sign of the cellular stress which at long term may induce cellular apoptosis.[235] Further investigations on cell extracts are needed to deepen the effects of these pollutants and better outline the mechanisms triggered by these interactions.

Conclusion

Due to the complexity of the aqueous environment NPs are exposed to several chemical hazardous compounds and pollutants. The ability of NPs to interact with living organisms could made them a “trojan-horse” for the internalization of many of these hazardous pollutants such as heavy metal ions, drugs and pesticides. The interactions and the binding of contaminants with the NPs determine the change of the chemical identity of the nanoparticles themselves. Since PET NPs are internalized by cells and can pass through intestinal barrier models, the risk of exposure to these pollutants is extended to the bloodstream and therefore to the entire body. The hydrophobicity and the presence of carboxylic groups, characteristic of the degraded PET polymer, allow

the formation of interactions, of various types and intensities, with contaminants. Physicochemical characterizations have validated the hypothetical ability of PET NPs to bind the three model substances with a high capacity: Levofloxacin 0.036 g/g_{NP}, Glyphosate 0.034 g/g_{NP} and Hg 0.014 g/g_{NP}. The absorption of molecules on NPs causes an alteration of their colloidal stability in water by inducing the formation of clusters and the increase of the D_H of colloids, in contrast with what described in chapter 1 for the pure NPs sample stably dispersed in water up to 6 months. The study of the biological effects of NPs and complexes produced with the contaminants on Caco-2 and MFs has shown conflicting results. Even in this case no differences were seen between the treated samples and the controls applying the standard assays of cell viability and ROS production, but approaching with an omics strategy it was possible to observe numerous small changes in cell physiology. The enormous amount of data produced, is relative only to the analysis of the medium, but from the results it is already easily distinguishable a correlation between treatment and the effects produced.

these promising preliminary results will be further complemented by the ongoing analysis on cell extracts and lipids, giving a holistic view on the mechanisms that drive the interactions between cells and NPs.

Chapter III

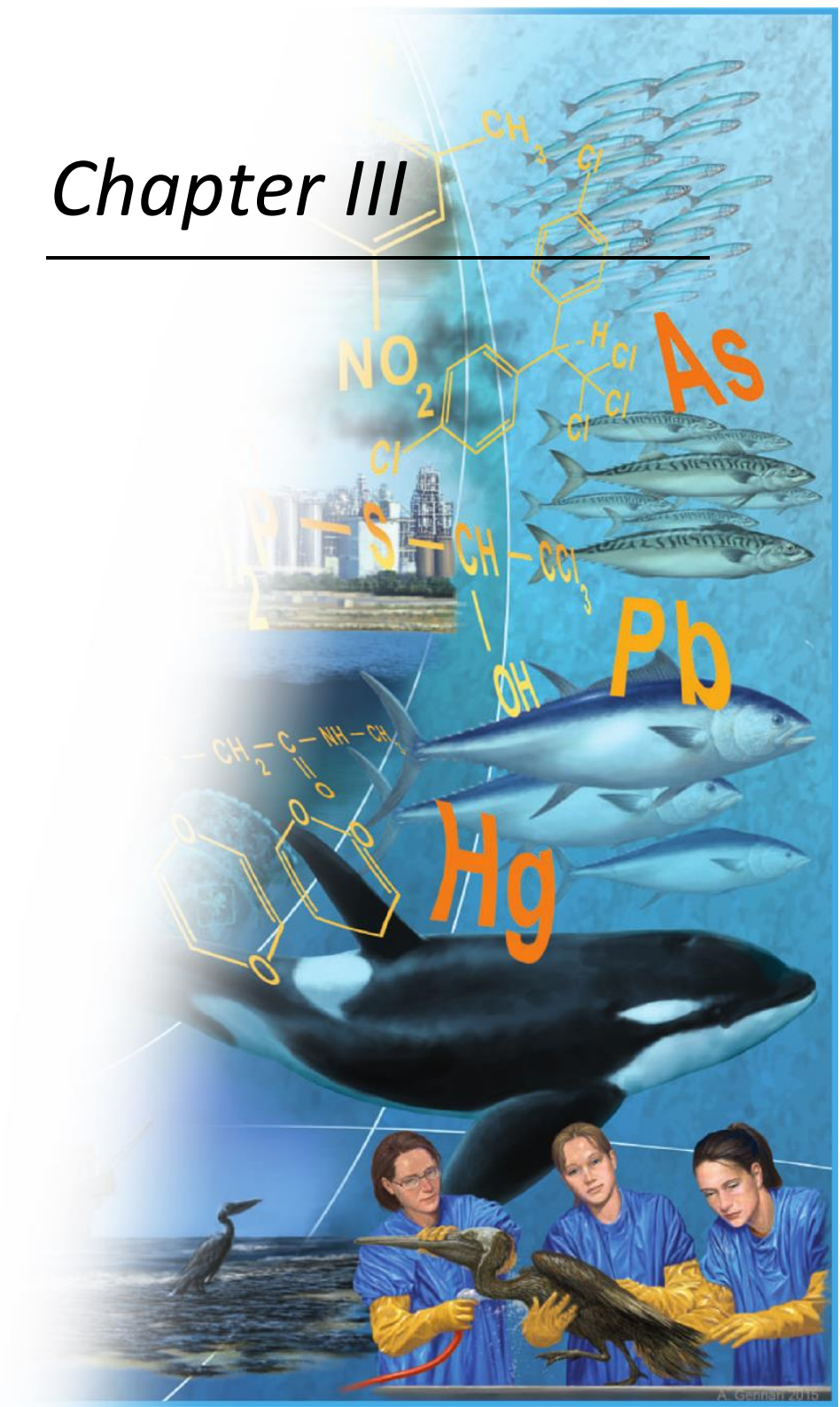

Titanates-fibroin nanocomposites for the heavy metal ions removal from water

State of the art

Heavy metal ions pollution

The intense agricultural and industrial activity, related to the continuous increase of the world population, has caused a severe rise in the environmental pollutants. Among them, heavy metal ions represent one of the most important classes of heterogeneous persistent pollutants. The name “heavy metals” is not due to the high atomic weight of these elements (in this case between 63.5 and 207.2 g / mol) but to their high specific gravity

of more than 5.0 g/cm^3.[203] Due to their widespread presence in the environment, heavy metal contamination is a worldwide recognized environmental and public-health hazard. The sources of these toxic elements, being a natural component of the earth's crust, can be natural (mineral weathering, volcanic activities, etc.) or can be related to numerous anthropogenic activities and industrial sectors (Table 9).[8] In the water environment heavy metals

Table 9. Heavy metals emissions from different industrial sectors.[8]

Industrial sector	Cd	Cr	Cu	Hg	Pb	Ni	Sn	Zn
Paper industry	–	✓	✓	✓	✓	✓	–	✓
Petrochemistry and refineries	✓	✓	✓	✓	✓	✓	✓	✓
Production of chlorine	✓	✓	–	✓	✓	–	✓	✓
Fertilizer industry	✓	✓	✓	✓	✓	✓	–	✓
Steelworks and ironworks	✓	✓	✓	✓	✓	✓	✓	✓
Motor vehicles, air craft	✓	✓	✓	✓	✓	–	✓	✓

can exist in form of colloid, particulate or dissolved ions, remaining suspended in the water column, precipitating on the bottom, or can be taken up by organisms.[236,237] WHO listed four of those elements (As, Pb, Hg, and Cd) between the top 10 chemicals of major public-health concern.[8] In fact, even at low environmental concentration, in the range of few µg/L, heavy metal ions can be a risk for humans.[5,203] As described in the previous chapter at

the highest levels of the food chain the concentrations of these persistent contaminants tend to increase by biomagnification due to their tendency to accumulate in living organisms, and can provoke serious health implications.[5,203] Therefore, some food, in particular certain types of seafood, are already subject to regulation.[238]

Some of the heavy metals are essential to life (e.g., Se, Zn, Co) and for maintenance of a number of biological functions. Contrarily, other elements, such as Pb, Hg, As, and Mb, have no nutritional properties and the intake can induce serious toxic effects. Even the essential elements in excess can be harmful; cobalt for example is the central atom of vitamin B12 (cobalamin) but its excess induces symptoms of poisoning in the gastrointestinal tract, heart, and kidney.[8] The elemental speciation and the chemical form may play a significant role in the interaction and toxicity of heavy metals. Toxicity of heavy metal can increase in the chelating process and due to the creation of sulfide with biologically active substances and enzymes.[202] Organometallic compounds of Hg, Pb, Cr, and Se exhibit a particularly acute effect.[8,239] Therefore, considerable attention is being devoted to the development

of low-cost and environmentally safe materials for the removal of heavy-metal ions from polluted waters.[240–242] This thesis work, was focused in particular on Pb, Cu, hereinafter briefly introduced, and Hg, already discussed in chapter 2.

Figure 56. Lead element properties, and an image of its bulk appearance.

Over 50% of Pb (Figure 56) emissions in the atmosphere have been originated from petrol and have polluted our environment, but fortunately due to the introduction of unleaded petrol the air concentration is slowly decreasing.[203] Other anthropogenic sources of Pb include the combustion of coal but also processing and manufacturing of additives and pesticides.[243] Pb is systemic poison causing anemia, kidney malfunction, brain damages and even death. Pb can affect fertility of women while at children, Pb reduces the physical and mental growth.[244] Pb can compete with calcium inactivating enzymes, altering

its incorporation into bones and interfering with nerve transmission.[245] The 0.01 mg/l concentration limit for Pb in waters, established by the WHO, is often exceeded in many developing countries.[246–248] Pb from air and water can accumulate in soil, especially in soil with high organic contents, where it remains for thousands of years. There, displacing other metals within organic matter, accumulates in plants reducing the rate of photosynthesis inducing damages also to agricultural production and to the food quality.[8]

Figure 57. Copper element properties, and an image of its appearance

Cu (Figure 57) is a micronutrient which interestingly is both essential and toxic to humans, depending on the dose ingested. It is difficult defining the milder effects of Cu deficiency or excess as the limits of homeostatic regu-

lation are not known. Adverse effects associated with excess of copper are damages to liver and kidneys.[249,250] The effects of Cu exposure are further severe in people with a genetic condition known as Wilson disease, in these people Cu levels rise strongly in the body due to a lack of specific liver enzymes.[249] Acquired Cu deficiency is described in children recovering from malnutrition, in low-birth-weight neonates, and in patients receiving copper-free total parenteral nutrition.[249]

Cu compounds are applied in wood preservatives, electroplating, azo dye manufacture, engraving, lithography, petroleum refining, pyrotechnics and as additives in food industry.[251,252] Are also largely used in agriculture as fungicides, insecticides and as algicides in surface water facilitating the environmental pollution.[253] A number of studies from Europe, Canada and the United States indicated that the Cu concentrations in surface- and drinking-water can reach values up to 30 mg/L, although these values vary greatly depending on the pH and hardness characteristics of the water and on the source of contamination.[252]

Ion exchange and water treatment processes

As discussed above, nowadays heavy metals are an environmental priority pollutant, and therefore there is a continuous investment for the development of methods and technologies for their removal from the environment and in particular from the waste water.[254] To date, the removal of heavy metal ions has been achieved by several methods herein listed and described:

- Ion-exchange processes are based on the exchange of an ions from a solution with a similarly charged ion present on a stable solid phase, the exchanger. This process commonly occurs in a reversible chemical reaction and has been widely used to remove heavy metal ions from wastewater due to the high treatment capacity, high removal efficiency and fast removal kinetics.[255] The most common cation exchangers are strongly acidic resins with sulfonic acid groups ($-SO_3H$) and weakly acid resins with carboxylic acid groups (-COOH).[254]

- Chemical precipitation is the most widely used process in industry because it is relatively simple and inexpensive to operate.[256] In precipitation processes, heavy metal ions interact with chemicals to form insoluble precipitates, which can be separated through sedimentation or filtration. The conventional chemical forms resulting by the precipitation processes include hydroxide and sulphide.[254] Although the solubilities of the metal sulphide precipitates are lower than hydroxide precipitates this last precipitation approach remains the most diffused due to its relative simplicity, low cost and ease of pH control.[257] An alternative to these two chemical precipitations methods is the use of chelating precipitants such as thiol or organic chelators. This technique can be combined with other methods such as ion-exchange or nanofiltration.[254]
- Adsorption is an effective and economic method for heavy metal wastewater treatment which offers flexibility in the operation and produce good-quality results. Sometimes adsorbents can be regenerated by suitable desorption processes. The most used absorbent in the

removal of heavy metal contaminants is activated carbon. Carbon nanotubes (CNTs), have been largely studied as adsorbents, demonstrating good potential for removing many heavy metal ions such as lead, copper, and nickel from wastewater, but their use is still expensive.[258–260] Therefore, considerable attention is being devoted to the development of low cost adsorbents and hundreds of studies have been focused on the use of natural substances, agricultural wastes, or industrial by-products for the heavy metal wastewater treatment.[240–242]

- Membrane filtration technologies with different types of membranes show high efficiency, easy operation and space saving. The membrane processes used to remove metals from the wastewater are ultrafiltration, reverse osmosis, nanofiltration and electrodialysis.[254] High removal efficiency of metal ions can be obtained through micellar enhanced ultrafiltration and polymer enhanced ultrafiltration based on the addition of surfactants or polymers to wastewater to “entrap” and bind selectivity metal, but these methods are not widespread in the industry. Reverse osmosis process uses a semi-permeable

membrane, which allows the fluid passages while rejecting the contaminants.[254] Reverse osmosis can remove a wide range of dissolved species from water, but even if widely applied, it involves a high energy consumption due to the pumping pressures and to the restoration of the membranes.[254] Nanofiltration is the intermediate process between ultrafiltration and reverse osmosis. Nanofiltration is easy to use, reliable and effective both in terms of energy and in the removal of pollutants.[261] Electrodialysis is another membrane process where the separation of ions is performed across a charged ion-exchange membrane using an electric field as the driving force. This process has been used in the processes of desalination of sea water for drinking.[262]

- Coagulation and flocculation followed by sedimentation and filtration is also employed to remove heavy metal ions from wastewaters. Neutralizing the repulsive forces using coagulants such as aluminium, ferrous sulphate and ferric chloride, destabilized colloids coagulate.[254] Coagulation is one of the most important methods for wastewater treatment, but the main objects of coagulation are only the hydrophobic colloids and suspended

particles. In order to remove both, new kinds of coagulants, the amphoteric polyelectrolytes, are developed [263] Flocculation is performed by bonds formation between polymers (the flocs) and the contaminants into large agglomerates or clumps, removed by filtration or floatation.[254]

- Flotation has nowadays found extensive use in wastewater treatment. Flotation has been employed to separate heavy metal ions from a liquid phase using bubble attachment.[254] Ion flotation and precipitation flotation are the main flotation processes for the removal of metal ions from solution. The process of ion flotation is based on conveying the ionic metal species in wastewaters hydrophobic by the use of surfactants and by subsequently removing these hydrophobic species by air bubbles.[264] Precipitate flotation process is based on the formation of precipitate and subsequent removal by attachment to air bubbles. Depending on the concentration of the metal solution, the precipitation may proceed via metal hydroxide formation or as a salt with a specific anion (sulphide, carbonate, etc.).[265]
- Electrochemical methods involve the plating-out of

metal ions on a cathode surface and can recover metals in the elemental metal state.[266] This technology involves large capital investment and energy consumption, so they have not been widely applied.[254] In addition to electrodeposition, electrocoagulation and electroflotation can be applied. Both the processes involve the generation of coagulants in situ by dissolving electrically either aluminium or iron ions from electrodes and allow a solid/liquid separation of heavy metals.[267]

Among the various wastewater treatments, ion exchange has emerged as a good compromise between removal rate and capacity, which also offers the possibility to regenerate and reuse the sorbent.[268] When metal contaminated solution is in contact with ion exchangers the positive charged toxic metal cations are exchanged with the positive charged ions from the solid insoluble exchanger such as hydrogen and sodium ions in equivalent amount in the solution (Figure 58), the same goes for negatively charged unwanted anions.[255] These systems are commonly based on synthetic resins, natural zeolites and silicates.[269] Nevertheless, such conventional materials also

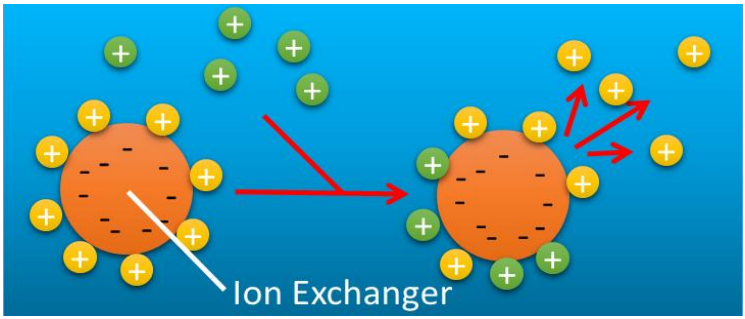

Figure 58. Schematic diagram of the ion exchange mechanism.

suffer from several drawbacks: difficulties to manage concentrated metal solution as the matrix gets easily fouled with lose of performance, poor regeneration (organic resins), slow sorption kinetics (zeolites and clays), limited selectivity, and relatively low thermal and chemical stability (resins).[268] Moreover, ion-exchange resins must be regenerated by chemical reagents when they are exhausted and the regeneration can cause serious secondary pollution.[254] Recently, several kinds of nanostructured inorganic materials were synthesized and studied for this purpose.[270,271] In particular, metal oxides and other nanomaterials have been already applied as pollutant sorbents due to their high surface/volume ratio, high reactivity, and ion exchange capacity.[271,272]

Titanates and nanomaterials in heavy metal ions removal from water

Recently, due to their unique physicochemical properties, economic benefit, efficiency and environmental friendliness, much attention has been paid to nanomaterials in water quality management. The small sizes and thus large specific surface areas of nanomaterials allow them to have strong adsorption capacities and reactivity. Not only heavy metal ions but also organic pollutants, inorganic anions, and bacteria have been reported to be successfully removed by various kinds of nanomaterials.[273] At present, the most extensively studied nanomaterials for water and wastewater treatment mainly include CNTs, metal oxides nanoparticles, and nanocomposites. Single-walled and multi-walled CNTs are good adsorption materials for the removal of organics and heavy metal ions including Pb^{2+}, Cd^{2+}, Ni^{2+} and Zn^{2+}.[274] The carbon nanotubes adsorption capability by far superior to the activated carbon performance. CNTs maximum adsorption capacity

for Cd^{2+}, Cu^{2+} and Pb^{2+} was calculated as 11.2, 167.2 and 101.05 mg/g respectively.[275] Although CNTs significant advantages, their use on a large scale is not expected in the midterm because of high production costs. Nanoscale metal oxides are promising alternatives to carbon-based materials as effective systems to remove heavy metal ions due to their high specific sorption capacity at the nanoscale owing to the fact that sorption sites reside predominantly on the surface.[271,276] γ-Fe_2O_3, MnO_2, ZnO, TiO_2, γ-AlOOH, and γ-Al_2O_3 etc. were used as adsorbents and they were combined with various matrices.[277] Some of these nanoscale metal oxides (eg, nanomaghemite and nanomagnetite) are superparamagnetic, which facilitates separation and recovery by a low-gradient magnetic field. Iron oxide nanomaterials could adsorb a variety of heavy metal ions.[278] Nano-magnetite showed an adsorption capacity for Cu^{2+}, Cd^{2+}, Ni^{2+}, Zn^{2+}, Pb^{2+} as 79.1, 88.4, 95.4, 107.3 and 112.9 mg/g, respectively.[279] Although the natural occurrence of iron and their facile synthesis, their application is still at the laboratory scale.[280] Nanosized manganese oxides have been exploited for sorption of

cationic or anionic pollutants from natural waters. Compared to commercial resins manganese oxides showed high selectivity towards heavy metal ions.[281,282] Alumina (Al_2O_3) is a traditional adsorbent for heavy metals. The chemical or physical modification of Al_2O_3 nanoparticles, with specific functional groups containing donor atoms, improves their sorption and selectivity toward heavy metals with a maximum adsorption capacity values of 100.0 mg/g for Pb^{2+} in multiple-metal solution.[283] Recently, it was found that nanostructured ZnO too can efficiently remove heavy metal ions and particularly Cu^{2+} with an adsorption capacity >1600 mg/g.[283,284]

Titanium oxides have many applications. Titanium is the ninth most abundant element in the Earth's crust, and therefore it is cheap, and its oxides were able to simultaneously remove multiple metal ions in the aqueous phase.[285] In terms of distribution coefficient (Kd), Titanium oxide nanostructures performed better than commercial activated carbon and many other metal oxides.

A particularly performing group of titanium oxide is that of titanates. In their early discovery, these materials have

been mistakenly assigned as anatase TiO_2, while they were actually a different class of layered materials, with a general formula $M_xTi_yO_{x/2+2y}{\cdot}zH2O$ (M=H, Li, Na, K, etc.), called titanates.[286] Titanates have been produced in various shapes, such as nanotubes, nanowires, and nanoflowers, but their base structures is constitute as 2D layers formed by connected TiO_6 octahedral blocks, with cations and neutral molecules inserted into the interlayer space (Figure 59). Every single structural entity is joined by corner to the other structural entities related forming a continuous 2D sheet.[286] The various stoichiometry of titanates is related to the number of TiO_6 octahedra composing the structural entity.[286] Thanks to their open crystal structure, their interlayer distance adaptability, titanates can accommodate many varieties of cations

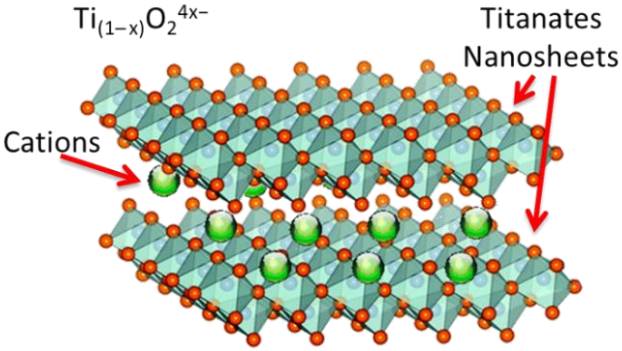

Figure 59. Titanates sheet layers structure.

in the interlayer spaces balancing their negatively charges and endowing them unique physiochemical properties.[287–291]

Layered titanates have been largely investigated due to the very good cation exchange capability. Because of the negative charge on the titanate sheet, it can adsorb positively charged molecular species effectively such as heavy metal ions showing better performance compared to other metal oxides, reaching a removal capacity of up to 550 mg/g in the case of lead ions.[287–291] Titanate nanosheets (TNSs), in particular, are novel two-dimensional (2D) nanomaterials with a layered nanostructure and a $Ti_{(1-x)}O_2^{4x-}$ composition. Usually, depending on their preparation method, diverse TNS lamellar structures can be formed by single Ti-O sheets in a TiO_6 octahedral configuration intercalated by organic cations.[292–295] These 2D crystals of sub-stoichiometric TiO_2 have small sizes (one-unit-cell thickness and length of 2−6 nm) and very high surface-to-volume ratio, whereas they present high refractive index values.[292–294] On top, it has been already

demonstrated that the cations present in the TNS structures can be efficiently substituted by sodium or other metal ions, making them interesting materials for diverse types of applications, among which is also the environmental remediation by ion exchange.[292,295,296] In particular, TNSs, have shown their appealing ability to irreversibly exchange and tightly immobilize hazardous metal ions, such as Pb^{2+}.[287,295]

However, due to their nanometric size, the increased surface energy unavoidably leads to the poor stability TNSs in aqueous ambient. Consequently, TNSs as other nanosized metal oxides are prone to agglomeration.[283] In addition, the environmental fate and the possible hazardous effects of nanomaterials are still unknown. Indeed, human health and ecological risk assessment of nanomaterials are limited.[297] So, to improve the applicability of these performing materials in real wastewater treatment, it is possible to incorporate them into solid supports obtaining nanocomposite adsorbents.[298–300]

Nano-biocomposites are a class of composites obtained by adding nanofillers to biopolymers. Biopolymers are

commonly destined to different short-term applications e.g. packaging, agriculture or hygiene and biomedical devices, and have already showed, in combination with nanomaterials, improved properties with preservation of their biodegradability, representing an emerging answer for improved and eco-friendly materials.[301] Recently, due to their facile synthesis and low cost, the application of nano-biocomposites has become a novel approach for environmental applications.[302] Nano-biocomposites have been reported for the removal of heavy metal ions from wastewater.[303] Biopolymers can derive from natural sources such as carbohydrates and protein (e.g. starch, cellulose, chitosan, alginate), can be chemically synthesized biodegradable polymers (e.g. poly-lactic acid (PLA), polyvinyl alcohol (PVA)) or produced by microbial fermentation (e.g. polyhydroxybutyrate (PHB), polyhydroxyalkanoates (PHA).[304] In the context of this thesis, in order to produce a reliable and good-performing nano-biocomposite, silk fibroin was used as a support for titanates, and for this reason its main characteristics will be explored in the next paragraph.

Silk fibroin

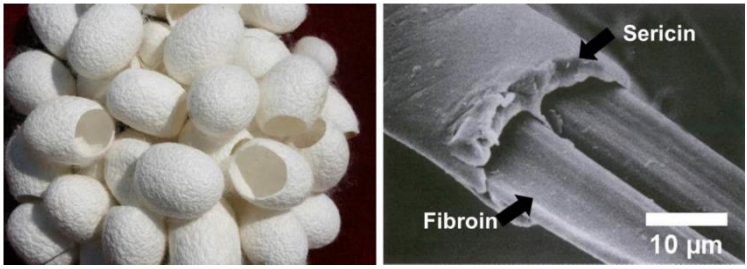

Figure 60. Silkworm cocoons (left) and a SEM micrograph of a cocoons yarn structure (right).

Silk is a natural fibre extracted from the cocoons of the *Bombyx mori* and constitute of two protein: 72-81% of fibroin and a 19-28% of sericin, a gum-like protein that coat a backbone of fibroin (Figure 46).[305,306] Fibroin is made up by a heavy (H) and a light (L) chain with a molecular weight of 325 kDa and 25 kDa respectively linked by a disulphide bond, forming the H-L complex.[307,308] The peculiar aminoacidic composition gives to this protein unique properties. H chain consists of repeated hexapeptide Gly-Ala-Gly-Ala-Gly-Ser and the dipeptide Gly-Ala/Ser/Tyr, which self-assemble in hydrophobic antiparallel β-sheets during the silk worms spinning.[307] L chain is more hydrophilic and is principally composed of valine, isoleucine

and leucine and acidic amino acids.[307,309]

Due to its composition fibroin results characterized by a semi-crystalline structure formed by the crystalline hydrophobic antiparallel β-sheets part, which is alternated with a less organized phase.[310] The crystalline part confers its strength, toughness, refractive index, water solubility and degradation properties to silk, while flexibility and elasticity are depending on the amorphous component.[310–313]

Silk fibroin was generally used for its high strength, such as fabric and fiber especially in textile industry.[312,314] The development of new protocols of extraction and regeneration has made possible to obtain pure fibroin in water solutions, already widely used for the production of materials for biomedical purposes due to its proven biocompatibility and low immunogenicity.[314] The regenerated silk fibroin is in fact soluble in water and more easily processable in several of films, fibers, sponges and nanoparticles.[305,308,314–318] It is possible to tune the water stability of fibroin by modifying the amount of β-sheets through crystallization. A crystalline state with high β-sheets content can be obtained by water vapor annealing or by the

exposure of the silk fibroin to organic solvents, such as methanol, making silk a suitable material for the development of composites with a low environmental impact, also applicable in aqueous environment.[313,319,320] Recently silk fibroin has been proposed as matrix support to produce nano-biocomposites. Thanks to its high transparency and stability, and to the development of novel nanofabrication methods, it was possible to embed TNS in silk fibroin producing biocompatible nanocomposites, applied in resorbable electronics, implantable and optical devices and sensing applications.[292,296,321]

Materials and methods

Fabrication of TNSs.

TNSs were synthesized by Prof. Martucci's group, using a sol-gel process.[293,322] Initially, 12 mmol of titanium tetraisopropoxide $Ti(OPri)_4$ were added to 107 mmol of warm (110 °C), dehydrated and degassed ethylene glycol (EG). Subsequently, 9 mmol of tetramethylammonium hydroxide (TMAH) (Sigma-Aldrich) dissolved in 54 mL of water were injected in the solution, which became optically clear after few seconds. The reaction run for four hours

at 110 °C. After cooling the solution at room temperature (RT) an excess of acetone was added to induce the flocculation. TNSs were then precipitate by centrifugation at 4000 rpm for 4 minutes. The TNSs pellet was washed twice with acetone and twice with methanol then was dried under vacuum. A stock dispersion of TNSs was obtained by dispersing 200 mg of TNSs in 1 mL of 0.1 M TMAH aqueous solution.

SF extraction.

SF aqueous solution was prepared according to a previously published protocol.[314] Cocoons of Bombyx mori were cut in little pieces and boiled for 30 min in a solution of 0.02 M sodium carbonate (Sigma-Aldrich) to remove the sericin. The boiled silk was rinsed with MilliQ water and, after drying, the fibers were dissolved in 9.3 M LiBr (Sigma-Aldrich) solution at 60°C for 4 h. The solution was dialyzed against distilled water using a dialysis membrane (Molecular weight cut-off 3500, 6.74 mL /cm, Fisherbrand) for 2 days to remove the LiBr salts. The silk fibroin

solution, obtained after dialysis, was transferred in a 50 mL tube and was centrifuged twice at 9000 rpm at 4 °C for 20 minutes and transferred in a clean tube to remove impurities. The concentration of fibroin in aqueous solution was in the range between 6-8% (w/v) for the different batches. The SF solution with a 5% concentration used in the present work was prepared by diluting the more concentrated solutions in milliQ water.

TNSs-SF nanocomposite formation.

TNSs-SF nanocomposites were formed by mixing the fibroin solution with the water dispersion of TNSs. Aliquots of the TNSs dispersion were added to aqueous solutions of SF (50 mg/mL) and mixed gently to avoid the fibroin flocculation. The solutions were drop-casted and dried under the fume hood at RT to obtain films. The composite films were then dipped in methanol overnight at RT to induce fibroin crystallization and dried for 24 hours under hood.[292] The methanol annealing process allows the stability of the nanocomposite in water and at the same time

permits an efficient interaction of the polluted water with the TNSs fillers.[292,308,314,323] TNSs-SF films with TNSs to silk ratios of 50/50, 70/30 and 90/10 were synthesized.

Ion Exchange Process.

To test the removal of heavy metal ions from the water solution, the nanocomposite films were incubated in aqueous solutions of lead nitrate ($Pb(NO_3)_2$ 99%), mercury chloride ($HgCl_2$ 99.999%), copper chloride ($CuCl_2$ 97%) and sodium chloride (NaCl 95%) (Sigma-Aldrich). Different metal ion concentrations were prepared (from 25 to 1000 mg/L) starting from stock solutions concentrated at 1000 mg/L. For each ion exchange experiment, 20 mg of the TNSs-SF films were enclosed in a dialysis membrane (Molecular weight cut-off 3500, 1.15 mL/cm, Fisherbrand) to facilitate the sampling operations and dipped in 20 mL of ion solution. All the tests were performed under stirring at 700 rpm. At the various time point, aliquots of 250 µl of ion solution were collected for further characterization. At the end of the adsorption

process, the solid films were collected and used for further analysis.

Inductive Coupled Plasma-Optical Emission Spectroscopy.

Inductive Coupled Plasma-Optical Emission Spectroscopy (ICP-OES) was used to determine the ions concentration with an iCAP 6500 spectrometer (Thermo). All the samples collected were previously treated with 2.5 mL of aqua regia (1HNO_3:3HCl) overnight. Then the digested samples were diluted up to 25 mL with milliQ water and filtered through Nylon syringe filters (diameter 25 mm and a pore size of 0.2 µm, Sartorius). From the ICP-OES data, the sorption capacity of the films q_e (mg/g) was calculated as follows:

$$q_e = \frac{(C_0 - C_e) \times V}{W} \quad \text{Eq.3}$$

where C_e (mol/L) is the concentrations of the heavy metal ions at the equilibrium, C_0 (mol/L) is the initial

concentration, V (L) is the volume of the solution and W (g) is the mass of the adsorbent.

Energy Dispersive X-ray Spectrometry.

Energy Dispersive X-ray Spectrometry (EDX) analysis was carried out using a Scanning Electron Microscopy (JEOL JSM-6490LA, Tokyo, Japan) equipped with a tungsten (W) thermionic electron source working in low vacuum. The composite samples were incubated in a 1000 mg/L lead ions solution for 24 hours. After the incubation, the samples were washed in milliQ water and after drying were coated with 10 nm thick AuPd film using a sputter coater (Cressington 208HR).

Transmission Electron Microscopy.

Transmission Electron Microscopy (TEM) analysis was carried out using a JEM 1400-Plus JEOL microscope operating at an acceleration voltage of 120 kV. The composite

samples before and after ion exchange were grinded and dispersed in water. Few drops of the composite suspension were deposited onto copper grids coated with an amorphous layer of lacey carbon film. Then the grids were dried under vacuum overnight to remove water. High Angle Annular Dark Field Scanning Transmission Electron Microscope (HAADF-STEM) images were acquired using an image Cs-corrected JEOL JEM-2200FS TEM with a Schottky emitter equipped with a Quantax 400 STEM system, operated at 200 kV. EDS analyses were carried out in HAADF-STEM mode using the same microscope and an XFlash 5060 silicon-drift detector (SDD, 60 mm^2 active area).

Fourier Transform Infrared.

Fourier Transform Infrared (FTIR) measurements were carried out on the films using a Vertex 80 (Bruker) spectrometer in attenuated total reflectance (ATR) and in transmission mode. The spectra were acquired between

4000 and 400 cm^{-1} with a resolution of 2 cm^{-1}. X-ray diffraction (XRD) measurements were performed on a PANalytical Empyrean X-ray diffractometer using a Cu Kα anode (λ=1.5406 Å) operating at 45 kV and 40 mA. The diffraction patterns were collected in the range 2–70° 2θ with a 0.04° step size. X-ray Photoelectron Spectroscopy (XPS) analysis was performed using a SPECS-Lab spectrometer with Al Kα source (hv= 1486.6 eV) operated at 15 kV with an emission current of 10 mA. Charge neutralizer consisting of low-energy (ca. 7 eV) electrons was applied and energy scale calibration was performed by setting the C-C/C-H component of C1s spectrum at 285 eV.

Results and discussion

TNSs-SF composite characterization

The first step for the development of a composite is to know the interspecific effects of the components and

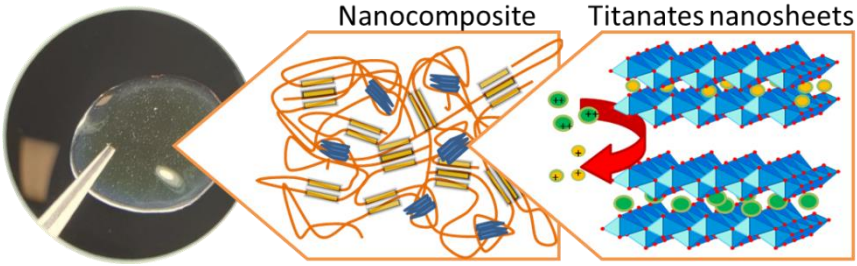

Figure 61. Schematic representation of TNSs-SF composite. In yellow/orange the SF matrix random coiled secondary structure and β-sheets, in blue the TNSs intercalated by cations during ion exchange.

those induced by the synthesis process. The sketch in Figure 61 illustrates with various magnifications the components constituting TNSs-SF composite. Being titanates the active part of the composite the effect of incorporation into SF matrix on the nanostructures was investigated. Studying the XRD patterns of the as synthesized TNSs powder and of the TNSs-SF composite before and after methanol annealing, typical peaks ascribable to the TNSs

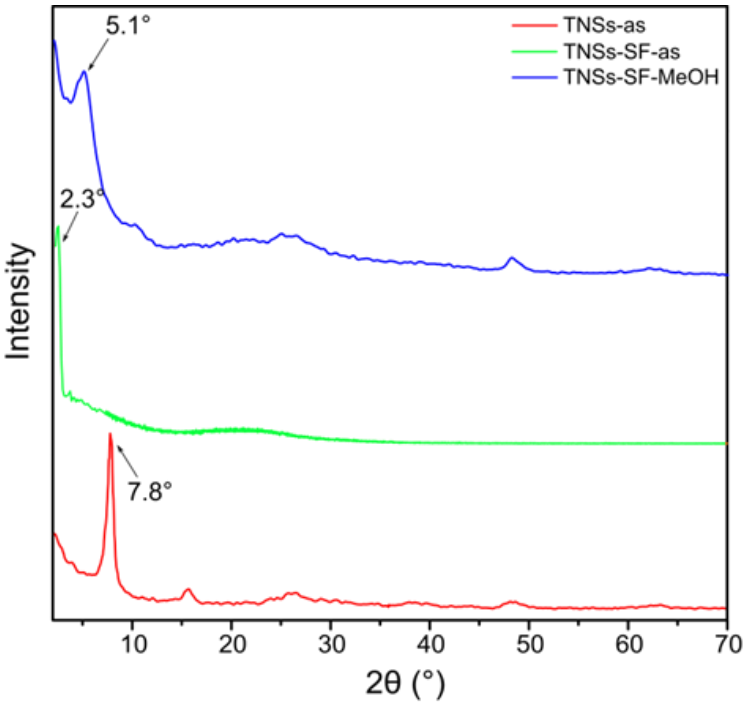

Figure 62. XRD patterns of bare TNSs (red trace) and TNS−SF nanocomposites before (green trace) and after (blue trace) methanol treatment.

have been observed (Figure 62). These peeks were consistent with the typical titanate layered structure.[293,294] The comparison between the patterns showed that, the strong reflection peak at a low angle, shift lower in presence of SF matrix. The value pass from the 7.8° for the as-synthesized TNS powder to the and 5.1° of TNSs-SF after methanol annealing and 2.3° before the treatment. As derived from the Bragg's law, the interlamellar spacings variated form 1.1 nm in the as-synthesized TNSs to 3.8 and 1.8 nm, for TNSs-SF before and after methanol respectively. This variation can be attributed to the different degree of hydration of the films due to the nanocomposite fabrication procedure. The highly hydrated environment of SF matrix affects the TNSs interlamellar spacing which recover after the dehydration induced by methanol annealing process, necessary for the crystallization of the SF matrix.[292]

The validation of the TNS nanostructure integrity after their introduction in the SF matrix has been carried out by TEM characterization. The as-synthesized TNSs and the TNSs-SF nanocomposites were analysed and as shown in Figure 63, the presence of the layered lamellar structures

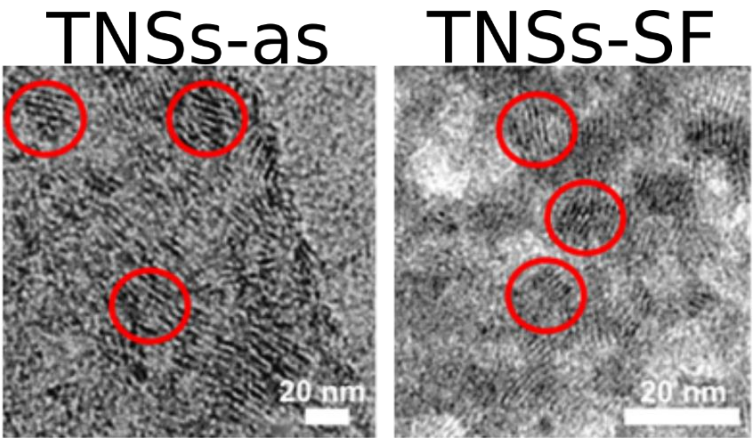

Figure 63. TEM images of as-prepared TNSs and TNSs dispersed in the SF matrix. Data presented for the TNS−SF nanocomposite refer to a 50/50 composition. TNSs appear as an alternation of darker lines due to the higher electronic density of Titanium, spaced by the less electrondense intercalated cation.

of ~10 nm in length, ascribable to the TNSs are present in both cases. The dark layers indicate the presence of a stronger scattering material (i.e. TNSs) in contrast with the organic moieties that lay invisible between each titanate lamella (Figure 63).

The influence of the hydration on the TNSs structure was also emerged via FTIR analysis (Figure 64). The vibrational modes of the TNSs [Ti-O] lattice experience some modifications when the TNSs are incorporated in the silk matrix. The change in the coordination environment of surface atoms induced by water absorption modified the band of

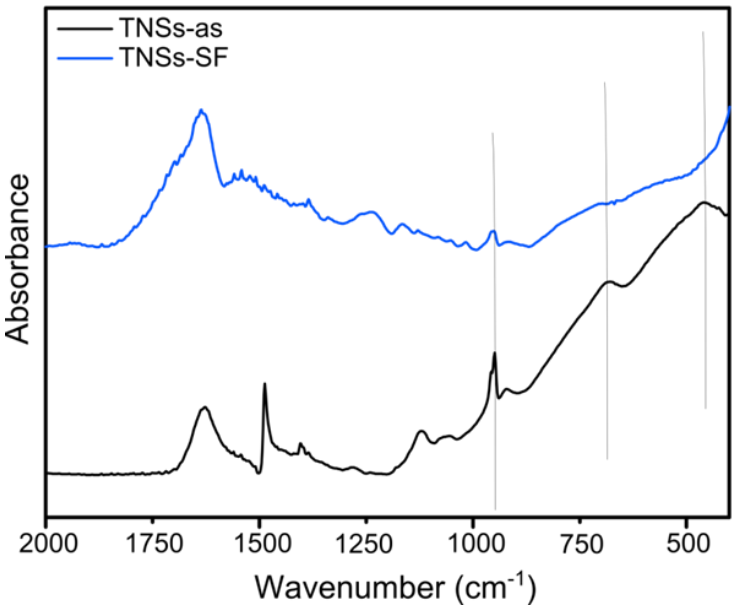

Figure 64. FTIR spectra of the as synthesized TNSs and TNSs-SF.

Ti-O bond related to stretching- and bending-type vibrations observable below 900 cm^{-1} (i.e. infrared-active A_{2u} and E_u modes, respectively).[324] In the composite, the function of SF should be limited to support and retain TNSs.

Nevertheless, in order to have a clearer knowledge about the materials employed any possible contribution of the SF matrix to the adsorption of the heavy metal ions was assessed. Pure SF films, and three TNSs-SF nanocomposite films, prepared with different ratio of TNS/SF (50/50,

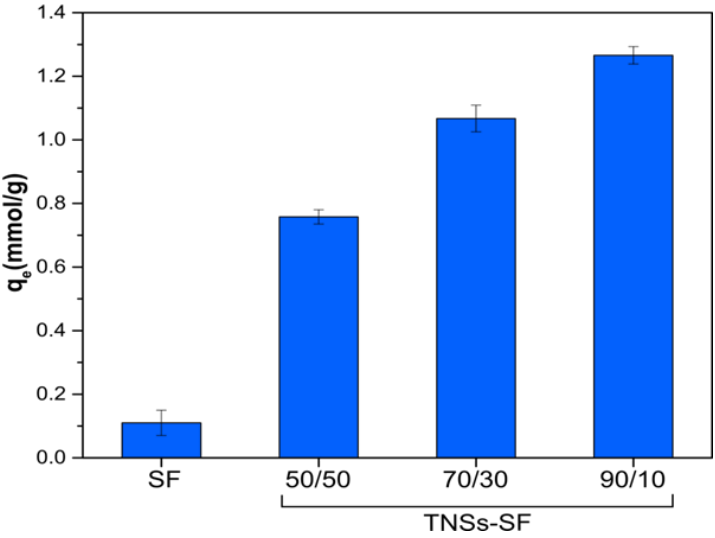

Figure 65. The histograms report the dependence of the absorption capacity in relation to the TNSs amount in the composites (TNSs-SF 50/50, 70/30, 90/10) and the negligible contribution of pure SF.

70/30 and 90/10, TNSs/SF respectively) were incubated in a 1000 mg/L Pb^{2+} aqueous solutions, for 24 h. Subsequently ICP-OES analysis of the ions solution was carried out, and the results presented in Figure 65 showed that the Pb^{2+} removal capacity of the bare biopolymer is negligible (0.1 mmol/g). The little amount of ions removed may be mostly attributed to the presence of glutamic acid, cysteine and histidine in the aminoacidic sequence of SF, such as, generally involved in metal ions removal.[37,38] Contrariwise, the TNSs-SF absorption capacity

increased in accordance with TNSs concentration. Specifically, for the 50/50 TNSs/SF the removal capacity was 0.75 mmol/g, progressively rising to 1.1 mmol/g for the 70/30 up to 1.3 mmol/g for the 90/10 TNSs/SF. The increase in the amount of TNSs within the composite causes strong structural decompensation, contradicting the objective of developing a stable and safe material for environmental applications. After 24h of incubation in the ions solution the composite experienced several structural alterations. Higher concentrations of TNSs caused swelling and weakening of the structure, and consequently increasing the risk of TNSs loss in the aqueous medium. Only the films having a 50/50 TNSs/SF composition retained his solid native appearance. Nonetheless, in all cases, the ICP-OES measurements carried out on the solutions after the adsorption process reveal a negligible titanium presence, indicating the good operation of SF in retain the nanostructures. Because of the good structural and operational compromise, the 50/50 TNSs-SF composition was chosen to further pursue the material characterization and the studies on its heavy metal ions removal capacity.

TNSs-SF response to ion exchange

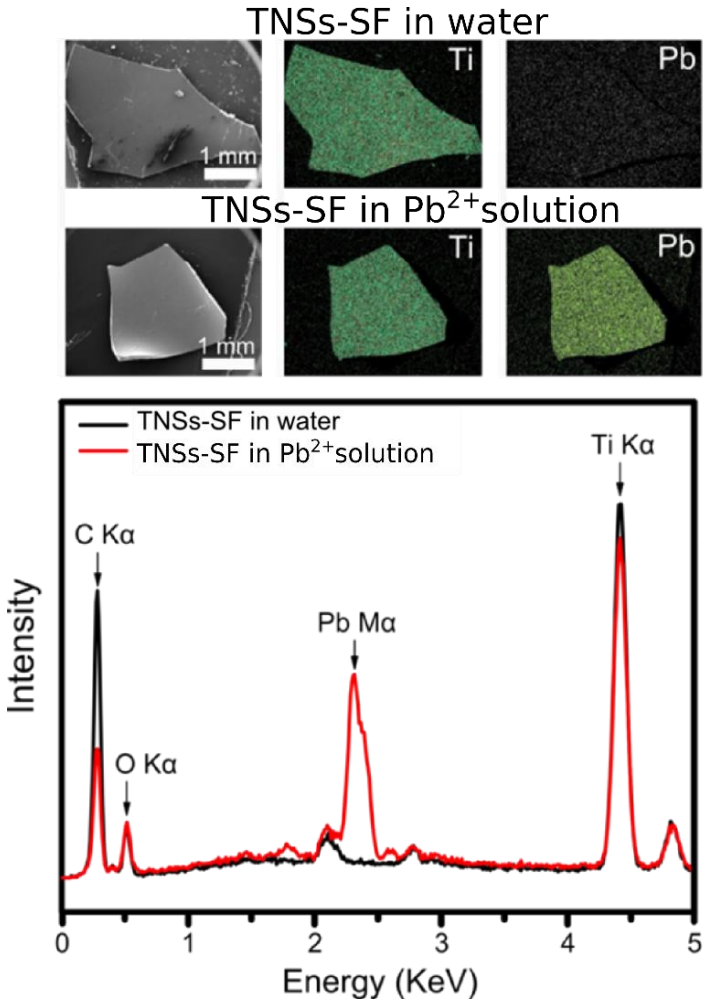

Figure 66. On the top, SEM images of the TNSs-SF (50/50) samples before and after the ion exchange with Pb^{2+}, respectively. The corresponding EDX maps are related to the Ti Kα and Pb Mα lines. On the bottom, representative EDX spectra of the TNSs-SF samples before (black line) and after Pb^{2+} exchange (red line).

The SEM analysis and the related titanium EDX mapping of the 50/50 composite shows that the TNSs are evenly distributed in the fibroin matrix (Figure 66), and this is preserved even after the dipping of the nanocomposite in the Pb^{2+} solution (1000 mg/l for 24h). Mapping of the Pb Mα line after dipping, lead signal appears homogeneously distributes on the whole surface of the TNSs-SF film. The EDX analysis gives also information about the ion exchange process occurred upon the Pb^{2+} interaction with the nanocomposite. Looking at the EDX spectra, the Pb Mα signal arises with an intense band at 2.4 keV after the dipping process, while Ti and O contribution still unchanged in both the samples. The stable intensity ratio of the Ti Kα (4.5 keV) over O Kα (0.5 keV) signals before and after the interaction with the Pb^{2+} ions (Ti/O~ 6.5) prove that TNSs persist within the composite. On the other hand, the C Kα signal (0.3 keV) significantly decrease with respect to the unchanged O Kα (0.5 keV), with C/O intensity ratio of 5.2 and 2.3 before and after the interaction of the film with the Pb^{2+}, respectively. This variation is coherently attributable to the loss of TMA^{+}, the organic counterion present between the TNSs layers, in favor of

the absorption of Pb^{2+}. The substitution of the ions intercalated in the titanates lamellar structure, in this case TMA^{+}, with a mono- or a divalent cation, such as Pb^{2+}, is a general accepted mechanism for the ions exchange process in TNSs.[292,327]

The TMA^{+} exchange in the solid nanocomposite is further confirmed by the high resolution XPS analysis of the N1s band of the samples before and after the interaction with the Pb^{2+} aqueous solution (1000 mg/L for 24h) (Figure 67). Specifically, in the TNSs-SF films the band analysis revealed the presence of two distinct N-C contributions: the first one centered at 399.8 eV is typical of the N-C bonds of the SF matrix[328] and the second at 402.7 eV is consistent with the presence of the quaternary nitrogen present in the TMAH component.[329] After the ion exchange

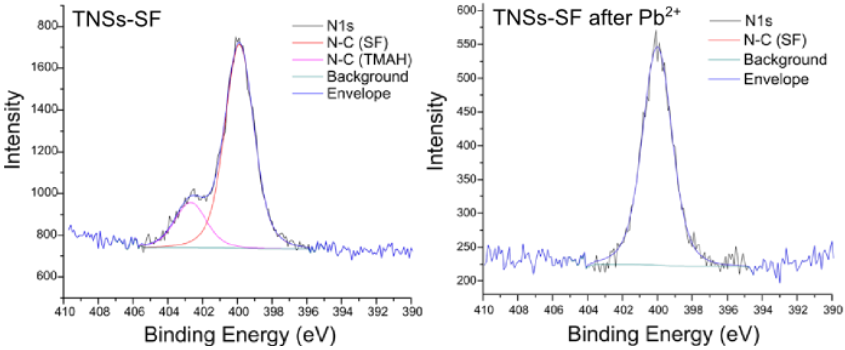

Figure 67. High resolution N1s XPS spectra of the TNSs-SF before and (e) after the Pb2+ exchange.

process, the latter peak disappears, while the N-C bonds of the SF component at 399.8 eV remain.

Cation exchange kinetics and efficiency of the TNSs-SF films have been assessed with three different metal ions: Pb^{2+}, Hg^{2+} and Cu^{2+}. The process of ion exchange was monitored during time measuring the concentration of ions in solution up to 24 hours. Every ion exchange kinetics assessment was performed for using three different concentrations of ions: 25, 200 and 1000 mg/l. As shown

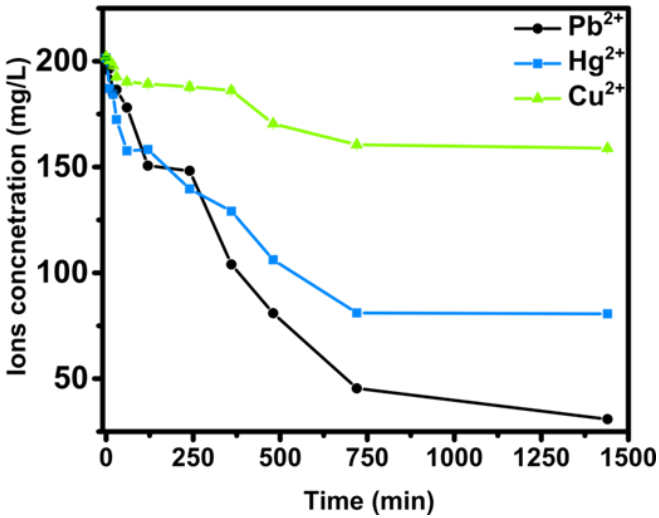

Figure 68. Kinetics of removal of Pb^{2+}, Hg^{2+} and Cu^{2+} ions after dipping the TNSs-SF in the ion solutions for 24 hours (1440 minutes). The analyzed samples were incubated in 20 ml solutions of 200 mg/L which correspond to Pb^{2+}=0.96 mM, Hg^{2+}=0.99 mM, and Cu^{2+}=3.15 mM. The standard deviation is below 0.6% for each point displayed in the plot, as determined from ICP analysis.

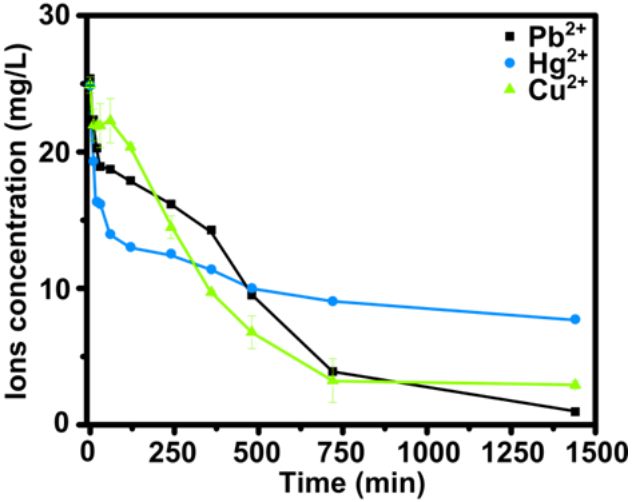

Figure 69. Kinetics of removal of Pb^{2+}, Hg^{2+} and Cu^{2+} ions after dipping the TNSs-SF in the ion solutions for 24 hours (1440 minutes). The analyzed samples were incubated in 20 ml solutions of 25 mg/l.

in Figure 68, starting from an initial concentration of 200 mg/l in all cases, the metal ion concentration is reduced during time. In the case of Pb^{2+} and Hg^{2+}, there is a significant decrease of the concentration in the first 120 minutes of incubation with up to 25% of metal ions removed. Until 720 minutes the films continue to entrap the ions, but slower compared to the initial phase, with removal efficiencies of 75% for Pb^{2+} and 60% for Hg^{2+} until the system reaches the equilibrium. In the case of Cu^{2+} ions, the initial adsorption stage is concluded after 60 minutes, while at the second stage the removal rate is

slower compared to the other ions, reaching up to 20% of metal ions removal in 720 minutes. This effect, observable also in the lowest initial concentration test (25 mg/l) (Figure 69), could be attributed to the higher initial concentration of the ions in the water solution, due to the Cu^{2+} smaller size, which might result in a faster saturation of the available active sites of the composite upon interaction with the ions.[330] In fact, 200 mg/l in terms of molarity corresponds to 3.15 mM of Cu^{2+}, more than 3 times higher compared to the 0.96 mM and 0.99 mM for Pb^{2+} and Hg^{2+} respectively. This is further emphasized testing

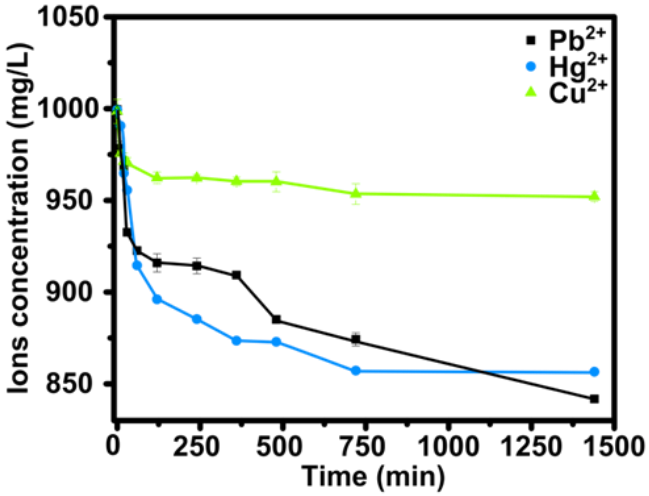

Figure 70. Kinetics of removal of Pb^{2+}, Hg^{2+} and Cu^{2+} ions after dipping the TNSs-SF in the ion solutions for 24 hours (1440 minutes). The analyzed samples were incubated in 20 ml solutions of 1000 mg/l.

the highest initial concentrations of 1000 mg/L (Figure 70). The Cu^{2+} concentration significantly affected its adsorption kinetics. In the first 120 minutes the 21%, 30%, and 78% of the total ions removed was reached when the TNSs-SF films are incubated in a solution of 25 mg/L, 200 mg/L and 1000 mg/L respectively.

Another parameter that characterize an ion exchanger is its ion removal capacity in the equilibrium state (q_e). Therefore, the TNSs-SF films were dipped for 24 hours in water solutions containing different concentrations of the Pb^{2+}, Hg^{2+} and Cu^{2+}, and the q_e was calculated (see Eq. 3) in each case as shown in Figure 71. For a correct interpretation of the results q_e data were presented in mmol/g. In all cases, two distinct sorption regimes can be distinguished. In the first one, between 25 and 200 mg/l for Pb^{2+} and Hg^{2+}, and between 25 and 100 mg/L for copper (higher concentrated in terms of moles), a sharp rise of the removal capacity was observed increasing the concentration of the ions. For initial concentrations higher than 200 mg/L for Pb^{2+} and Hg^{2+}higher than 100 for Cu^{2+}, the films changed regime and reached their maximum

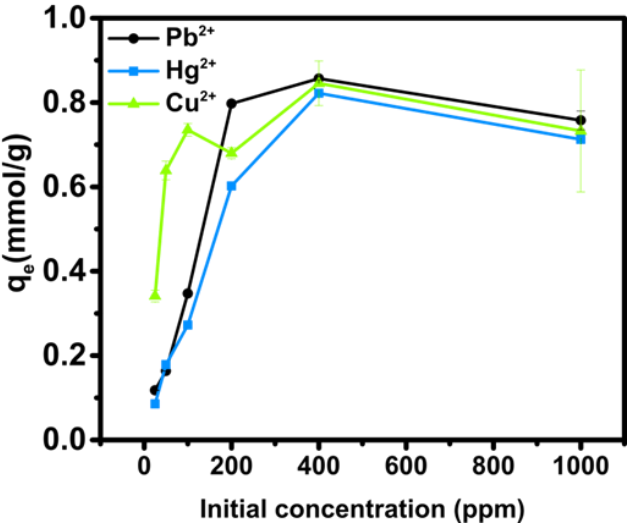

Figure 71. Removal capacity q_e in mmol/g after 24h of incubation at different of ions concentration (Pb^{2+}, Hg^{2+} and Cu^{2+}, respectively).

sorption capacity (q_{max}). This behavior was due to the complete saturation of the active sites of the TNSs, thus beyond this concentration threshold the composite cannot remove other ions. As expected, the q_{max} is similar for all the ions studied and a mean value of 0.73 ± 0.02 mmol/g was calculated at 1000 mg/L. The q_{max} results are compliant with the values described in literature for other titanates shape.[287–289,295,331] The reported q_{max} values for Pb^{2+} removal from aqueous solution in the range between 0.50 and 2.64 mmol/g were referred to free-standing titanate nanopowder, dispersed directly in the

metal ions solution. In our case the TNSs are embedded in a solid and compact SF matrix and q_{max} of 0.73 mmol/g was calculated with respect to the weight of the entire nanocomposite. Calculating q_{max} with respect to the weight of the TNSs inside the nanocomposite (50%) the q_{max} becomes resulted 1.46 mmol/g. Although the process is slower compared to the freely dispersed titanates, due to the limited diffusion induced by the SF matrix, the incorporation of the TNSs in the biopolymer did not affect the TNSs ions sorption capability.[288,289,295,331] Despite the diffusion limits imposed by the SF matrix, the TNSs-SF removal kinetics (24 hours) is faster compared to conventional adsorbents such as zeolites and/or TNs nanofibers, that need up to 50-100 hours to reach the equilibrium of absorption.[331,332]

TNSs-Na-SF composite characterization

The aim of this work is to produce a highly efficient environmentally friendly water treatment system, and therefore the system was improved to avoid concerns on the

release of TMA+ to the environment. In fact, during ion exchange, TMA^+ is substituted by the heavy metal ions inside the composite remaining dispersed in water. As already reported is possible to pre-treat the TNSs-SF films with Na^+ solutions, in order to exchange the TMA^+ with Na^+ ions,[292] and resulting in a new type of composite indicated as TNSs-Na-SF.

The FTIR analysis (Figure 72) of the TNSs-SF films before and after their dipping in a 1000 mg/L Na^+ solution for 24 hours confirms the complete TMA^+ removal from the material: the absorption band at 949 cm^{-1}, referred to the C-

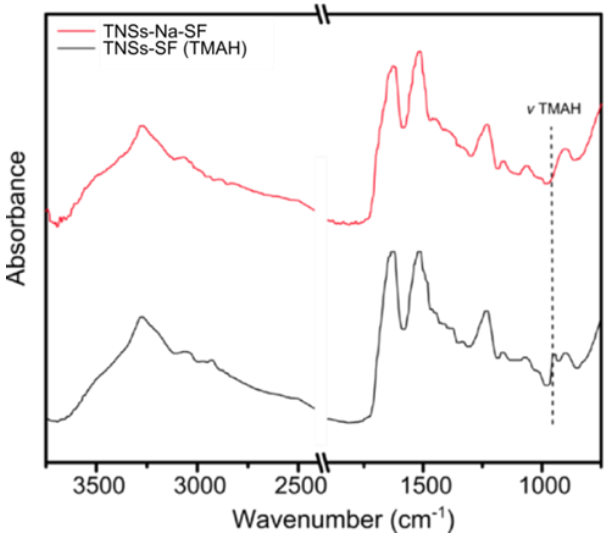

Figure 72. FTIR spectra of the TNSs-SF films before and after the incubation in Na^+ solution. The dotted line indicates the wavenumber at 949 cm^{-1} related to the identifiable peak of the TMAH.

N stretching characteristic for the TMAH molecules disappears.[292] The contribution of SF is still well recognizable from the relative amide I (1600-1700 cm^{-1}) and II (1540 cm^{-1}) bands.[292]

The sorption capacity of the bionanocomposite after the exchange of TMA^+ with the Na^+ was studied. As shown in Figure 73, in order to ascertain the functioning of the system, following the first ion exchange in a 1000 mg/L (43.5 mM) Na^+ solution for 24 hours, the TNSs-Na-SF has been incubated in an aqueous solution of Pb^{2+}. As already

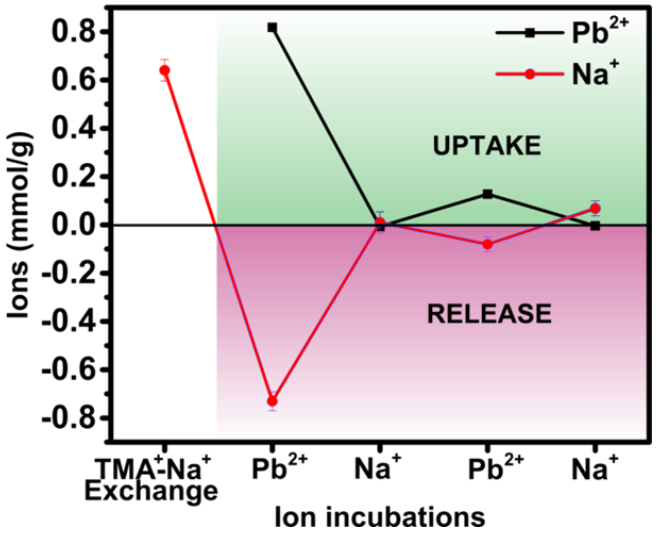

Figure 73. ICP-OES result of a successive incubations of the TNSs-SF nanocomposite in solutions of Na^+ and Pb^{2+}. After the initial substitution of TMA^+ by Na^+, the material was incubated alternatively in Pb^{2+} and Na^+ of the same initial concentration 2.1 mM for 24 hours, each time.

demonstrated through FTIR analysis after the incubation, the TMA^+ was exchanged with the Na^+ and 0.65 mmol/g of such ions are entrapped in the TNSs-SF system. Subsequently the modified TNSs-Na-SF nanocomposite was dipped in a Pb^{2+} ions solution of 435 mg/L (2.1 mM) for 24 hours. As shown, all the Na^+ ions were released from the composite and replaced by the Pb^{2+} ions (Pb^{2+} sorption capacity 0.81 mmol/g). Performing more uptake cycle, dipping the Pb^{2+}-modified TNSs-Pb-SF system in the Na^+ solution, with a concentration of 2.1 mM, did not cause any release of Pb^{2+} or uptake of Na^+. On the other hand, the subsequent dipping in Pb^{2+} ions induced the slight increase of the sorption capacity of the system, since an additional small amount of Pb^{2+} was uptaken and an equivalent amount of Na^+ was released (~0.1 mmol/g), possibly due to the not complete exchange process of the first Pb^{2+} exchange cycle. Therefore, it is evident that although the Pb^{2+} is easily absorbed in substitution to the Na^+, the latter cannot replace Pb^{2+} even in conditions of unbalanced concentrations equilibrium. This behavior indicates that the adsorption of the Pb^{2+} ions was irreversible, facilitating thus the safe disposal after adsorption.

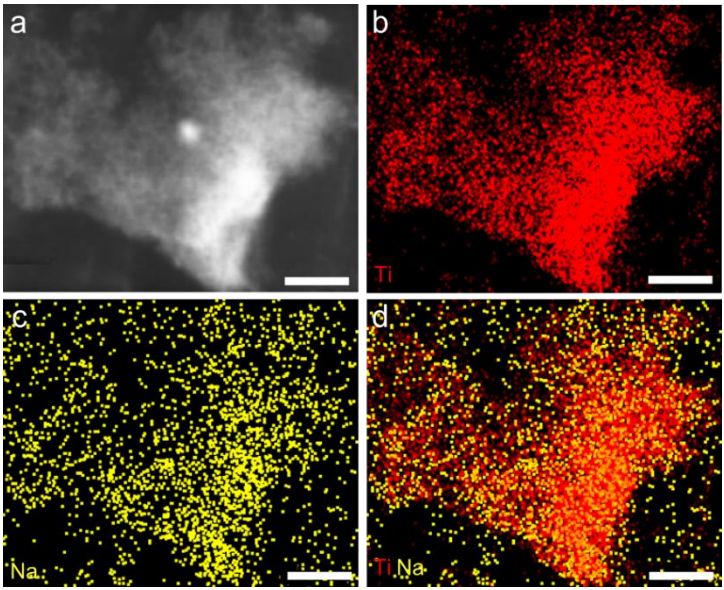

Figure 74. STEM-EDX of TNSs-SF samples after ion exchange with Na+. In (a) STEM image of the nanocomposite; in (b-c-d) EDX maps of titanium (b), sodium (c) and the merge of the two signals. The Ti/Na ratio is 4.6. Scale bar 100 nm.

In Figures 74 is shown the STEM images and the related EDX mapping of TNSs-Na-SF before the exchange with Pb^{2+}. Na^{+} looks homogeneously intercalated inside the TNSs matrix further proving the efficacy of the TMA^{+} removal. Upon dipping the TNSs-Na-SF in the Pb^{2+} solution, the STEM-EDX study reveals the presence of Pb^{2+} dispersed throughout the TNSs structure without any signature of residual Na^{+}(Figure 75).

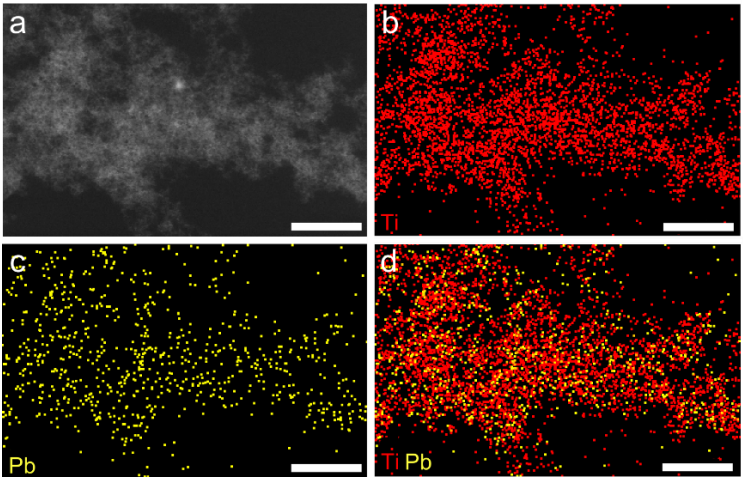

Figure 76. STEM-EDX of TNSs-SF samples after ion exchange with Na^+ and then with Pb^{2+}. In (a) STEM image of the nanocomposite; in (b-c-d) EDX maps of titanium (b), lead (c) and the merge of the two signals. The Ti/Pb ratio is 4.9. Scale bar 200 nm.

The XPS analysis corroborate these results. As the XPS

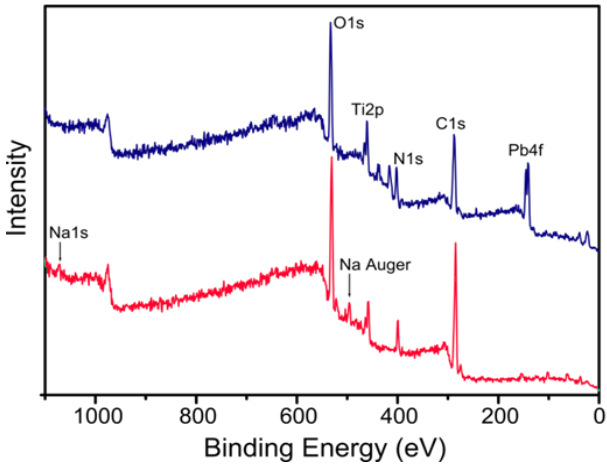

Figure 75. XPS survey spectra of TNSs-Na-SF composites before (red line) and after incubation with Pb^{2+} (blue line).

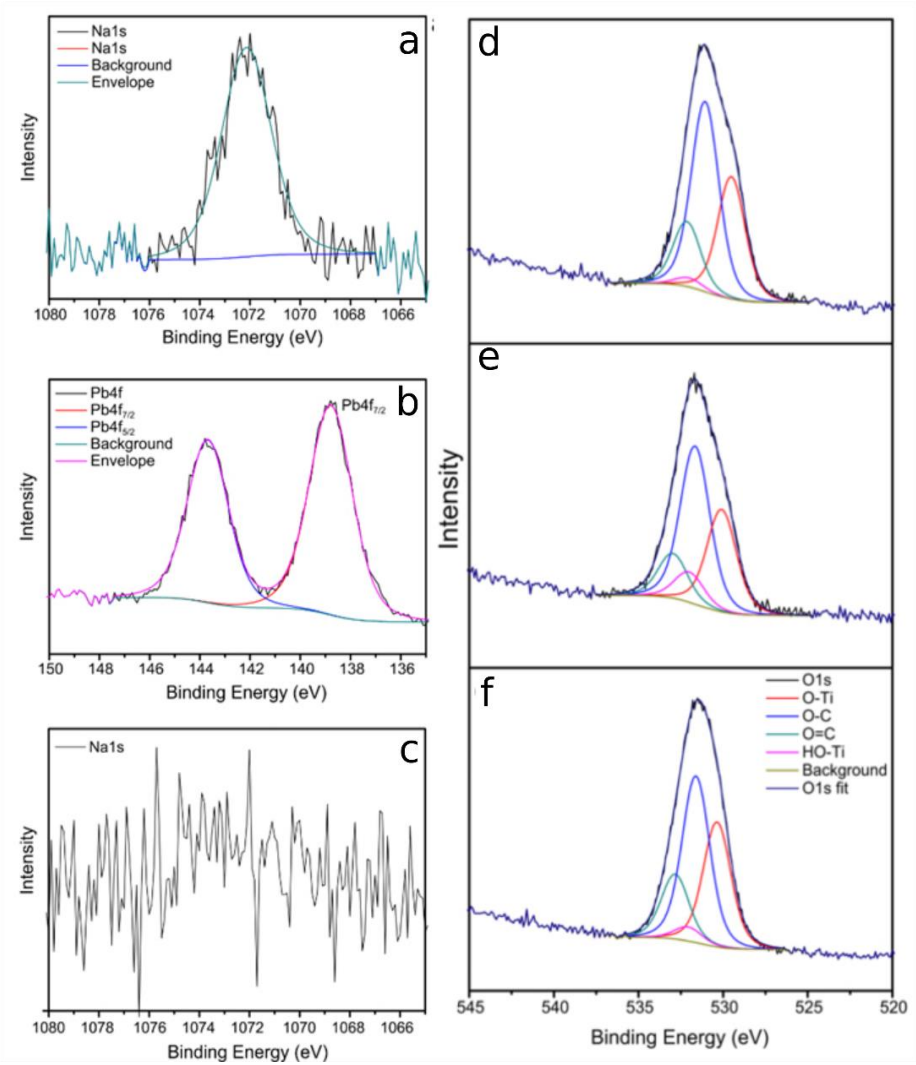

Figure 77. XPS high resolution spectra of TNSs-SF after incubation with Na^+ and Pb^{2+}. In (a) and (c) Na1s spectra respectively before and after Pb^{2+} exchange; in (b) Pb4f spectrum (after Pb^{2+} exchange). (d-e-f) O1s spectra referred to: (a) TNSs-SF, (b) TNSs-Na-SF, (c) TNSs-Pb-SF composites.

survey spectra show (Figure 76), after the incubation in

the Pb^{2+} solution the signal related to Na1s, as well as the strong Auger peak at 497 eV, disappear, while at the same time the Pb signal emerges. Furthermore, the high resolution XPS spectra of the Na1s signal (Figure 77) centred at the typical binding energy of 1072.2 eV[333] becomes negligible after dipping in the Pb^{2+} solution. On the other hand, the signal ascribed to the $Pb4f_{7/2}$ at 138.8 eV emerges after the dipping process. The difference of binding energies (Δ=4.89 eV) between the $Pb4f_{5/2}$ and $Pb4f_{7/2}$ is consistent with the Pb in +2 oxidation state.[334] The high resolution O1s XPS spectra of the TNSs-SF nanocomposite after ion exchange with Na^+ and Pb^{2+} (Figure 77 d, e, f) show that the [Ti-O] component ascribed to the TNSs lattice experiences very little changes. This behaviour is consistent with the TNSs structure retention and an ion exchange process accordingly to what observed by Liu et al.[287] In contrast with ion exchange theory, where a bivalent cation exchanges two monovalent cations, after the Na^+ exchange with the TMA^+, the TNSs-Na-SF sorbs ~0.81mmol/g of Pb^{2+} and releases a comparable amount of Na^+ (~0.73 mmol/g). Nonetheless, XPS analysis showed

that the hydroxyl moieties increase after the Na^+ exchange with the TMA^+ component (2.4%±0.5% for the TNSs-SF and 10.0%±0.5% for the TNSs-Na-SF), indicating that the Na^+ the TNSs interaction sites, leaving a higher content of available -OH groups, which belong to the TNSs structure. On the other hand, after the interaction of the TNSs-Na-SF sample with the Pb^{2+} the -OH component decreases to 3.8±0.5%, indicating that the Pb^{2+} not only replaces all the Na^+ but also a great amount of the -OH groups (Table 10).

Table 10. Species percentage calculated on O1s components XPS spectra

Samples	O-Ti (%)	O-C (%)	HO-Ti (%)	O=C (%)
TNSs-SF	31.6±0.5	49.2±0.5	2.4±0.5	16.8±0.5
TNSs-Na-SF	30.5±0.5	47.2±0.5	10.0±0.5	13.3±0.5
TNSs-Pb-SF	33.7±0.5	45.0±0.5	3.8±0.5	17.5±0.5

Furthermore, the variation of the carboxylic moieties towards higher binding energies of the O1s components (Figure 77 d, e) upon the Na^+ and Pb^{2+} ions sorption could be an indication of ions chelation also from the SF species.[335] The substitution of the interlamellar counter ion could affect the structure of the TNSs influencing the relative interlamellar distance. The diffractograms related to

the samples before and after the various ion exchange procedure are shown in Figure 78. Interestingly, calculating the interlamellar distances using the Bragg's law, it was observed that when the TNSs are enwrapped in the fibroin matrix and subsequently exposed to the ion exchange procedure, the peak at 7.8° experiences a shift to-

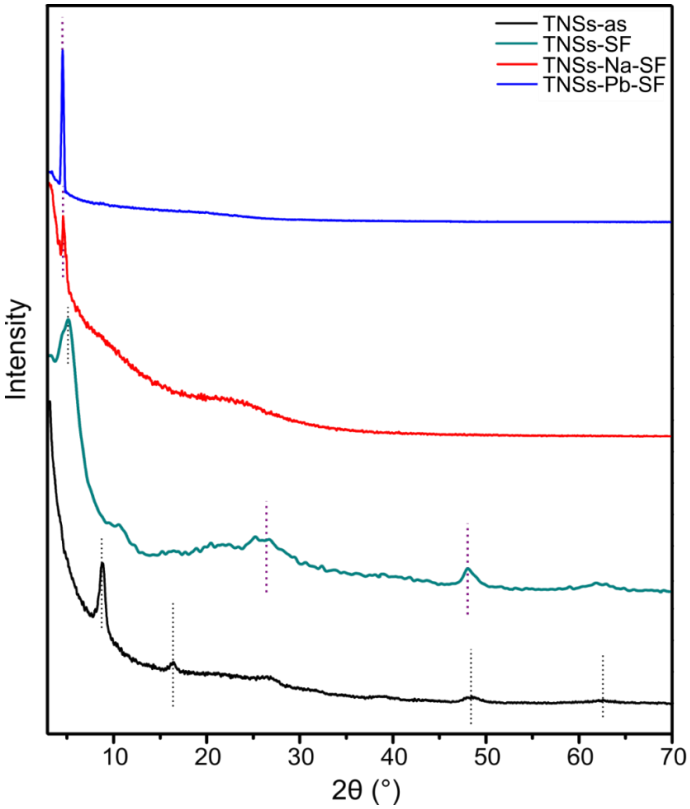

Figure 78. XRD patterns referred to as-prepared TNSs and to the different treated TNSs-SF composites.

wards lower angles. In particular, the lamellae are separated with a distance of 1.8, 2.6 and 2.8 nm for the TNSs-SF, TNSs-Na-SF and TNSs-Pb-SF samples, respectively. The interlamellar distance expansion can be attributed to the presence of diverse hydrated phases of the ions and to their effect towards the crystalline structures, as already demonstrated for similar Ti-based compounds.[336] So, the interlamellar distance of the TNSs embedded in the SF films increases after the TMA^+ exchange with Na^+, and even more after the exchange of the Na^+ with Pb^{2+}. This effect could be explained in terms of the corresponding ion salt hydration degree and ion size.

Characterization of the TNSs-SF selectivity

The ion exchange behavior of the nanocomposites, and the effect of Na^+ on the sorption process were studied exposing the material to multiple ions simultaneously. The histogram in Figure 79a shows the amount of ions exchanged (uptaken or released) by the TNSs-Na-SF nanocomposite. The incubation was performed in a solution

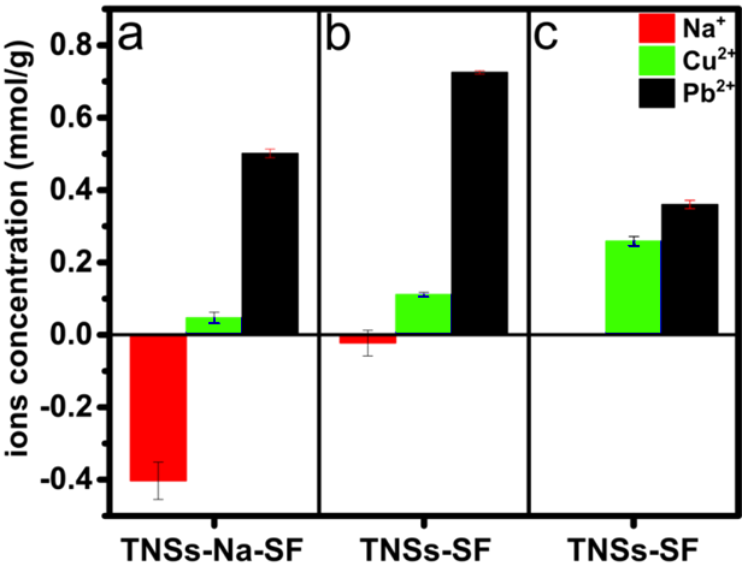

Figure 79. (a) Histogram of ions exchange (uptaken=positive values, released=negative values) on a TNSs-SF sample previously exchanged with Na^+ (TNSs-Na-SF) in a solution of Cu^{2+} and Pb^{2+} (2.1mM each) for 24 hours; (b) histogram related to TNSs-SF nanocomposite in competitive condition using a complex system constituted from three cations (Cu^{2+}, Na^+ and Pb^{2+} of 2.1mM each) after 24 hours; (c) histogram of adsorption of a TNSs-SF sample in a solution of Cu^{2+} and Pb^{2+} (2.1 mM each) for 24 hours.

containing equal concentrations of Pb^{2+} and Cu^{2+} (2.1 mM of each ion, which corresponds to 435 mg/L for Pb^{2+} and 133 mg/L for Cu^{2+}). As shown Pb^{2+} sorption capacity (0.50±0.01 mmol/g) is not affected considerably by the presence of the Cu^{2+} (Pb^{2+} sorption capacity was 0.81 mmol/g without the presence of Cu^{2+}). Contrarily, the Cu^{2+} uptake is very low, showing a sorption capacity of

0.05±0.01 mmol/g. As described above, Na^+ release is proportional to the amount of adsorbed ions. This result demonstrated that the TNSs-Na-SF samples selectively uptake Pb^{2+} in the presence of Cu^{2+}. To understand the Na^+ role in the selectivity of the nanocomposites towards Pb^{2+} TNSs-SF film have been incubated in a solution containing equal concentrations of Na^+, Cu^{2+} and Pb^{2+} (2.1 mM of each ion) (Figure 79b). Again, TNSs-SF sample demonstrated to favor the sorption of Pb^{2+}, which was removed with a sorption capacity of 0.73±0.01 mmol/g, similarly to what observed in the only-Pb^{2+} ions solution, reported above. Only 0.11 mmol/g of Cu^{2+} and no Na^+ ions were sorbed. The results changed in the absence of Na^+. As shown in Figure 79c, the TNSs-SF sample is slightly more selective for the Pb^{2+} with respect to the Cu^{2+} with sorption capacities of about 0.36±0.01 and 0.26±0.01 mmol/g, respectively. The two sorption values are comparable lower than the single ion removal for both types of ions. The sum of the two ion contributions gives a sorption capacity value of 0.62mmol/g, close to the previously calculated maximum sorption capacity of the system. The stronger affinity of Pb^{2+} towards the TNSs compared to

Cu^{2+} can be related to the different hydration energy of the ions.[287,337] Although ions with smaller radii such as Cu^{2+} (0.73 Å, lower compared to Pb^{2+} having a radius of 1.19 Å)[338] can diffuse easily, ions with a lower hydration energy such as the Pb^{2+} (the free energy of hydration of Pb^{2+} is 1425 kJ/mol while for Cu^{2+} is 2085 kJ/mol)[339] dissociated easily from water molecules making their exchange in the titanate layers more energy favorable.[287] During the sorption of the cations in the TNSs structure diverse mechanisms take place.[20,36] Initially, the hydrated metal ions are dissociated into bare ions, then the cations are electrostatically attracted by negatively charged titanates. Metal cations with higher valence are attracted with a larger electrostatic force. Finally, the cations are exchanged with the existing interlayered ions. The mechanism efficiency is strictly dependent on the cation hardness or softness according to Pearson's hard-soft acid-base (HSAB) principle,[340] where hard acids bind strongly to hard bases and soft acids bind strongly to soft bases. In this context Pb^{2+}, considered an acid softer than Na^{+} (absolute hardness of Pb^{2+} 8.5 and of Na^{+} 21.1), [341] is advantaged in the interaction with a soft base such as TNSs.[327]

Copper, on the other hand, is strongly afflicted by the presence Na^+ that alters significantly its weak interaction with TNSs compromising its sorption.[287] The high affinity of Pb^{2+} towards TNSs resultant, supported by similar observations obtained on Titanate-nanotubes,[287] could promote the application of TNSs-SF based composites in complex aquatic environments such as oceans.

Conclusion

Metal oxide nanostructures exhibit good properties for the removal of heavy metal ions from water and can be structured in several shapes. However, focusing on the application in the environmental field should not underestimate the risks related to the dispersion of nanomaterials in the environment. In fact, to date the use of nanomaterials for water treatment is limited both by production costs and by the difficult management of the material itself. This study demonstrated that nanocomposites are an efficient alternative to combine the good heavy metal removal performance of metal oxides

nanostructures with the stability and safety of solid polymeric material. The TNSs-SF nanocomposite produced showed high sorption capacity of 0.73 ± 0.02 mmol/g towards Pb^{2+}, Hg^{2+} and Cu^{2+}. When transformed to the maximum removal capacity of the bare TNSs fraction inside the composite it reaches 1.46 mmol/g, which is in the upper limit of the values presented so far in the literature for freestanding titanates (between 0.50 and 2.64 mmol/g).[287–289,295,331] Therefore the SF matrix does not affects the ability of the titanates to efficiently interact with the metal ions. Therefore entrapping the TNSs in the solid structure, prevents the risk of release of those nanostructures in the aqueous medium without affecting their efficiency to remove metal ions. Moreover, the TNSs-SF selectivity toward Pb^{2+} is significantly affected by the presence of Na^{+}, paving the way to the application of TNS–SF-based composites under real condition, in complex aquatic environments.

Conclusions

Managing the problem of global water pollution requires the implementation of new policies, technologies and scientific advances. Persistent contaminants such as plastics and heavy metal ions, capable of infiltrating the food chain and accumulating, are a great risk to the health of the ecosystem and of human. Sometimes, as for NPs, due to the lack of suitable methodologies, the study of emerging pollutants is limited to the use of inaccurate synthetic models and needs to find new approaches. In other cases, the obstacle to tackling the water pollution problem is due to the difficulty in exporting the technologies developed in the laboratory on a real scale.

In this thesis, it was explored the development of a new NP model and the investigation on its behaviour and fate in aqueous and biological environment. Furthermore, the possibility of exploiting the high efficiency of nanotechnologies for the removal of heavy metal ions from water has been investigated, overcoming the application limits by developing a nanocomposite.

In particular, the following conclusions can be deduced from this thesis work:

Nanoplastics: model development and assessment:

- Pulsed Laser ablation in water is a versatile top-down approach to synthesize NPs. Pulsed laser ablation allowed to produce nanoparticles without impurities, chemical precursors, and their by-products.

- Chemical analysis demonstrated the validity of the developed PET NP model, since, in accordance to what has been observed in UV-exposed plastic materials in the environment, organic acid groups are exposed on the surface of laser-ablated NPs.

- NPs showed a long-term colloidal stability in pure water. Salt concentration higher than 700 mM affect the system stability inducing homo-aggregation and precipitation. In the biological media the formation of a protein corona leads to a stability even beyond the critical coagulation concentration.

- NPs can be uptaken by cells and can pass through the Caco-2 intestinal barrier model. However no acute toxicity has been observed.

Interactions of Nanoplastics with water contaminants and their impact on cells

- The chemical characteristic of the PET NPs allows the formation of interactions with contaminants. The ability of NPs to accumulate up to 0.036 g/g_{NP} of Levofloxacin, 0.034 g/g_{NP} of Glyphosate and 0.014 g/g_{NP} of Hg^{2+} has been demonstrated.

- The absorption of molecules on NPs influences the physical and chemical properties of the pollutant and causes the alteration of their colloidal

stability in water, inducing the formation of cluster and the increase of their D_H.

- The biological effect of the complex contaminant-NP assessed *in vitro* on Caco-2 cells and macrophages indicate no acute toxicity. Nevertheless, the preliminary metabolomic results reported an alteration of the metabolic pattern. Results are different in the two cell types and change in presence of bare NPs or contaminant-NP complexes.

Titanates-fibroin nanocomposites for the heavy metal removal from water

- It was produced and characterized a nanocomposite made of TNSs immobilized in a solid matrix of regenerated silk-fibroin as a novel heavy metal ions removal solid system. The capacity of this nanocomposite to remove Pb^{2+}, Hg^{2+} and Cu^{2+} from water was investigated, reveling a removal capacity of ~73 mmol/g for all the ions tested.

- The composite can efficiently retain the adsorbed ions and the TNSs. This prevents the risk of release of the nanostructures in the aqueous medium and

eliminates any possible concern due to side-contamination.

- The substitution of TMA^+ with Na^+, inside the titanates nanostructures allows to produce a more environmentally friendly material, without affecting its performance in heavy metal ions removal. Moreover, the presence of Na^+ in the material increased its sorption selectivity toward Pb^{2+}.

List of publications

- **Davide Magrì**, Gianvito Caputo, Giovanni Perotto, Alice Scarpellini, Elena Colusso, Filippo Drago, Alessandro Martucci, Athanassia Athanassiou, Despina Fragouli, "Titanate Fibroin Nanocomposites: A Novel Approach for the Removal of Heavy-Metal Ions from water" ACS applied materials & interfaces, (2017), 10 (1), 651-659
- Javier Pinto, **Davide Magrì,** Paola Valentini, Francisco Palazon, José Alejandro Heredia-Guerrero, Simone Lauciello, Suset Barroso-Solares, Luca Ceseracciu, Pier Paolo Pompa, Athanassia Athanassiou, Despina Fragouli, "Antibacterial melamine foams decorated with in situ synthesized silver nanoparticles",ACS applied materials & interfaces, (2018), 10 (18), 16095-16104
- **Davide Magrì**, Paola Sánchez-Moreno, Gianvito Caputo, Francesca Gatto, Marina Veronesi, Giuseppe Bardi, Tiziano Catelani, Daniela Guarnieri, Athanassia Athanassiou, Pier Paolo Pompa, Despina Fragouli "Laser Ablation as a Versatile Tool To Mimic Polyethylene Terephthalate Nanoplastic Pollutants: Characterization and Toxicology Assessment", ACS Nano, (2018), 12 (8), 7690-7700
- Enrique Lallana-Ozores, Roberto Donno, **Davide Magrì**, Katie Barker, Zahid Nazir, Kevin Treacher, M. Jayne Lawrence, Marianne Ashford, Nicola Tirelli, "Microfluidic-assisted nanoprecipitation of (PEGylated) poly (d,llactic acid- co-caprolactone): Effect of macromolecular and

microfluidic parameters on particle size and paclitaxel encapsulation", International Journal of Pharmaceutics, (2018), 548 (1), 530-539

- Laura Campagnolo, Davide Morselli, **Davide Magrì**, Alice Scarpellini, Cansunur Demirci, Massimo Colombo, Athanassia Athanassiou, Despina Fragouli, "Silk Fibroin/Orange Peel Foam: An Efficient Biocomposite for Water Remediation", Advanced Sustainable Systems, (2019), 3, 1800097

Oral presentations and posters

- Oral contribution "Merck Young Chemists Symposium", Rimini (Italy), October 25th-27th, 2017;
- Poster contribution "NanoBio&Med2017 International Conference", Barcelona (Spain), November 22nd-24th, 2017;
- Oral contribution "Nanotexnology 2018 International Conference", Thessaloniki, Greece, July 2nd-6th 2018.

References

(1) 2009 - Water in a Changing World | United Nations Educational, Scientific and Cultural Organization http://www.unesco.org/new/en/natural-sciences/environment/water/wwap/wwdr/wwdr3-2009/ (accessed Oct 18, 2018).

(2) Huntington, T. G. Evidence for Intensification of the Global Water Cycle: Review and Synthesis. *J. Hydrol.* **2006**, *319* (1), 83–95. https://doi.org/10.1016/j.jhydrol.2005.07.003.

(3) Oki, T.; Kanae, S. Global Hydrological Cycles and World Water Resources. *Science* **2006**, *313* (5790), 1068–1072. https://doi.org/10.1126/science.1128845.

(4) Schwarzenbach, R. P.; Escher, B. I.; Fenner, K.; Hofstetter, T. B.; Johnson, C. A.; Gunten, U. von; Wehrli, B. The Challenge of Micropollutants in Aquatic Systems. *Science* **2006**, *313* (5790), 1072–1077. https://doi.org/10.1126/science.1127291.

(5) Schwarzenbach, R. P.; Egli, T.; Hofstetter, T. B.; von Gunten, U.; Wehrli, B. Global Water Pollution and Human Health. *Annu. Rev. Environ. Resour.* **2010**, *35* (1), 109–136. https://doi.org/10.1146/annurev-environ-100809-125342.

(6) Álvarez-Muñoz, D.; Llorca, M.; Blasco, J.; Barceló, D. Chapter 1 - Contaminants in the Marine Environment. In *Marine Ecotoxicology*; Blasco, J., Chapman, P. M., Campana, O., Hampel, M., Eds.; Academic Press, 2016; pp 1–34. https://doi.org/10.1016/B978-0-12-803371-5.00001-1.

(7) Shao, M.; Tang, X.; Zhang, Y.; Li, W. City Clusters in China: Air and Surface Water Pollution. *Front. Ecol. Environ.* **2006**, *4* (7), 353–361. https://doi.org/10.1890/1540-9295(2006)004[0353:CCICAA]2.0.CO;2.

(8) Calvo-Flores, F. G.; Isac-Garcia, J.; Jiménez, J. A. D.; Dobado, J. A. *Emerging Pollutants: Origin, Structure, and Properties*; John Wiley & Sons, 2018.

(9) Albaigés, J. Environmental Organic Chemistry, 3rd Edition, by R. P. Schwarzenbach, Ph. M. Gschwend and D. M. Imboden, New Jersey, USA, Wiley-Interscience, 2017, 1026 Pp., € 144 (Paperback), € 129.99 (E-Book), ISBN 978-1-118-76723-8. *Int. J. Environ. Anal. Chem.* **2017**, *97* (4), 398–399. https://doi.org/10.1080/03067319.2017.1318869.

(10) Boxall, A. B. A. New and Emerging Water Pollutants Arising from Agriculture. **2012**, 49.

(11) Plastics Europe. Plastics - the Facts 2017 https://www.plasticseurope.org/en/resources/publications/274-plastics-facts-2017 (accessed Oct 18, 2018).

(12) Mateo-Sagasta, J.; Zadeh, S., M.; Turral, H.; Burke, J. *Water Pollution from Agriculture: A Global Review. Executive Summary*; Rome, Italy: FAO Colombo, Sri Lanka: International Water Management Institute (IWMI). CGIAR Research Program on Water, Land and Ecosystems (WLE)., 2017.

(13) Nizzoli, D.; Bartoli, M.; Azzoni, R.; Longhi, D.; Castaldelli, G.; Viaroli, P. Denitrification in a Meromictic Lake and Its Relevance to Nitrogen Flows within a Moderately Impacted Forested Catchment. *Biogeochemistry* **2018**, *137* (1), 143–161. https://doi.org/10.1007/s10533-017-0407-9.

(14) Jobling, S.; Nolan, M.; Tyler, C. R.; Brighty, G.; Sumpter, J. P. Widespread Sexual Disruption in Wild Fish. *Environ. Sci. Technol.* **1998**, *32* (17), 2498–2506.

(15) Ohe, T.; Watanabe, T.; Wakabayashi, K. Mutagens in Surface Waters: A Review. *Mutat. Res. Mutat. Res.* **2004**, *567* (2), 109–149. https://doi.org/10.1016/j.mrrev.2004.08.003.

(16) Ross, P. S. Report of the Study Group on Marine Pollutants http://meetings.pices.int/publications/scientific-reports/Report46/Rpt46.pdf (accessed Jul 25, 2018).

(17) King, J.; Comeau, C.; Cantwell, M.; Borden, T. Chapter 9, Legacy Contaminants. In *The State of Narragansett Bay and Its Watershed Technical Report*; 2017; pp 192–210.

(18) Goutte, A.; Barbraud, C.; Herzke, D.; Bustamante, P.; Angelier, F.; Tartu, S.; Clément-Chastel, C.; Moe, B.; Bech, C.; Gabrielsen, G. W.; et al. Survival Rate and Breeding Outputs in a High Arctic Seabird Exposed to Legacy Persistent Organic Pollutants and Mercury. *Environ. Pollut.* **2015**, *200*, 1–9. https://doi.org/10.1016/j.envpol.2015.01.033.

(19) Tchounwou, P. B.; Yedjou, C. G.; Patlolla, A. K.; Sutton, D. J. Heavy Metals Toxicity and the Environment. *EXS* **2012**, *101*, 133–164. https://doi.org/10.1007/978-3-7643-8340-4_6.

(20) Farré, M. la; Pérez, S.; Kantiani, L.; Barceló, D. Fate and Toxicity of Emerging Pollutants, Their Metabolites and Transformation Products in the Aquatic Environment. *TrAC Trends Anal. Chem.* **2008**, *27* (11), 991–1007. https://doi.org/10.1016/j.trac.2008.09.010.

(21) Iñiguez, M. E.; Conesa, J. A.; Fullana, A. Microplastics in Spanish Table Salt. *Sci. Rep.* **2017**, *7* (1), 8620. https://doi.org/10.1038/s41598-017-09128-x.

(22) Reed, C. Dawn of the Plasticene Age. *New Sci.* **2015**, *225* (3006), 28–32. https://doi.org/10.1016/S0262-4079(15)60215-9.

(23) Ross, N. L. The "Plasticene" Epoch? *Elements* **2018**, *14* (5), 291–291. https://doi.org/10.2138/gselements.14.5.291.

(24) Zalasiewicz, J.; Waters, C. N.; Ivar do Sul, J. A.; Corcoran, P. L.; Barnosky, A. D.; Cearreta, A.; Edgeworth, M.; Gałuszka, A.; Jeandel, C.; Leinfelder, R.; et al. The Geological Cycle of Plastics and Their Use as a Stratigraphic Indicator of the Anthropocene. *Anthropocene* **2016**, *13*, 4–17. https://doi.org/10.1016/j.ancene.2016.01.002.

(25) Geyer, R.; Jambeck, J. R.; Law, K. L. Production, Use, and Fate of All Plastics Ever Made. *Sci. Adv.* **2017**, *3* (7), e1700782. https://doi.org/10.1126/sciadv.1700782.

(26) Andrady, A. L.; Neal, M. A. Applications and Societal Benefits of Plastics. *Philos. Trans. R. Soc. B Biol. Sci.* **2009**, *364* (1526), 1977–1984. https://doi.org/10.1098/rstb.2008.0304.

(27) Rochman, C. M.; Browne, M. A.; Halpern, B. S.; Hentschel, B. T.; Hoh, E.; Karapanagioti, H. K.; Rios-Mendoza, L. M.; Takada, H.; Teh, S.; Thompson, R. C. Policy: Classify Plastic Waste as Hazardous. *Nature* **2013**, *494* (7436), 169–171. https://doi.org/10.1038/494169a.

(28) Rochman, C. M.; Cook, A.-M.; Koelmans, A. A. Plastic Debris and Policy: Using Current Scientific Understanding to Invoke Positive Change. *Environ. Toxicol. Chem.* **2016**, *35* (7), 1617–1626. https://doi.org/10.1002/etc.3408.

(29) Addamo, A. M.; Hanke, G.; Laroche, P.; MSFD Technical Group on Marine Litter; European Commission; Joint Research Centre. *Top Marine Beach Litter Items in Europe a Review and Synthesis Based on Beach Litter Data.*; 2017.

(30) Jambeck, J. R.; Geyer, R.; Wilcox, C.; Siegler, T. R.; Perryman, M.; Andrady, A.; Narayan, R.; Law, K. L. Plastic Waste Inputs from Land into the Ocean. *Science* **2015**, *347* (6223), 768–771. https://doi.org/10.1126/science.1260352.

(31) Browne, M. A.; Chapman, M. G.; Thompson, R. C.; Amaral Zettler, L. A.; Jambeck, J.; Mallos, N. J. Spatial and Temporal Patterns of Stranded Intertidal Marine Debris: Is There a Picture of Global Change? *Environ. Sci. Technol.* **2015**, *49* (12), 7082–7094. https://doi.org/10.1021/es5060572.

(32) Eriksen, M.; Lebreton, L. C. M.; Carson, H. S.; Thiel, M.; Moore, C. J.; Borerro, J. C.; Galgani, F.; Ryan, P. G.; Reisser, J. Plastic Pollution in the World's Oceans: More than 5 Trillion Plastic Pieces Weighing over 250,000 Tons Afloat at Sea. *PloS One* **2014**, *9* (12), e111913. https://doi.org/10.1371/journal.pone.0111913.

(33) Eriksen, M.; Mason, S.; Wilson, S.; Box, C.; Zellers, A.; Edwards, W.; Farley, H.; Amato, S. Microplastic Pollution in the Surface Waters of the Laurentian Great Lakes. *Mar. Pollut. Bull.* **2013**, *77* (1–2), 177–182.

(34) Galgani, F.; Hanke, G.; Maes, T. Global Distribution, Composition and Abundance of Marine Litter. In *Marine Anthropogenic Litter*; Bergmann, M., Gutow, L., Klages, M., Eds.; Springer International Publishing: Cham, 2015; pp 29–56. https://doi.org/10.1007/978-3-319-16510-3_2.

(35) Browne, M. A.; Galloway, T. S.; Thompson, R. C. Spatial Patterns of Plastic Debris along Estuarine Shorelines. *Environ. Sci. Technol.* **2010**, *44* (9), 3404–3409. https://doi.org/10.1021/es903784e.

(36) Katsanevakis, S.; Verriopoulos, G.; Nicolaidou, A.; Thessalou-Legaki, M. Effect of Marine Litter on the Benthic Megafauna of Coastal Soft Bottoms: A Manipulative Field Experiment. *Mar. Pollut. Bull.* **2007**, *54* (6), 771–778. https://doi.org/10.1016/j.marpolbul.2006.12.016.

(37) Donohue, M. J.; Boland, R. C.; Sramek, C. M.; Antonelis, G. A. Derelict Fishing Gear in the Northwestern Hawaiian Islands: Diving Surveys and Debris Removal in 1999 Confirm Threat to Coral Reef Ecosystems. *Mar. Pollut. Bull.* **2001**, *42* (12), 1301–1312.

(38) Woodall, L. C.; Robinson, L. F.; Rogers, A. D.; Narayanaswamy, B. E.; Paterson, G. L. J. Deep-Sea Litter: A Comparison of Seamounts, Banks and a Ridge in the Atlantic and Indian Oceans Reveals Both Environmental and Anthropogenic Factors Impact Accumulation and Composition. *Front. Mar. Sci.* **2015**, *2*. https://doi.org/10.3389/fmars.2015.00003.

(39) Obbard, R. W.; Sadri, S.; Wong, Y. Q.; Khitun, A. A.; Baker, I.; Thompson, R. C. Global Warming Releases Microplastic Legacy Frozen in Arctic Sea Ice. *Earths Future* **2014**, *2* (6), 315–320. https://doi.org/10.1002/2014EF000240.

(40) Imhof, H. K.; Ivleva, N. P.; Schmid, J.; Niessner, R.; Laforsch, C. Contamination of Beach Sediments of a Subalpine Lake with Microplastic Particles. *Curr. Biol. CB* **2013**, *23* (19), R867-868. https://doi.org/10.1016/j.cub.2013.09.001.

(41) Zbyszewski, M.; Corcoran, P. L.; Hockin, A. Comparison of the Distribution and Degradation of Plastic Debris along Shorelines of the Great Lakes, North America. *J. Gt. Lakes Res.* **2014**, *40* (2), 288–299. https://doi.org/10.1016/j.jglr.2014.02.012.

(42) Lechner, A.; Keckeis, H.; Lumesberger-Loisl, F.; Zens, B.; Krusch, R.; Tritthart, M.; Glas, M.; Schludermann, E. The Danube so Colourful: A Potpourri of Plastic Litter Outnumbers Fish Larvae in Europe's Second Largest River. *Environ. Pollut. Barking Essex 1987* **2014**, *188* (100), 177–181. https://doi.org/10.1016/j.envpol.2014.02.006.

(43) Bergmann, M.; Tekman, M. B.; Gutow, L. Marine Litter: Sea Change for Plastic Pollution. *Nature* **2017**, *544* (7650), 297–297. https://doi.org/10.1038/544297a.

(44) Webb, H. K.; Arnott, J.; Crawford, R. J.; Ivanova, E. P. Plastic Degradation and Its Environmental Implications with Special Reference to Poly(Ethylene Terephthalate). *Polymers* **2012**, *5* (1), 1–18. https://doi.org/10.3390/polym5010001.

(45) Levchik, S. V.; Weil, E. D. A Review on Thermal Decomposition and Combustion of Thermoplastic Polyesters. *Polym. Adv. Technol.* **2004**, *15* (12), 691–700. https://doi.org/10.1002/pat.526.

(46) Bergeret, A.; Ferry, L.; Ienny, P. Influence of the Fibre/Matrix Interface on Ageing Mechanisms of Glass Fibre Reinforced Thermoplastic Composites (PA-6,6, PET, PBT) in a Hygrothermal Environment. *Polym. Degrad. Stab.* **2009**, *9* (94), 1315–1324. https://doi.org/10.1016/j.polymdegradstab.2009.04.009.

(47) Kint, D.; Muñoz-Guerra, S. A Review on the Potential Biodegradability of Poly(Ethylene Terephthalate). *Polym. Int.* **1999**, *48* (5), 346–352. https://doi.org/10.1002/(SICI)1097-0126(199905)48:5<346::AID-PI156>3.0.CO;2-N.

(48) Khoonkari, M.; Haghighi, A. H.; Sefidbakht, Y.; Shekoohi, K.; Ghaderian, A. Chemical Recycling of PET Wastes with Different Catalysts

https://www.hindawi.com/journals/ijps/2015/124524/ref/ (accessed Nov 21, 2018). https://doi.org/10.1155/2015/124524.
(49) Plastic Europe. Plastics - the Facts 2016 http://www.plasticseurope.org/Document/plastics---the-facts-2016-15787.aspx?FolID=2 (accessed Oct 17, 2017).
(50) Köpnick, H.; Schmidt, M.; Brügging, W.; Rüter, J.; Kaminsky, W. Polyesters. In *Ullmann's Encyclopedia of Industrial Chemistry*; American Cancer Society, 2000. https://doi.org/10.1002/14356007.a21_227.
(51) Worm, B.; Lotze, H. K.; Jubinville, I.; Wilcox, C.; Jambeck, J. Plastic as a Persistent Marine Pollutant. *Annu. Rev. Environ. Resour.* **2017**, *42* (1), 1–26. https://doi.org/10.1146/annurev-environ-102016-060700.
(52) Greven, A.-C.; Merk, T.; Karagöz, F.; Mohr, K.; Klapper, M.; Jovanović, B.; Palić, D. Polycarbonate and Polystyrene Nanoplastic Particles Act as Stressors to the Innate Immune System of Fathead Minnow (Pimephales Promelas). *Environ. Toxicol. Chem.* **2016**, *35* (12), 3093–3100. https://doi.org/10.1002/etc.3501.
(53) Andrady, A. L. Assessment of Environmental Biodegradation of Synthetic Polymers. *J. Macromol. Sci. Part C* **1994**, *34* (1), 25–76. https://doi.org/10.1080/15321799408009632.
(54) Andrady, A. L. Microplastics in the Marine Environment. *Mar. Pollut. Bull.* **2011**, *62* (8), 1596–1605. https://doi.org/10.1016/j.marpolbul.2011.05.030.
(55) Gewert, B.; Plassmann, M. M.; MacLeod, M. Pathways for Degradation of Plastic Polymers Floating in the Marine Environment. *Environ. Sci. Process. Impacts* **2015**, *17* (9), 1513–1521. https://doi.org/10.1039/c5em00207a.
(56) Mattsson, K.; Hansson, L.-A.; Cedervall, T. Nano-Plastics in the Aquatic Environment. *Environ. Sci. Process. Impacts* **2015**, *17* (10), 1712–1721. https://doi.org/10.1039/C5EM00227C.
(57) Wei, R.; Zimmermann, W. Microbial Enzymes for the Recycling of Recalcitrant Petroleum-Based Plastics: How Far Are We? *Microb. Biotechnol.* **2017**, *10* (6), 1308–1322. https://doi.org/10.1111/1751-7915.12710.
(58) Zhang, J.; Wang, X.; Gong, J.; Gu, Z. A Study on the Biodegradability of Polyethylene Terephthalate Fiber and Diethylene Glycol Terephthalate. *J. Appl. Polym. Sci.* **2004**, *93* (3), 1089–1096. https://doi.org/10.1002/app.20556.
(59) Danso, D.; Schmeisser, C.; Chow, J.; Zimmermann, W.; Wei, R.; Leggewie, C.; Li, X.; Hazen, T.; Streit, W. R. New Insights into the Function and Global Distribution of Polyethylene Terephthalate (PET)-Degrading Bacteria and Enzymes in Marine and Terrestrial Metagenomes. *Appl Env. Microbiol* **2018**, *84* (8), e02773-17. https://doi.org/10.1128/AEM.02773-17.
(60) Yoshida, S.; Hiraga, K.; Takehana, T.; Taniguchi, I.; Yamaji, H.; Maeda, Y.; Toyohara, K.; Miyamoto, K.; Kimura, Y.; Oda, K. A Bacterium That Degrades and Assimilates Poly(Ethylene Terephthalate). *Science* **2016**, *351* (6278), 1196–1199. https://doi.org/10.1126/science.aad6359.
(61) Suaria, G.; Avio, C. G.; Mineo, A.; Lattin, G. L.; Magaldi, M. G.; Belmonte, G.; Moore, C. J.; Regoli, F.; Aliani, S. The Mediterranean Plastic Soup: Synthetic Polymers in Mediterranean Surface Waters. *Sci. Rep.* **2016**, *6*, 37551. https://doi.org/10.1038/srep37551.
(62) Koelmans, A. A.; Kooi, M.; Law, K. L.; Sebille, E. van. All Is Not Lost: Deriving a Top-down Mass Budget of Plastic at Sea. *Environ. Res. Lett.* **2017**, *12* (11), 114028. https://doi.org/10.1088/1748-9326/aa9500.
(63) Gigault, J.; Pedrono, B.; Maxit, B.; Halle, A. T. Marine Plastic Litter: The Unanalyzed Nano-Fraction. *Environ. Sci. Nano* **2016**, *3* (2), 346–350. https://doi.org/10.1039/C6EN00008H.
(64) Lusher, A. Microplastics in the Marine Environment: Distribution, Interactions and Effects. In *Marine Anthropogenic Litter*; Springer, Cham, 2015; pp 245–307. https://doi.org/10.1007/978-3-319-16510-3_10.
(65) Koelmans, A. A.; Besseling, E.; Shim, W. J. Nanoplastics in the Aquatic Environment. Critical Review. In *Marine Anthropogenic Litter*; Springer, Cham, 2015; pp 325–340. https://doi.org/10.1007/978-3-319-16510-3_12.

(66) Koelmans, A. A.; Gouin, T.; Thompson, R.; Wallace, N.; Arthur, C. Plastics in the Marine Environment. *Environ. Toxicol. Chem.* **2014**, *33* (1), 5–10. https://doi.org/10.1002/etc.2426.

(67) Cózar, A.; Echevarría, F.; González-Gordillo, J. I.; Irigoien, X.; Úbeda, B.; Hernández-León, S.; Palma, Á. T.; Navarro, S.; García-de-Lomas, J.; Ruiz, A.; et al. Plastic Debris in the Open Ocean. *Proc. Natl. Acad. Sci.* **2014**, *111* (28), 10239–10244. https://doi.org/10.1073/pnas.1314705111.

(68) Girão, A. V.; Caputo, G.; Ferro, M. C. Chapter 6 - Application of Scanning Electron Microscopy–Energy Dispersive X-Ray Spectroscopy (SEM-EDS). In *Comprehensive Analytical Chemistry*; Rocha-Santos, T. A. P., Duarte, A. C., Eds.; Characterization and Analysis of Microplastics; Elsevier, 2017; Vol. 75, pp 153–168. https://doi.org/10.1016/bs.coac.2016.10.002.

(69) Cole, M.; Galloway, T. S. Ingestion of Nanoplastics and Microplastics by Pacific Oyster Larvae. *Environ. Sci. Technol.* **2015**, *49* (24), 14625–14632. https://doi.org/10.1021/acs.est.5b04099.

(70) EFSA Panel on Contaminants in the Food Chain (CONTAM). Presence of Microplastics and Nanoplastics in Food, with Particular Focus on Seafood. *EFSA J.* **2016**, *14* (6), 1–30. https://doi.org/10.2903/j.efsa.2016.4501.

(71) da Costa, J. P.; Santos, P. S. M.; Duarte, A. C.; Rocha-Santos, T. (Nano)Plastics in the Environment – Sources, Fates and Effects. *Sci. Total Environ.* **2016**, *566–567*, 15–26. https://doi.org/10.1016/j.scitotenv.2016.05.041.

(72) Zhang, H.; Kuo, Y.-Y.; Gerecke, A. C.; Wang, J. Co-Release of Hexabromocyclododecane (HBCD) and Nano- and Microparticles from Thermal Cutting of Polystyrene Foams. *Environ. Sci. Technol.* **2012**, *46* (20), 10990–10996. https://doi.org/10.1021/es302559v.

(73) Stephens, B.; Azimi, P.; El Orch, Z.; Ramos, T. Ultrafine Particle Emissions from Desktop 3D Printers. *Atmos. Environ.* **2013**, *79*, 334–339. https://doi.org/10.1016/j.atmosenv.2013.06.050.

(74) Alimi, O. S.; Farner Budarz, J.; Hernandez, L. M.; Tufenkji, N. Microplastics and Nanoplastics in Aquatic Environments: Aggregation, Deposition, and Enhanced Contaminant Transport. *Environ. Sci. Technol.* **2018**, *52* (4), 1704–1724. https://doi.org/10.1021/acs.est.7b05559.

(75) Zbyszewski, M.; Corcoran, P. L. Distribution and Degradation of Fresh Water Plastic Particles Along the Beaches of Lake Huron, Canada. *Water. Air. Soil Pollut.* **2011**, *220* (1), 365–372. https://doi.org/10.1007/s11270-011-0760-6.

(76) Galloway, T. S.; Cole, M.; Lewis, C. Interactions of Microplastic Debris throughout the Marine Ecosystem. *Nat. Ecol. Evol.* **2017**, *1* (5), 0116. https://doi.org/10.1038/s41559-017-0116.

(77) Galloway, T. S.; Cole, M.; Lewis, C. Interactions of Microplastic Debris throughout the Marine Ecosystem. *Nat. Ecol. Evol.* **2017**, *1* (5).

(78) Lowry, G. V.; Gregory, K. B.; Apte, S. C.; Lead, J. R. Transformations of Nanomaterials in the Environment. *Environ. Sci. Technol.* **2012**, *46* (13), 6893–6899. https://doi.org/10.1021/es300839e.

(79) Wegner, A.; Besseling, E.; Foekema, E. M.; Kamermans, P.; Koelmans, A. A. Effects of Nanopolystyrene on the Feeding Behavior of the Blue Mussel (Mytilus Edulis L.). *Environ. Toxicol. Chem.* **2012**, *31* (11), 2490–2497. https://doi.org/10.1002/etc.1984.

(80) Clark, J. R.; Cole, M.; Lindeque, P. K.; Fileman, E.; Blackford, J.; Lewis, C.; Lenton, T. M.; Galloway, T. S. Marine Microplastic Debris: A Targeted Plan for Understanding and Quantifying Interactions with Marine Life. *Front. Ecol. Environ.* **2016**, *14* (6), 317–324. https://doi.org/10.1002/fee.1297.

(81) Ter Halle, A.; Jeanneau, L.; Martignac, M.; Jardé, E.; Pedrono, B.; Brach, L.; Gigault, J. Nanoplastic in the North Atlantic Subtropical Gyre. *Environ. Sci. Technol.* **2017**, *51* (23), 13689–13697. https://doi.org/10.1021/acs.est.7b03667.

(82) Gigault, J.; Halle, A. ter; Baudrimont, M.; Pascal, P.-Y.; Gauffre, F.; Phi, T.-L.; El Hadri, H.; Grassl, B.; Reynaud, S. Current Opinion: What Is a Nanoplastic? *Environ. Pollut.* **2018**, *235*, 1030–1034. https://doi.org/10.1016/j.envpol.2018.01.024.

(83) Lusher, A. L.; Welden, N. A.; Sobral, P.; Cole, M. Sampling, Isolating and Identifying Microplastics Ingested by Fish and Invertebrates. *Anal. Methods* **2017**, *9* (9), 1346–1360. https://doi.org/10.1039/C6AY02415G.

(84) Cole, M.; Lindeque, P. K.; Fileman, E.; Clark, J.; Lewis, C.; Halsband, C.; Galloway, T. S. Microplastics Alter the Properties and Sinking Rates of Zooplankton Faecal Pellets. *Environ. Sci. Technol.* **2016**, *50* (6), 3239–3246. https://doi.org/10.1021/acs.est.5b05905.

(85) European Food Safety Authority (EFSA); Kass, G.; Moon, J.; Robinson, T. Horizon 2020: EFSA's Priority Research Topics. *EFSA Support. Publ.* **2017**, *14* (1), 1–11. https://doi.org/10.2903/sp.efsa.2017.EN-1166.

(86) Browne, M. A.; Dissanayake, A.; Galloway, T. S.; Lowe, D. M.; Thompson, R. C. Ingested Microscopic Plastic Translocates to the Circulatory System of the Mussel, Mytilus Edulis (L). *Environ. Sci. Technol.* **2008**, *42* (13), 5026–5031.

(87) von Moos, N.; Burkhardt-Holm, P.; Köhler, A. Uptake and Effects of Microplastics on Cells and Tissue of the Blue Mussel Mytilus Edulis L. after an Experimental Exposure. *Environ. Sci. Technol.* **2012**, *46* (20), 11327–11335. https://doi.org/10.1021/es302332w.

(88) Lee, K.-W.; Shim, W. J.; Kwon, O. Y.; Kang, J.-H. Size-Dependent Effects of Micro Polystyrene Particles in the Marine Copepod Tigriopus Japonicus. *Environ. Sci. Technol.* **2013**, *47* (19), 11278–11283. https://doi.org/10.1021/es401932b.

(89) Rochman, C. M.; Kurobe, T.; Flores, I.; Teh, S. J. Early Warning Signs of Endocrine Disruption in Adult Fish from the Ingestion of Polyethylene with and without Sorbed Chemical Pollutants from the Marine Environment. *Sci. Total Environ.* **2014**, *493*, 656–661. https://doi.org/10.1016/j.scitotenv.2014.06.051.

(90) Besseling, E.; Wang, B.; Lürling, M.; Koelmans, A. A. Nanoplastic Affects Growth of S. Obliquus and Reproduction of D. Magna. *Environ. Sci. Technol.* **2014**, *48* (20), 12336–12343. https://doi.org/10.1021/es503001d.

(91) Chen, Q.; Gundlach, M.; Yang, S.; Jiang, J.; Velki, M.; Yin, D.; Hollert, H. Quantitative Investigation of the Mechanisms of Microplastics and Nanoplastics toward Zebrafish Larvae Locomotor Activity. *Sci. Total Environ.* **2017**, *584–585*, 1022–1031. https://doi.org/10.1016/j.scitotenv.2017.01.156.

(92) Bouwmeester, H.; Hollman, P. C. H.; Peters, R. J. B. Potential Health Impact of Environmentally Released Micro- and Nanoplastics in the Human Food Production Chain: Experiences from Nanotoxicology. *Environ. Sci. Technol.* **2015**, *49* (15), 8932–8947. https://doi.org/10.1021/acs.est.5b01090.

(93) Chen, Q.; Yin, D.; Jia, Y.; Schiwy, S.; Legradi, J.; Yang, S.; Hollert, H. Enhanced Uptake of BPA in the Presence of Nanoplastics Can Lead to Neurotoxic Effects in Adult Zebrafish. *Sci. Total Environ.* **2017**, *609*, 1312–1321. https://doi.org/10.1016/j.scitotenv.2017.07.144.

(94) Wright, S. L.; Kelly, F. J. Plastic and Human Health: A Micro Issue? *Environ. Sci. Technol.* **2017**, *51* (12), 6634–6647. https://doi.org/10.1021/acs.est.7b00423.

(95) Nel, A.; Xia, T.; Mädler, L.; Li, N. Toxic Potential of Materials at the Nanolevel. *Science* **2006**, *311* (5761), 622–627. https://doi.org/10.1126/science.1114397.

(96) EUROPEAN COMMISSION HEALTH & CONSUMER PROTECTION DIRECTORATE-GENERAL. The Appropriateness of Existing Methodologies to Assess the Potential Risks Associated with Engineered and Adventitious Products. **2006**, No. SCENIHR/002/05.

(97) Mahler, G. J.; Esch, M. B.; Tako, E.; Southard, T. L.; Archer, S. D.; Glahn, R. P.; Shuler, M. L. Oral Exposure to Polystyrene Nanoparticles Affects Iron Absorption. *Nat. Nanotechnol.* **2012**, *7* (4), 264–271. https://doi.org/10.1038/nnano.2012.3.

(98) Koeneman, B. A.; Zhang, Y.; Westerhoff, P.; Chen, Y.; Crittenden, J. C.; Capco, D. G. Toxicity and Cellular Responses of Intestinal Cells Exposed to Titanium Dioxide. *Cell Biol. Toxicol.* **2010**, *26* (3), 225–238. https://doi.org/10.1007/s10565-009-9132-z.

(99) Bhattacharya, P.; Lin, S.; Turner, J. P.; Ke, P. C. Physical Adsorption of Charged Plastic Nanoparticles Affects Algal Photosynthesis. *J. Phys. Chem. C* **2010**, *114* (39), 16556–16561. https://doi.org/10.1021/jp1054759.

(100) Chen, C.-S.; Anaya, J. M.; Zhang, S.; Spurgin, J.; Chuang, C.-Y.; Xu, C.; Miao, A.-J.; Chen, E. Y.-T.; Schwehr, K. A.; Jiang, Y.; et al. Effects of Engineered Nanoparticles on the Assembly of Exopolymeric Substances from Phytoplankton. *PLOS ONE* **2011**, *6* (7), e21865. https://doi.org/10.1371/journal.pone.0021865.

(101) Mattsson, K.; Ekvall, M. T.; Hansson, L.-A.; Linse, S.; Malmendal, A.; Cedervall, T. Altered Behavior, Physiology, and Metabolism in Fish Exposed to Polystyrene Nanoparticles. *Environ. Sci. Technol.* **2015**, *49* (1), 553–561. https://doi.org/10.1021/es5053655.

(102) Cedervall, T.; Hansson, L.-A.; Lard, M.; Frohm, B.; Linse, S. Food Chain Transport of Nanoparticles Affects Behaviour and Fat Metabolism in Fish. *PLOS ONE* **2012**, *7* (2), e32254. https://doi.org/10.1371/journal.pone.0032254.

(103) Kashiwada, S. Distribution of Nanoparticles in the See-through Medaka (Oryzias Latipes). *Environ. Health Perspect.* **2006**, *114* (11), 1697. https://doi.org/10.1289/ehp.9209.

(104) Bergami, E.; Bocci, E.; Vannuccini, M. L.; Monopoli, M.; Salvati, A.; Dawson, K. A.; Corsi, I. Nano-Sized Polystyrene Affects Feeding, Behavior and Physiology of Brine Shrimp Artemia Franciscana Larvae. *Ecotoxicol. Environ. Saf.* **2016**, *123*, 18–25. https://doi.org/10.1016/j.ecoenv.2015.09.021.

(105) Manabe, M.; Tatarazako, N.; Kinoshita, M. Uptake, Excretion and Toxicity of Nano-Sized Latex Particles on Medaka (Oryzias Latipes) Embryos and Larvae. *Aquat. Toxicol. Amst. Neth.* **2011**, *105* (3–4), 576–581. https://doi.org/10.1016/j.aquatox.2011.08.020.

(106) Cui, R.; Kim, S. W.; An, Y.-J. Polystyrene Nanoplastics Inhibit Reproduction and Induce Abnormal Embryonic Development in the Freshwater Crustacean Daphnia Galeata. *Sci. Rep.* **2017**, *7* (1), 12095. https://doi.org/10.1038/s41598-017-12299-2.

(107) Brown, D. M.; Wilson, M. R.; MacNee, W.; Stone, V.; Donaldson, K. Size-Dependent Proinflammatory Effects of Ultrafine Polystyrene Particles: A Role for Surface Area and Oxidative Stress in the Enhanced Activity of Ultrafines. *Toxicol. Appl. Pharmacol.* **2001**, *175* (3), 191–199. https://doi.org/10.1006/taap.2001.9240.

(108) Della Torre, C.; Bergami, E.; Salvati, A.; Faleri, C.; Cirino, P.; Dawson, K. A.; Corsi, I. Accumulation and Embryotoxicity of Polystyrene Nanoparticles at Early Stage of Development of Sea Urchin Embryos Paracentrotus Lividus. *Environ. Sci. Technol.* **2014**, *48* (20), 12302–12311. https://doi.org/10.1021/es502569w.

(109) Ward, J. E.; Kach, D. J. Marine Aggregates Facilitate Ingestion of Nanoparticles by Suspension-Feeding Bivalves. *Mar. Environ. Res.* **2009**, *68* (3), 137–142. https://doi.org/10.1016/j.marenvres.2009.05.002.

(110) Booth, A. M.; Hansen, B. H.; Frenzel, M.; Johnsen, H.; Altin, D. Uptake and Toxicity of Methylmethacrylate-Based Nanoplastic Particles in Aquatic Organisms. *Environ. Toxicol. Chem.* **2016**, *35* (7), 1641–1649. https://doi.org/10.1002/etc.3076.

(111) Sussarellu, R.; Suquet, M.; Thomas, Y.; Lambert, C.; Fabioux, C.; Pernet, M. E. J.; Le Goïc, N.; Quillien, V.; Mingant, C.; Epelboin, Y.; et al. Oyster Reproduction Is Affected by Exposure to Polystyrene Microplastics. *Proc. Natl. Acad. Sci. U. S. A.* **2016**, *113* (9), 2430–2435. https://doi.org/10.1073/pnas.1519019113.

(112) Vauthier, C.; Bouchemal, K. Methods for the Preparation and Manufacture of Polymeric Nanoparticles. *Pharm. Res.* **2009**, *26* (5), 1025–1058. https://doi.org/10.1007/s11095-008-9800-3.

(113) Lambert, S.; Wagner, M. Formation of Microscopic Particles during the Degradation of Different Polymers. *Chemosphere* **2016**, *161*, 510–517. https://doi.org/10.1016/j.chemosphere.2016.07.042.

(114) Magrì, D.; Sánchez-Moreno, P.; Caputo, G.; Gatto, F.; Veronesi, M.; Bardi, G.; Catelani, T.; Guarnieri, D.; Athanassiou, A.; Pompa, P. P.; et al. Laser Ablation as a Versatile Tool To Mimic Polyethylene Terephthalate Nanoplastic Pollutants: Characterization and Toxicology Assessment. *ACS Nano* **2018**, *12* (8), 7690–7700. https://doi.org/10.1021/acsnano.8b01331.

(115) Brown, M. S.; Arnold, C. B. Fundamentals of Laser-Material Interaction and Application to Multiscale Surface Modification. In *Laser Precision Microfabrication*; Sugioka, K., Meunier, M., Piqué, A., Eds.; Springer Series in Materials Science; Springer Berlin Heidelberg: Berlin, Heidelberg, 2010; pp 91–120. https://doi.org/10.1007/978-3-642-10523-4_4.

(116) Mihailescu, I. N.; Caricato, A. P. *Pulsed Laser Ablation: Advances and Applications in Nanoparticles and Nanostructuring Thin Films*; CRC Press, 2018.

(117) Bäuerle, D. W. *Laser Processing and Chemistry*, 4th ed.; Springer-Verlag: Berlin Heidelberg, 2011.

(118) Hirayama, Y.; Obara, M. Heat Effects of Metals Ablated with Femtosecond Laser Pulses. *Appl. Surf. Sci.* **2002**, *197–198*, 741–745. https://doi.org/10.1016/S0169-4332(02)00403-8.
(119) Elaboudi, I.; Lazare, S.; Belin, C.; Talaga, D.; Labrugère, C. Underwater Excimer Laser Ablation of Polymers. *Appl. Phys. A* **2008**, *92* (4), 743–748. https://doi.org/10.1007/s00339-008-4567-2.
(120) Martínez-Tong, D. E.; Sanz, M.; Ezquerra, T. A.; Nogales, A.; Marco, J. F.; Castillejo, M.; Rebollar, E. Formation of Polymer Nanoparticles by UV Pulsed Laser Ablation of Poly (Bisphenol A Carbonate) in Liquid Environment. *Appl. Surf. Sci.* **2017**, *418* (Part B), 522–529. https://doi.org/10.1016/j.apsusc.2016.11.186.
(121) Elaboudi, I.; Lazare, S.; Belin, C.; Talaga, D.; Labrugère, C. From Polymer Films to Organic Nanoparticles Suspensions by Means of Excimer Laser Ablation in Water. *Appl. Phys. A* **2008**, *93* (4), 827–831. https://doi.org/10.1007/s00339-008-4746-1.
(122) Berthe, L.; Fabbro, R.; Peyre, P.; Tollier, L.; Bartnicki, E. Shock Waves from a Water-Confined Laser-Generated Plasma. *J. Appl. Phys.* **1997**, *82* (6), 2826–2832. https://doi.org/10.1063/1.366113.
(123) Kukreja, L. M.; Kaul, R.; Paul, C. P.; Ganesh, P.; Rao, B. T. Emerging Laser Materials Processing Techniques for Future Industrial Applications. In *Laser-Assisted Fabrication of Materials*; Springer Series in Materials Science; Springer, Berlin, Heidelberg, 2013; pp 423–478. https://doi.org/10.1007/978-3-642-28359-8_10.
(124) Streubel, R.; Barcikowski, S.; Gökce, B. Continuous Multigram Nanoparticle Synthesis by High-Power, High-Repetition-Rate Ultrafast Laser Ablation in Liquids. *Opt. Lett.* **2016**, *41* (7), 1486–1489. https://doi.org/10.1364/OL.41.001486.
(125) Peula, J. M.; Santos, R.; Forcada, J.; Hidalgo-Alvarez, R.; de las Nieves, F. J. Study on the Colloidal Stability Mechanisms of Acetal-Functionalized Latexes. *Langmuir* **1998**, *14* (22), 6377–6384. https://doi.org/10.1021/la9805488.
(126) Ozaki, Y. Frontiers of Far-Ultraviolet Spectroscopy in the Solid and Liquid States http://www.spectroscopyonline.com/frontiers-far-ultraviolet-spectroscopy-solid-and-liquid-states (accessed Jul 31, 2018).
(127) Jie-Rong, C.; Xue-Yan, W.; Tomiji, W. Wettability of Poly(Ethylene Terephthalate) Film Treated with Low-Temperature Plasma and Their Surface Analysis by ESCA. *J. Appl. Polym. Sci.* **1999**, *72* (10), 1327–1333. https://doi.org/10.1002/(SICI)1097-4628(19990606)72:10<1327::AID-APP13>3.0.CO;2-0.
(128) Gupta, B.; Plummer, C.; Bisson, I.; Frey, P.; Hilborn, J. Plasma-Induced Graft Polymerization of Acrylic Acid onto Poly(Ethylene Terephthalate) Films: Characterization and Human Smooth Muscle Cell Growth on Grafted Films. *Biomaterials* **2002**, *23* (3), 863–871. https://doi.org/10.1016/S0142-9612(01)00195-8.
(129) Girardeaux, C.; Zammatteo, N.; Art, M.; Gillon, B.; Pireaux, J. J.; Caudano, R. Amination of Poly(Ethylene-Terephthalate) Polymer Surface for Biochemical Applications. *Plasmas Polym.* **1996**, *1* (4), 327–346. https://doi.org/10.1007/BF02532829.
(130) Riccardi, C.; Barni, R.; Selli, E.; Mazzone, G.; Massafra, M. R.; Marcandalli, B.; Poletti, G. Surface Modification of Poly(Ethylene Terephthalate) Fibers Induced by Radio Frequency Air Plasma Treatment. *Appl. Surf. Sci.* **2003**, *211* (1), 386–397. https://doi.org/10.1016/S0169-4332(03)00265-4.
(131) Peeling, J.; Courval, G.; Jazzar, M. S. ESCA and Contact-Angle Studies of the Surface Modification of Poly(Ethylene Terephthalate) Film: Photooxidation and Aging. *J. Polym. Sci. Polym. Chem. Ed.* **1984**, *22* (2), 419–428. https://doi.org/10.1002/pol.1984.170220213.
(132) Fechine, G. J. M.; Rabello, M. S.; Souto Maior, R. M.; Catalani, L. H. Surface Characterization of Photodegraded Poly(Ethylene Terephthalate). The Effect of Ultraviolet Absorbers. *Polymer* **2004**, *45* (7), 2303–2308. https://doi.org/10.1016/j.polymer.2004.02.003.
(133) Wypych, G. *Weathering of Plastics: Testing to Mirror Life Performance*; William Andrew, 1999.
(134) Culbert, B.; Christel, A. Continuous Solid-State Polycondensation of Polyesters. In *Modern Polyesters: Chemistry and Technology of Polyesters and Copolyesters*; Scheirs, J., Long, T.

E., Eds.; John Wiley & Sons, Ltd, 2004; pp 143–194. https://doi.org/10.1002/0470090685.ch4.

(135) Allen, N. S.; Edge, M.; Mohammadian, M.; Jones, K. Hydrolytic Degradation of Poly(Ethylene Terephthalate): Importance of Chain Scission versus Crystallinity. *Eur. Polym. J.* **1991**, *27* (12), 1373–1378. https://doi.org/10.1016/0014-3057(91)90237-I.

(136) Babij, N. R.; McCusker, E. O.; Whiteker, G. T.; Canturk, B.; Choy, N.; Creemer, L. C.; Amicis, C. V. D.; Hewlett, N. M.; Johnson, P. L.; Knobelsdorf, J. A.; et al. NMR Chemical Shifts of Trace Impurities: Industrially Preferred Solvents Used in Process and Green Chemistry. *Org. Process Res. Dev.* **2016**, *20* (3), 661–667. https://doi.org/10.1021/acs.oprd.5b00417.

(137) Molina-Bolívar, J. A.; Ortega-Vinuesa, J. L. How Proteins Stabilize Colloidal Particles by Means of Hydration Forces. *Langmuir* **1999**, *15* (8), 2644–2653. https://doi.org/10.1021/la981445s.

(138) Torcello-Gómez, A.; Santander-Ortega, M. J.; Peula-García, J. M.; Maldonado-Valderrama, J.; Gálvez-Ruiz, M. J.; Ortega-Vinuesa, J. L.; Martín-Rodríguez, A. Adsorption of Antibody onto Pluronic F68-Covered Nanoparticles: Link with Surface Properties. *Soft Matter* **2011**, *7* (18), 8450–8461. https://doi.org/10.1039/C1SM05570D.

(139) Molina-Bolívar, J. A.; Galisteo-González, F.; Hidalgo-Alvarez, R. Particle Enhanced Immunoassays Stabilized by Hydration Forces: A Comparative Study between IgG and F(Ab)2 Immunoreactivity. *J. Immunol. Methods* **1998**, *211* (1–2), 87–95.

(140) Monopoli, M. P.; Aberg, C.; Salvati, A.; Dawson, K. A. Biomolecular Coronas Provide the Biological Identity of Nanosized Materials. *Nat. Nanotechnol.* **2012**, *7* (12), 779–786. https://doi.org/10.1038/nnano.2012.207.

(141) Cedervall, T.; Lynch, I.; Lindman, S.; Berggård, T.; Thulin, E.; Nilsson, H.; Dawson, K. A.; Linse, S. Understanding the Nanoparticle-Protein Corona Using Methods to Quantify Exchange Rates and Affinities of Proteins for Nanoparticles. *Proc. Natl. Acad. Sci. U. S. A.* **2007**, *104* (7), 2050–2055. https://doi.org/10.1073/pnas.0608582104.

(142) Bouwmeester, H.; Hollman, P.; Peters, R. Potential Health Impact of Environmentally Released Micro- and Nanoplastics in the Human Food Production Chain: Experiences from Nanotoxicology. *Environ. Sci. Technol.* **2015**, *49*. https://doi.org/10.1021/acs.est.5b01090.

(143) Bergin, I. L.; Witzmann, F. A. Nanoparticle Toxicity by the Gastrointestinal Route: Evidence and Knowledge Gaps. *Int. J. Biomed. Nanosci. Nanotechnol.* **2013**, *3* (1–2), 163–210. https://doi.org/10.1504/IJBNN.2013.054515.

(144) Kim, J. A.; Åberg, C.; Salvati, A.; Dawson, K. A. Role of Cell Cycle on the Cellular Uptake and Dilution of Nanoparticles in a Cell Population. *Nat. Nanotechnol.* **2011**, *7* (1), 62–68. https://doi.org/10.1038/nnano.2011.191.

(145) Baltazar, G. C.; Guha, S.; Lu, W.; Lim, J.; Boesze-Battaglia, K.; Laties, A. M.; Tyagi, P.; Kompella, U. B.; Mitchell, C. H. Acidic Nanoparticles Are Trafficked to Lysosomes and Restore an Acidic Lysosomal PH and Degradative Function to Compromised ARPE-19 Cells. *PloS One* **2012**, *7* (12), e49635. https://doi.org/10.1371/journal.pone.0049635.

(146) Varela, J. A.; Bexiga, M. G.; Åberg, C.; Simpson, J. C.; Dawson, K. A. Quantifying Size-Dependent Interactions between Fluorescently Labeled Polystyrene Nanoparticles and Mammalian Cells. *J. Nanobiotechnology* **2012**, *10*, 39. https://doi.org/10.1186/1477-3155-10-39.

(147) Walczak, A. P.; Kramer, E.; Hendriksen, P. J. M.; Helsdingen, R.; van der Zande, M.; Rietjens, I. M. C. M.; Bouwmeester, H. In Vitro Gastrointestinal Digestion Increases the Translocation of Polystyrene Nanoparticles in an in Vitro Intestinal Co-Culture Model. *Nanotoxicology* **2015**, *9* (7), 886–894. https://doi.org/10.3109/17435390.2014.988664.

(148) Moglianetti, M.; De Luca, E.; Pedone, D.; Marotta, R.; Catelani, T.; Sartori, B.; Amenitsch, H.; Retta, S. F.; Pompa, P. P. Platinum Nanozymes Recover Cellular ROS Homeostasis in an Oxidative Stress-Mediated Disease Model. *Nanoscale* **2016**, *8* (6), 3739–3752. https://doi.org/10.1039/c5nr08358c.

(149) Pedone, D.; Moglianetti, M.; De Luca, E.; Bardi, G.; Pompa, P. P. Platinum Nanoparticles in Nanobiomedicine. *Chem. Soc. Rev.* **2017**, *46* (16), 4951–4975. https://doi.org/10.1039/c7cs00152e.

(150) Kang, T.; Guan, R.; Chen, X.; Song, Y.; Jiang, H.; Zhao, J. In Vitro Toxicity of Different-Sized ZnO Nanoparticles in Caco-2 Cells. *Nanoscale Res. Lett.* **2013**, *8* (1), 496. https://doi.org/10.1186/1556-276X-8-496.

(151) Ivask, A.; Titma, T.; Visnapuu, M.; Vija, H.; Kakinen, A.; Sihtmae, M.; Pokhrel, S.; Madler, L.; Heinlaan, M.; Kisand, V.; et al. Toxicity of 11 Metal Oxide Nanoparticles to Three Mammalian Cell Types In Vitro. *Curr. Top. Med. Chem.* **2015**, *15* (18), 1914–1929.

(152) Tarantini, A.; Lanceleur, R.; Mourot, A.; Lavault, M.-T.; Casterou, G.; Jarry, G.; Hogeveen, K.; Fessard, V. Toxicity, Genotoxicity and Proinflammatory Effects of Amorphous Nanosilica in the Human Intestinal Caco-2 Cell Line. *Toxicol. Vitro Int. J. Publ. Assoc. BIBRA* **2015**, *29* (2), 398–407. https://doi.org/10.1016/j.tiv.2014.10.023.

(153) Song, Y.; Guan, R.; Lyu, F.; Kang, T.; Wu, Y.; Chen, X. In Vitro Cytotoxicity of Silver Nanoparticles and Zinc Oxide Nanoparticles to Human Epithelial Colorectal Adenocarcinoma (Caco-2) Cells. *Mutat. Res.* **2014**, *769*, 113–118. https://doi.org/10.1016/j.mrfmmm.2014.08.001.

(154) Auewiriyavit, S.; Phummiratch, D.; Maniratanachote, R. Mechanistic Study on the Biological Effects of Silver and Gold Nanoparticles in Caco-2 Cells--Induction of the Nrf2/HO-1 Pathway by High Concentrations of Silver Nanoparticles. *Toxicol. Lett.* **2014**, *224* (1), 73–83. https://doi.org/10.1016/j.toxlet.2013.09.020.

(155) Saha, D.; Heldt, C. L.; Gencoglu, M. F.; Vijayaragavan, K. S.; Chen, J.; Saksule, A. A Study on the Cytotoxicity of Carbon-Based Materials. *Mater. Sci. Eng. C Mater. Biol. Appl.* **2016**, *68*, 101–108. https://doi.org/10.1016/j.msec.2016.05.094.

(156) Chai, G.-H.; Xu, Y.; Chen, S.-Q.; Cheng, B.; Hu, F.-Q.; You, J.; Du, Y.-Z.; Yuan, H. Transport Mechanisms of Solid Lipid Nanoparticles across Caco-2 Cell Monolayers and Their Related Cytotoxicology. *ACS Appl. Mater. Interfaces* **2016**, *8* (9), 5929–5940. https://doi.org/10.1021/acsami.6b00821.

(157) Guarnieri, D.; Paola Sánchez-Moreno, P.; Del Rio Castillo, A. E.; Bonaccorso, F.; Gatto, F.; Bardi, G.; Martin, C.; Vázquez, E.; Catelani, T.; Sabella, S.; et al. Biotransformation and Biological Interaction of Graphene and Graphene Oxide during Simulated Oral Ingestion. *Small*. 2018, p (under revision).

(158) Kucki, M.; Diener, L.; Bohmer, N.; Hirsch, C.; Krug, H. F.; Palermo, V.; Wick, P. Uptake of Label-Free Graphene Oxide by Caco-2 Cells Is Dependent on the Cell Differentiation Status. *J. Nanobiotechnology* **2017**, *15* (1), 46. https://doi.org/10.1186/s12951-017-0280-7.

(159) Beloqui, A.; des Rieux, A.; Préat, V. Mechanisms of Transport of Polymeric and Lipidic Nanoparticles across the Intestinal Barrier. *Adv. Drug Deliv. Rev.* **2016**, *106*, 242–255. https://doi.org/10.1016/j.addr.2016.04.014.

(160) Lin, I.-C.; Liang, M.; Liu, T.-Y.; Ziora, Z. M.; Monteiro, M. J.; Toth, I. Interaction of Densely Polymer-Coated Gold Nanoparticles with Epithelial Caco-2 Monolayers. *Biomacromolecules* **2011**, *12* (4), 1339–1348. https://doi.org/10.1021/bm200116z.

(161) Ranaldi, G.; Marigliano, I.; Vespignani, I.; Perozzi, G.; Sambuy, Y. The Effect of Chitosan and Other Polycations on Tight Junction Permeability in the Human Intestinal Caco-2 Cell Line(1). *J. Nutr. Biochem.* **2002**, *13* (3), 157–167.

(162) Liu, Y.; Chiu, G. N. C. Dual-Functionalized PAMAM Dendrimers with Improved P-Glycoprotein Inhibition and Tight Junction Modulating Effect. *Biomacromolecules* **2013**, *14* (12), 4226–4235. https://doi.org/10.1021/bm401057c.

(163) Coyuco, J. C.; Liu, Y.; Tan, B.-J.; Chiu, G. N. C. Functionalized Carbon Nanomaterials: Exploring the Interactions with Caco-2 Cells for Potential Oral Drug Delivery. *Int. J. Nanomedicine* **2011**, *6*, 2253–2263. https://doi.org/10.2147/IJN.S23962.

(164) Ye, D.; Bramini, M.; Hristov, D. R.; Wan, S.; Salvati, A.; Åberg, C.; Dawson, K. A. Low Uptake of Silica Nanoparticles in Caco-2 Intestinal Epithelial Barriers. *Beilstein J. Nanotechnol.* **2017**, *8*, 1396–1406. https://doi.org/10.3762/bjnano.8.141.

(165) Rochman, C. M. The Complex Mixture, Fate and Toxicity of Chemicals Associated with Plastic Debris in the Marine Environment. In *Marine Anthropogenic Litter*; Bergmann, M., Gutow, L., Klages, M., Eds.; Springer International Publishing: Cham, 2015; pp 117–140. https://doi.org/10.1007/978-3-319-16510-3_5.

(166) Lithner, D.; Larsson, A.; Dave, G. Environmental and Health Hazard Ranking and Assessment of Plastic Polymers Based on Chemical Composition. *Sci. Total Environ.* **2011**, *409* (18), 3309–3324. https://doi.org/10.1016/j.scitotenv.2011.04.038.

(167) Mato, Y.; Isobe, T.; Takada, H.; Kanehiro, H.; Ohtake, C.; Kaminuma, T. Plastic Resin Pellets as a Transport Medium for Toxic Chemicals in the Marine Environment. *Environ. Sci. Technol.* **2001**, *35* (2), 318–324.

(168) Ogata, Y.; Takada, H.; Mizukawa, K.; Hirai, H.; Iwasa, S.; Endo, S.; Mato, Y.; Saha, M.; Okuda, K.; Nakashima, A.; et al. International Pellet Watch: Global Monitoring of Persistent Organic Pollutants (POPs) in Coastal Waters. 1. Initial Phase Data on PCBs, DDTs, and HCHs. *Mar. Pollut. Bull.* **2009**, *58* (10), 1437–1446. https://doi.org/10.1016/j.marpolbul.2009.06.014.

(169) Suhrhoff, T. J.; Scholz-Böttcher, B. M. Qualitative Impact of Salinity, UV Radiation and Turbulence on Leaching of Organic Plastic Additives from Four Common Plastics - A Lab Experiment. *Mar. Pollut. Bull.* **2016**, *102* (1), 84–94. https://doi.org/10.1016/j.marpolbul.2015.11.054.

(170) Westerhoff, P.; Prapaipong, P.; Shock, E.; Hillaireau, A. Antimony Leaching from Polyethylene Terephthalate (PET) Plastic Used for Bottled Drinking Water. *Water Res.* **2008**, *42* (3), 551–556. https://doi.org/10.1016/j.watres.2007.07.048.

(171) Liu, J.; Ma, Y.; Zhu, D.; Xia, T.; Qi, Y.; Yao, Y.; Guo, X.; Ji, R.; Chen, W. Polystyrene Nanoplastics-Enhanced Contaminant Transport: Role of Irreversible Adsorption in Glassy Polymeric Domain. *Environ. Sci. Technol.* **2018**, *52* (5), 2677–2685. https://doi.org/10.1021/acs.est.7b05211.

(172) Velzeboer, I.; Kwadijk, C. J. A. F.; Koelmans, A. A. Strong Sorption of PCBs to Nanoplastics, Microplastics, Carbon Nanotubes, and Fullerenes. *Environ. Sci. Technol.* **2014**, *48* (9), 4869–4876. https://doi.org/10.1021/es405721v.

(173) Liu, L.; Fokkink, R.; Koelmans, A. A. Sorption of Polycyclic Aromatic Hydrocarbons to Polystyrene Nanoplastic. *Environ. Toxicol. Chem.* **2016**, *35* (7), 1650–1655. https://doi.org/10.1002/etc.3311.

(174) Chua, E. M.; Shimeta, J.; Nugegoda, D.; Morrison, P. D.; Clarke, B. O. Assimilation of Polybrominated Diphenyl Ethers from Microplastics by the Marine Amphipod, Allorchestes Compressa. *Environ. Sci. Technol.* **2014**, *48* (14), 8127–8134. https://doi.org/10.1021/es405717z.

(175) Llorca, M.; Farré, M.; Karapanagioti, H. K.; Barceló, D. Levels and Fate of Perfluoroalkyl Substances in Beached Plastic Pellets and Sediments Collected from Greece. *Mar. Pollut. Bull.* **2014**, *87* (1–2), 286–291. https://doi.org/10.1016/j.marpolbul.2014.07.036.

(176) Bao, L.-J.; You, J.; Zeng, E. Y. Sorption of PBDE in Low-Density Polyethylene Film: Implications for Bioavailability of BDE-209. *Environ. Toxicol. Chem.* **2011**, *30* (8), 1731–1738. https://doi.org/10.1002/etc.564.

(177) Hüffer, T.; Hofmann, T. Sorption of Non-Polar Organic Compounds by Micro-Sized Plastic Particles in Aqueous Solution. *Environ. Pollut. Barking Essex 1987* **2016**, *214*, 194–201. https://doi.org/10.1016/j.envpol.2016.04.018.

(178) Deng, R.; Lin, D.; Zhu, L.; Majumdar, S.; White, J. C.; Gardea-Torresdey, J. L.; Xing, B. Nanoparticle Interactions with Co-Existing Contaminants: Joint Toxicity, Bioaccumulation and Risk. *Nanotoxicology* **2017**, *11* (5), 591–612. https://doi.org/10.1080/17435390.2017.1343404.

(179) Koelmans, A. A.; Besseling, E.; Wegner, A.; Foekema, E. M. Plastic as a Carrier of POPs to Aquatic Organisms: A Model Analysis. *Environ. Sci. Technol.* **2013**, *47* (14), 7812–7820. https://doi.org/10.1021/es401169n.

(180) Teuten, E. L.; Saquing, J. M.; Knappe, D. R. U.; Barlaz, M. A.; Jonsson, S.; Björn, A.; Rowland, S. J.; Thompson, R. C.; Galloway, T. S.; Yamashita, R.; et al. Transport and Release of Chemicals from Plastics to the Environment and to Wildlife. *Philos. Trans. R. Soc. Lond. B. Biol. Sci.* **2009**, *364* (1526), 2027–2045. https://doi.org/10.1098/rstb.2008.0284.

(181) Holmes, L. A.; Turner, A.; Thompson, R. C. Interactions between Trace Metals and Plastic Production Pellets under Estuarine Conditions. *Mar. Chem.* **2014**, *167*, 25–32. https://doi.org/10.1016/j.marchem.2014.06.001.

(182) Brennecke, D.; Duarte, B.; Paiva, F.; Caçador, I.; Canning-Clode, J. Microplastics as Vector for Heavy Metal Contamination from the Marine Environment. *Estuar. Coast. Shelf Sci.* **2016**, *178*, 189–195. https://doi.org/10.1016/j.ecss.2015.12.003.
(183) Borggaard, O. K.; Gimsing, A. L. Fate of Glyphosate in Soil and the Possibility of Leaching to Ground and Surface Waters: A Review. *Pest Manag. Sci.* **2008**, *64* (4), 441–456. https://doi.org/10.1002/ps.1512.
(184) Vereecken, H. Mobility and Leaching of Glyphosate: A Review. *Pest Manag. Sci.* **2005**, *61* (12), 1139–1151. https://doi.org/10.1002/ps.1122.
(185) Torretta, V.; Katsoyiannis, I. A.; Viotti, P.; Rada, E. C. Critical Review of the Effects of Glyphosate Exposure to the Environment and Humans through the Food Supply Chain. *Sustainability* **2018**, *10* (4), 950. https://doi.org/10.3390/su10040950.
(186) Mercurio, P.; Flores, F.; Mueller, J. F.; Carter, S.; Negri, A. P. Glyphosate Persistence in Seawater. *Mar. Pollut. Bull.* **2014**, *85* (2), 385–390. https://doi.org/10.1016/j.marpolbul.2014.01.021.
(187) Carbon, C. Comparison of Side Effects of Levofloxacin versus Other Fluoroquinolones. *Chemotherapy* **2001**, *47 Suppl 3*, 9–14; discussion 44-48. https://doi.org/10.1159/000057839.
(188) Gudaganatti, M. S.; Hanagadakar, M. S.; Kulkarni, R. M.; Malladi, R. S.; Nagarale, R. K. Transformation of Levofloxacin during Water Chlorination Process: Kinetics and Pathways. *Prog. React. Kinet. Mech. 37* (4), 366–382.
(189) Aldred, K. J.; Kerns, R. J.; Osheroff, N. Mechanism of Quinolone Action and Resistance. *Biochemistry* **2014**, *53* (10), 1565–1574. https://doi.org/10.1021/bi5000564.
(190) Ahmad, I.; Bano, R.; Sheraz, M. A.; Ahmed, S.; Mirza, T.; Ansari, S. A. Photodegradation of Levofloxacin in Aqueous and Organic Solvents: A Kinetic Study. *Acta Pharm.* **2013**, *63* (2), 223–229. https://doi.org/10.2478/acph-2013-0011.
(191) Gao, C.-H.; Yu, L.-S.; Zeng, S.; Huang, Y.-W.; Zhou, Q. Personalized Therapeutics for Levofloxacin: A Focus on Pharmacokinetic Concerns. *Ther. Clin. Risk Manag.* **2014**, *10*, 217–227. https://doi.org/10.2147/TCRM.S59079.
(192) Orzoł, A.; Piotrowicz-Cieślak, A. I. Levofloxacin Is Phytotoxic and Modifies the Protein Profile of Lupin Seedlings. *Environ. Sci. Pollut. Res. Int.* **2017**, *24* (28), 22226–22240. https://doi.org/10.1007/s11356-017-9845-0.
(193) Zuccato, E.; Castiglioni, S.; Fanelli, R. Identification of the Pharmaceuticals for Human Use Contaminating the Italian Aquatic Environment. *J. Hazard. Mater.* **2005**, *122* (3), 205–209. https://doi.org/10.1016/j.jhazmat.2005.03.001.
(194) Abdullah, I. H.; Ahmed, N.; Mohamed, M. A.; Ragab, F. M. A.; Abdel-Wareth, M. T. A.; Allam, N. K. An Engineered Nanocomposite for Sensitive and Selective Detection of Mercury in Environmental Water Samples. *Anal. Methods* **2018**, *10* (21), 2526–2535. https://doi.org/10.1039/C8AY00618K.
(195) Jiang, Y.; He, T.; Chen, Y.; Ruan, Y.; Zhou, Y.; Tang, B. Z.; Qin, J.; Tang, Y. Quantitative Evaluation and in Vivo Visualization of Mercury Ion Bioaccumulation in Rotifers by Novel Aggregation-Induced Emission Fluorogen Nanoparticles. *Environ. Sci. Nano* **2017**, *4* (11), 2186–2192. https://doi.org/10.1039/C7EN00599G.
(196) Gumpu, M. B.; Sethuraman, S.; Krishnan, U. M.; Rayappan, J. B. B. A Review on Detection of Heavy Metal Ions in Water – An Electrochemical Approach. *Sens. Actuators B Chem.* **2015**, *213*, 515–533. https://doi.org/10.1016/j.snb.2015.02.122.
(197) Nolan, E. M.; Lippard, S. J. Tools and Tactics for the Optical Detection of Mercuric Ion. *Chem. Rev.* **2008**, *108* (9), 3443–3480. https://doi.org/10.1021/cr068000q.
(198) Gworek, B.; Bemowska-Kałabun, O.; Kijeńska, M.; Wrzosek-Jakubowska, J. Mercury in Marine and Oceanic Waters—a Review. *Water. Air. Soil Pollut.* **2016**, *227* (10). https://doi.org/10.1007/s11270-016-3060-3.
(199) Falcó, G.; Llobet, J. M.; Bocio, A.; Domingo, J. L. Daily Intake of Arsenic, Cadmium, Mercury, and Lead by Consumption of Edible Marine Species. *J. Agric. Food Chem.* **2006**, *54* (16), 6106–6112. https://doi.org/10.1021/jf0610110.
(200) Labuda, J.; K. Bubnicova, K.; Kovalova, L.; Vanickova, M.; Mattusch, J.; Wennrich, R. Voltammetric Detection of Damage to DNA by Arsenic Compounds at a DNA Biosensor. *Sensors* **2005**, *5* (6), 411–423. https://doi.org/10.3390/s5060411.

(201) Hoang, C. V.; Oyama, M.; Saito, O.; Aono, M.; Nagao, T. Monitoring the Presence of Ionic Mercury in Environmental Water by Plasmon-Enhanced Infrared Spectroscopy. *Sci. Rep.* **2013**, *3*, 1175. https://doi.org/10.1038/srep01175.

(202) Jaishankar, M.; Tseten, T.; Anbalagan, N.; Mathew, B. B.; Beeregowda, K. N. Toxicity, Mechanism and Health Effects of Some Heavy Metals. *Interdiscip. Toxicol.* **2014**, *7* (2), 60–72. https://doi.org/10.2478/intox-2014-0009.

(203) Järup, L. Hazards of Heavy Metal Contamination. *Br. Med. Bull.* **2003**, *68* (1), 167–182. https://doi.org/10.1093/bmb/ldg032.

(204) Barboza, L. G. A.; Vieira, L. R.; Branco, V.; Figueiredo, N.; Carvalho, F.; Carvalho, C.; Guilhermino, L. Microplastics Cause Neurotoxicity, Oxidative Damage and Energy-Related Changes and Interact with the Bioaccumulation of Mercury in the European Seabass, Dicentrarchus Labrax (Linnaeus, 1758). *Aquat. Toxicol.* **2018**, *195*, 49–57. https://doi.org/10.1016/j.aquatox.2017.12.008.

(205) Boerger, C. M.; Lattin, G. L.; Moore, S. L.; Moore, C. J. Plastic Ingestion by Planktivorous Fishes in the North Pacific Central Gyre. *Mar. Pollut. Bull.* **2010**, *60* (12), 2275–2278. https://doi.org/10.1016/j.marpolbul.2010.08.007.

(206) Mackay, D.; Boethling, R. S.; Boethling, R. S. Bioconcentration and Biomagnification in the Aquatic Environment https://www.taylorfrancis.com/ (accessed Dec 12, 2018). https://doi.org/10.1201/9781420026283-13.

(207) Mason, R. P.; Reinfelder, J. R.; Morel, F. M. M. Uptake, Toxicity, and Trophic Transfer of Mercury in a Coastal Diatom. *Environ. Sci. Technol.* **1996**, *30* (6), 1835–1845. https://doi.org/10.1021/es950373d.

(208) Farrell, P.; Nelson, K. Trophic Level Transfer of Microplastic: Mytilus Edulis (L.) to Carcinus Maenas (L.). *Environ. Pollut.* **2013**, *177*, 1–3. https://doi.org/10.1016/j.envpol.2013.01.046.

(209) Setälä, O.; Fleming-Lehtinen, V.; Lehtiniemi, M. Ingestion and Transfer of Microplastics in the Planktonic Food Web. *Environ. Pollut.* **2014**, *185*, 77–83. https://doi.org/10.1016/j.envpol.2013.10.013.

(210) Van Cauwenberghe, L.; Janssen, C. R. Microplastics in Bivalves Cultured for Human Consumption. *Environ. Pollut.* **2014**, *193*, 65–70. https://doi.org/10.1016/j.envpol.2014.06.010.

(211) Browne, M. A.; Niven, S. J.; Galloway, T. S.; Rowland, S. J.; Thompson, R. C. Microplastic Moves Pollutants and Additives to Worms, Reducing Functions Linked to Health and Biodiversity. *Curr. Biol. CB* **2013**, *23* (23), 2388–2392. https://doi.org/10.1016/j.cub.2013.10.012.

(212) Rochman, C. M.; Hoh, E.; Kurobe, T.; Teh, S. J. Ingested Plastic Transfers Hazardous Chemicals to Fish and Induces Hepatic Stress. *Sci. Rep.* **2013**, *3*, 3263. https://doi.org/10.1038/srep03263.

(213) Fossi, M. C.; Panti, C.; Guerranti, C.; Coppola, D.; Giannetti, M.; Marsili, L.; Minutoli, R. Are Baleen Whales Exposed to the Threat of Microplastics? A Case Study of the Mediterranean Fin Whale (Balaenoptera Physalus). *Mar. Pollut. Bull.* **2012**, *64* (11), 2374–2379. https://doi.org/10.1016/j.marpolbul.2012.08.013.

(214) Rossi, G.; Barnoud, J.; Monticelli, L. Polystyrene Nanoparticles Perturb Lipid Membranes. *J. Phys. Chem. Lett.* **2014**, *5* (1), 241–246. https://doi.org/10.1021/jz402234c.

(215) Salvati, A.; Aberg, C.; dos Santos, T.; Varela, J.; Pinto, P.; Lynch, I.; Dawson, K. A. Experimental and Theoretical Comparison of Intracellular Import of Polymeric Nanoparticles and Small Molecules: Toward Models of Uptake Kinetics. *Nanomedicine Nanotechnol. Biol. Med.* **2011**, *7* (6), 818–826. https://doi.org/10.1016/j.nano.2011.03.005.

(216) Chae, Y.; An, Y.-J. Effects of Micro- and Nanoplastics on Aquatic Ecosystems: Current Research Trends and Perspectives. *Mar. Pollut. Bull.* **2017**, *124* (2), 624–632. https://doi.org/10.1016/j.marpolbul.2017.01.070.

(217) Xia, T.; Kovochich, M.; Liong, M.; Zink, J. I.; Nel, A. E. Cationic Polystyrene Nanosphere Toxicity Depends on Cell-Specific Endocytic and Mitochondrial Injury Pathways. *ACS Nano* **2008**, *2* (1), 85–96. https://doi.org/10.1021/nn700256c.

(218) Forte, M.; Iachetta, G.; Tussellino, M.; Carotenuto, R.; Prisco, M.; De, M. F.; Laforgia, V.; Valiante, S. Polystyrene Nanoparticles Internalization in Human Gastric Adenocarcinoma Cells. *Toxicol. Vitro Int. J. Publ. Assoc. BIBRA* **2016**, *31*, 126–136. https://doi.org/10.1016/j.tiv.2015.11.006.

(219) Horgan, R. P.; Kenny, L. C. 'Omic' Technologies: Genomics, Transcriptomics, Proteomics and Metabolomics. *Obstet. Gynaecol.* **2011**, *13* (3), 189–195. https://doi.org/10.1576/toag.13.3.189.27672.

(220) Raja, K.; Patrick, M.; Gao, Y.; Madu, D.; Yang, Y.; Tsoi, L. C. A Review of Recent Advancement in Integrating Omics Data with Literature Mining towards Biomedical Discoveries https://www.hindawi.com/journals/ijg/2017/6213474/ (accessed Dec 13, 2018). https://doi.org/10.1155/2017/6213474.

(221) Werf, M. J. van der; Jellema, R. H.; Hankemeier, T. Microbial Metabolomics: Replacing Trial-and-Error by the Unbiased Selection and Ranking of Targets. *J. Ind. Microbiol. Biotechnol.* **2005**, *32* (6), 234–252. https://doi.org/10.1007/s10295-005-0231-4.

(222) Brown, M.; Wedge, D. C.; Goodacre, R.; Kell, D. B.; Baker, P. N.; Kenny, L. C.; Mamas, M. A.; Neyses, L.; Dunn, W. B. Automated Workflows for Accurate Mass-Based Putative Metabolite Identification in LC/MS-Derived Metabolomic Datasets. *Bioinformatics* **2011**, *27* (8), 1108–1112. https://doi.org/10.1093/bioinformatics/btr079.

(223) Dunn, W. B.; Ellis, D. I. Metabolomics: Current Analytical Platforms and Methodologies. *TrAC Trends Anal. Chem.* **2005**, *24* (4), 285–294. https://doi.org/10.1016/j.trac.2004.11.021.

(224) Castle, A. L.; Fiehn, O.; Kaddurah-Daouk, R.; Lindon, J. C. Metabolomics Standards Workshop and the Development of International Standards for Reporting Metabolomics Experimental Results. *Brief. Bioinform.* **2006**, *7* (2), 159–165. https://doi.org/10.1093/bib/bbl008.

(225) Tyers, M.; Mann, M. From Genomics to Proteomics. *Nature* **2003**, *422* (6928), 193–197. https://doi.org/10.1038/nature01510.

(226) Chandramouli, K.; Qian, P.-Y. Proteomics: Challenges, Techniques and Possibilities to Overcome Biological Sample Complexity. *Hum. Genomics Proteomics HGP* **2009**, *2009*. https://doi.org/10.4061/2009/239204.

(227) Meiboom, S.; Gill, D. Modified Spin-Echo Method for Measuring Nuclear Relaxation Times. *Rev. Sci. Instrum.* **1958**, *29* (8), 688–691. https://doi.org/10.1063/1.1716296.

(228) Guitton, Y.; Tremblay-Franco, M.; Le Corguillé, G.; Martin, J.-F.; Pétéra, M.; Roger-Mele, P.; Delabrière, A.; Goulitquer, S.; Monsoor, M.; Duperier, C.; et al. Create, Run, Share, Publish, and Reference Your LC-MS, FIA-MS, GC-MS, and NMR Data Analysis Workflows with the Workflow4Metabolomics 3.0 Galaxy Online Infrastructure for Metabolomics. *Int. J. Biochem. Cell Biol.* **2017**, *93*, 89–101. https://doi.org/10.1016/j.biocel.2017.07.002.

(229) Chegel, V.; Rachkov, O.; Lopatynskyi, A.; Ishihara, S.; Yanchuk, I.; Nemoto, Y.; Hill, J. P.; Ariga, K. Gold Nanoparticles Aggregation: Drastic Effect of Cooperative Functionalities in a Single Molecular Conjugate. *J. Phys. Chem. C* **2012**, *116* (4), 2683–2690. https://doi.org/10.1021/jp209251y.

(230) Schneider, C.; Hanisch, M.; Wedel, B.; Jusufi, A.; Ballauff, M. Experimental Study of Electrostatically Stabilized Colloidal Particles: Colloidal Stability and Charge Reversal. *J. Colloid Interface Sci.* **2011**, *358* (1), 62–67. https://doi.org/10.1016/j.jcis.2011.02.039.

(231) Joshi, H.; Shirude, P. S.; Bansal, V.; Ganesh, K. N.; Sastry, M. Isothermal Titration Calorimetry Studies on the Binding of Amino Acids to Gold Nanoparticles. *J. Phys. Chem. B* **2004**, *108* (31), 11535–11540. https://doi.org/10.1021/jp048766z.

(232) Freyer, M. W.; Lewis, E. A. Isothermal Titration Calorimetry: Experimental Design, Data Analysis, and Probing Macromolecule/Ligand Binding and Kinetic Interactions. *Methods Cell Biol.* **2008**, *84*, 79–113. https://doi.org/10.1016/S0091-679X(07)84004-0.

(233) Adamson, S. X.-F.; Wang, R.; Wu, W.; Cooper, B.; Shannahan, J. Metabolomic Insights of Macrophage Responses to Graphene Nanoplatelets: Role of Scavenger Receptor CD36. *PLoS ONE* **2018**, *13* (11). https://doi.org/10.1371/journal.pone.0207042.

(234) Ramirez, T.; Daneshian, M.; Kamp, H.; Bois, F. Y.; Clench, M. R.; Coen, M.; Donley, B.; Fischer, S. M.; Ekman, D. R.; Fabian, E.; et al. Metabolomics in Toxicology and Preclinical Research. *ALTEX* **2013**, *30* (2), 209–225.

(235) Wenzel, U.; Schoberl, K.; Lohner, K.; Daniel, H. Activation of Mitochondrial Lactate Uptake by Flavone Induces Apoptosis in Human Colon Cancer Cells. *J. Cell. Physiol.* **2005**, *202* (2), 379–390. https://doi.org/10.1002/jcp.20129.

(236) Olmedo, P.; Pla, A.; Hernández, A. F.; Barbier, F.; Ayouni, L.; Gil, F. Determination of Toxic Elements (Mercury, Cadmium, Lead, Tin and Arsenic) in Fish and Shellfish Samples. Risk Assessment for the Consumers. *Environ. Int.* **2013**, *59*, 63–72. https://doi.org/10.1016/j.envint.2013.05.005.

(237) Yılmaz, A. B.; Yanar, A.; Alkan, E. N. Review of Heavy Metal Accumulation on Aquatic Environment in Northern East Mediterrenean Sea Part I: Some Essential Metals. *Rev. Environ. Health* **2017**, *32* (1–2), 119–163. https://doi.org/10.1515/reveh-2016-0065.

(238) Fliedner, A.; Rüdel, H.; Knopf, B.; Lohmann, N.; Paulus, M.; Jud, M.; Pirntke, U.; Koschorreck, J. Assessment of Seafood Contamination under the Marine Strategy Framework Directive: Contributions of the German Environmental Specimen Bank. *Environ. Sci. Pollut. Res. Int.* **2018**, *25* (27), 26939–26956. https://doi.org/10.1007/s11356-018-2728-1.

(239) Francesconi, K. A. Toxic Metal Species and Food Regulations—Making a Healthy Choice. *Analyst* **2006**, *132* (1), 17–20. https://doi.org/10.1039/B610544K.

(240) Chavan, A. A.; Pinto, J.; Liakos, I.; Bayer, I. S.; Lauciello, S.; Athanassiou, A.; Fragouli, D. Spent Coffee Bioelastomeric Composite Foams for the Removal of Pb2+ and Hg2+ from Water. *ACS Sustain. Chem. Eng.* **2016**, *4* (10), 5495–5502. https://doi.org/10.1021/acssuschemeng.6b01098.

(241) Iqbal, M.; Saeed, A.; Zafar, S. I. FTIR Spectrophotometry, Kinetics and Adsorption Isotherms Modeling, Ion Exchange, and EDX Analysis for Understanding the Mechanism of Cd2+ and Pb2+ Removal by Mango Peel Waste. *J. Hazard. Mater.* **2009**, *164* (1), 161–171. https://doi.org/10.1016/j.jhazmat.2008.07.141.

(242) Sud, D.; Mahajan, G.; Kaur, M. P. Agricultural Waste Material as Potential Adsorbent for Sequestering Heavy Metal Ions from Aqueous Solutions - a Review. *Bioresour. Technol.* **2008**, *99* (14), 6017–6027. https://doi.org/10.1016/j.biortech.2007.11.064.

(243) Acharya, J.; Sahu, J. N.; Mohanty, C. R.; Meikap, B. C. Removal of Lead(II) from Wastewater by Activated Carbon Developed from Tamarind Wood by Zinc Chloride Activation. *Chem. Eng. J.* **2009**, *149* (1/3), 249–262.

(244) Chowdhury, S.; Mazumder, M. A. J.; Al-Attas, O.; Husain, T. Heavy Metals in Drinking Water: Occurrences, Implications, and Future Needs in Developing Countries. *Sci. Total Environ.* **2016**, *569–570*, 476–488. https://doi.org/10.1016/j.scitotenv.2016.06.166.

(245) Leonas, R.; Noor, Z.; Rasyid, H. N.; Madjid, T. H.; Tanjung, F. A. Effect of Lead Nanoparticles Inhalation on Bone Calcium Sensing Receptor, Hydroxyapatite Crystal and Receptor Activator of Nuclear Factor-Kappa B in Rats. *Acta Inform. Medica* **2016**, *24* (5), 343–346. https://doi.org/10.5455/aim.2016.24.343-346.

(246) Mebrahtu, G.; Zerabruk, S. Concentration and Health Implication of Heavy Metals in Drinking Water from Urban Areas of Tigray Region, Northern Ethiopia. *Momona Ethiop. J. Sci.* **2011**, *3* (1), 105-121–121. https://doi.org/10.4314/mejs.v3i1.63689.

(247) Kaplan, O.; Yildirim, N. C.; Yildirim, N.; Tayhan, N. Assessment of Some Heavy Metals in Drinking Water Samples of Tunceli, Turkey https://www.hindawi.com/journals/jchem/2011/370545/abs/ (accessed Dec 14, 2018). https://doi.org/10.1155/2011/370545.

(248) Raji, M. I. O.; Ibrahim, Y. K. E.; Ehinmidu, J. O. Physico-Chemical Characteristics and Heavy Metal Levels in Drinking Water Sources in Sokoto Metropolis in North-Western Nigeria. *J. Appl. Sci. Environ. Manag.* **2010**, *14* (3). https://doi.org/10.4314/jasem.v14i3.61473.

(249) Araya, M.; Olivares, M.; Pizarro, F.; González, M.; Speisky, H.; Uauy, R. Gastrointestinal Symptoms and Blood Indicators of Copper Load in Apparently Healthy Adults Undergoing Controlled Copper Exposure. *Am. J. Clin. Nutr.* **2003**, *77* (3), 646–650. https://doi.org/10.1093/ajcn/77.3.646.

(250) Sharma, R. K.; Agrawal, M. Biological Effects of Heavy Metals: An Overview. *J. Environ. Biol.* **2005**, *26* (2 Suppl), 301–313.

(251) Monser, L.; Adhoum, N. Modified Activated Carbon for the Removal of Copper, Zinc, Chromium and Cyanide from Wastewater. *Sep. Purif. Technol.* **2002**, *26* (2), 137–146. https://doi.org/10.1016/S1383-5866(01)00155-1.
(252) WHO | Copper in drinking-water http://www.who.int/water_sanitation_health/publications/copper/en/ (accessed Dec 15, 2018).
(253) Moore, L. R.; Durand, J. R.; Strickland, F. Copper Removal from Mine Effluents: From Lab to Field Evaluations. *Mine Water Environ.* **2013**, *32* (3), 239–246. https://doi.org/10.1007/s10230-013-0227-7.
(254) Fu, F.; Wang, Q. Removal of Heavy Metal Ions from Wastewaters: A Review. *J. Environ. Manage.* **2011**, *92* (3), 407–418. https://doi.org/10.1016/j.jenvman.2010.11.011.
(255) Kang, S.-Y.; Lee, J.-U.; Moon, S.-H.; Kim, K.-W. Competitive Adsorption Characteristics of Co2+, Ni2+, and Cr3+ by IRN-77 Cation Exchange Resin in Synthesized Wastewater. *Chemosphere* **2004**, *56* (2), 141–147. https://doi.org/10.1016/j.chemosphere.2004.02.004.
(256) Ku, Y.; Jung, I. L. Photocatalytic Reduction of Cr(VI) in Aqueous Solutions by UV Irradiation with the Presence of Titanium Dioxide. *Water Res.* **2001**, *35* (1), 135–142.
(257) Huisman, J. L.; Schouten, G.; Schultz, C. Biologically Produced Sulphide for Purification of Process Streams, Effluent Treatment and Recovery of Metals in the Metal and Mining Industry. *Hydrometallurgy* **2006**, *83* (1), 106–113. https://doi.org/10.1016/j.hydromet.2006.03.017.
(258) Kabbashi, N. A.; Atieh, M. A.; Al-Mamun, A.; Mirghami, M. E.; Alam, M.; Yahya, N. Kinetic Adsorption of Application of Carbon Nanotubes for Pb(II) Removal from Aqueous Solution. *J. Environ. Sci.* **2009**, *21* (4), 539–544. https://doi.org/10.1016/S1001-0742(08)62305-0.
(259) Li, Y.; Liu, F.; Xia, B.; Du, Q.; Zhang, P.; Wang, D.; Wang, Z.; Xia, Y. Removal of Copper from Aqueous Solution by Carbon Nanotube/Calcium Alginate Composites. *J. Hazard. Mater.* **2010**, *177* (1–3), 876–880. https://doi.org/10.1016/j.jhazmat.2009.12.114.
(260) Kandah, M. I.; Meunier, J. L. Removal of Nickel Ions from Water by Multi-Walled Carbon Nanotubes. *J. Hazard. Mater.* **2007**, *146* (1–2), 283–288. https://doi.org/10.1016/j.jhazmat.2006.12.019.
(261) Eriksson, P. Nanofiltration Extends the Range of Membrane Filtration. *Environ. Prog.* **1988**, *7* (1), 58–62. https://doi.org/10.1002/ep.3300070116.
(262) Sadrzadeh, M.; Mohammadi, T.; Ivakpour, J.; Kasiri, N. Neural Network Modeling of Pb2+ Removal from Wastewater Using Electrodialysis. *Chem. Eng. Process. Process Intensif.* **2009**, *8* (48), 1371–1381. https://doi.org/10.1016/j.cep.2009.07.001.
(263) Chang, Q.; Wang, G. Study on the Macromolecular Coagulant PEX Which Traps Heavy Metals. *Chem. Eng. Sci.* **2007**, *62* (17), 4636–4643. https://doi.org/10.1016/j.ces.2007.05.002.
(264) Polat, H.; Erdogan, D. Heavy Metal Removal from Waste Waters by Ion Flotation. *J. Hazard. Mater.* **2007**, *148* (1–2), 267–273. https://doi.org/10.1016/j.jhazmat.2007.02.013.
(265) Capponi, F.; Sartori, M.; Souza, M. L.; Rubio, J. Modified Column Flotation of Adsorbing Iron Hydroxide Colloidal Precipitates. *Int. J. Miner. Process.* **2006**, *79* (3), 167–173. https://doi.org/10.1016/j.minpro.2006.02.002.
(266) Issabayeva, G.; Aroua, M. K.; Sulaiman, N. M. N. Removal of Lead from Aqueous Solutions on Palm Shell Activated Carbon. *Bioresour. Technol.* **2006**, *97* (18), 2350–2355. https://doi.org/10.1016/j.biortech.2005.10.023.
(267) Chen, G. Electrochemical Technologies in Wastewater Treatment. *Sep. Purif. Technol.* **2004**, *38* (1), 11–41. https://doi.org/10.1016/j.seppur.2003.10.006.
(268) Kumar, P.; Pournara, A.; Kim, K.-H.; Bansal, V.; Rapti, S.; Manos, M. J. Metal-Organic Frameworks: Challenges and Opportunities for Ion-Exchange/Sorption Applications. *Prog. Mater. Sci.* **2017**, *86*, 25–74. https://doi.org/10.1016/j.pmatsci.2017.01.002.
(269) Rieman, W.; Walton, H. F. *Ion Exchange in Analytical Chemistry: International Series of Monographs in Analytical Chemistry*; Elsevier, 2013.

(270) Hu, J.-S.; Zhong, L.-S.; Song, W.-G.; Wan, L.-J. Synthesis of Hierarchically Structured Metal Oxides and Their Application in Heavy Metal Ion Removal. *Adv. Mater.* **2008**, *20* (15), 2977–2982. https://doi.org/10.1002/adma.200800623.

(271) Hua, M.; Zhang, S.; Pan, B.; Zhang, W.; Lv, L.; Zhang, Q. Heavy Metal Removal from Water/Wastewater by Nanosized Metal Oxides: A Review. *J. Hazard. Mater.* **2012**, *211*, 317–331. https://doi.org/10.1016/j.jhazmat.2011.10.016.

(272) Wang, X.; Guo, Y.; Yang, L.; Han, M.; Zhao, J.; Cheng, X. Nanomaterials as Sorbents to Remove Heavy Metal Ions in Wastewater Treatment. *J. Environ. Anal. Toxicol.* **2012**, *2*, 1000154. https://doi.org/10.4172/2161-0525.1000154.

(273) Khin, M. M.; Nair, A. S.; Babu, V. J.; Murugan, R.; Ramakrishna, S. A Review on Nanomaterials for Environmental Remediation. *Energy Environ. Sci.* **2012**, *5* (8), 8075–8109. https://doi.org/10.1039/C2EE21818F.

(274) Xue, X.; Cheng, R.; Shi, L.; Ma, Z.; Zheng, X. Nanomaterials for Water Pollution Monitoring and Remediation. *Environ. Chem. Lett.* **2017**, *15* (1), 23–27. https://doi.org/10.1007/s10311-016-0595-x.

(275) Tofighy, M. A.; Mohammadi, T. Adsorption of Divalent Heavy Metal Ions from Water Using Carbon Nanotube Sheets. *J. Hazard. Mater.* **2011**, *185* (1), 140–147. https://doi.org/10.1016/j.jhazmat.2010.09.008.

(276) Sarkar, S.; Guibal, E.; Quignard, F.; SenGupta, A. K. Polymer-Supported Metals and Metal Oxide Nanoparticles: Synthesis, Characterization, and Applications. *J. Nanoparticle Res.* **2012**, *14* (2), 715. https://doi.org/10.1007/s11051-011-0715-2.

(277) Lu, H.; Wang, J.; Stoller, M.; Wang, T.; Bao, Y.; Hao, H. An Overview of Nanomaterials for Water and Wastewater Treatment https://www.hindawi.com/journals/amse/2016/4964828/ (accessed Dec 15, 2018). https://doi.org/10.1155/2016/4964828.

(278) Ray, P. Z.; Shipley, H. J. Inorganic Nano-Adsorbents for the Removal of Heavy Metals and Arsenic: A Review. *RSC Adv.* **2015**, *5* (38), 29885–29907. https://doi.org/10.1039/C5RA02714D.

(279) Karami, H. Heavy Metal Removal from Water by Magnetite Nanorods. *Chem. Eng. J.* **2013**, *219*, 209–216. https://doi.org/10.1016/j.cej.2013.01.022.

(280) Xu, P.; Zeng, G. M.; Huang, D. L.; Feng, C. L.; Hu, S.; Zhao, M. H.; Lai, C.; Wei, Z.; Huang, C.; Xie, G. X.; et al. Use of Iron Oxide Nanomaterials in Wastewater Treatment: A Review. *Sci. Total Environ.* **2012**, *424*, 1–10. https://doi.org/10.1016/j.scitotenv.2012.02.023.

(281) Boujelben, N.; Bouzid, J.; Elouear, Z.; Feki, M. Retention of Nickel from Aqueous Solutions Using Iron Oxide and Manganese Oxide Coated Sand: Kinetic and Thermodynamic Studies. *Environ. Technol.* **2010**, *31* (14), 1623–1634. https://doi.org/10.1080/09593330.2010.482148.

(282) Trgo, M.; Perić, J. Interaction of the Zeolitic Tuff with Zn-Containing Simulated Pollutant Solutions. *J. Colloid Interface Sci.* **2003**, *260* (1), 166–175. https://doi.org/10.1016/S0021-9797(03)00042-0.

(283) Pathania, D.; Singh, P. Nanosized Metal Oxide-Based Adsorbents for Heavy Metal Removal: A Review. In *Advanced Materials for Agriculture, Food, and Environmental Safety*; Tiwari, A., Syväjärvi, M., Eds.; John Wiley & Sons, Inc., 2014; pp 243–263. https://doi.org/10.1002/9781118773857.ch9.

(284) Ghoshal, T.; Kar, S.; Chaudhuri, S. ZnO Doughnuts: Controlled Synthesis, Growth Mechanism, and Optical Properties. *Cryst. Growth Des.* **2007**, *7* (1), 136–141. https://doi.org/10.1021/cg060289h.

(285) Bavykin, D. V.; Friedrich, J. M.; Walsh, F. C. Protonated Titanates and TiO2 Nanostructured Materials: Synthesis, Properties, and Applications. *Adv. Mater.* **2006**, *18* (21), 2807–2824. https://doi.org/10.1002/adma.200502696.

(286) Zhang, Y.; Jiang, Z.; Huang, J.; Lim, L. Y.; Li, W.; Deng, J.; Gong, D.; Tang, Y.; Lai, Y.; Chen, Z. Titanate and Titania Nanostructured Materials for Environmental and Energy Applications: A Review. *RSC Adv.* **2015**, *5* (97), 79479–79510. https://doi.org/10.1039/C5RA11298B.

(287) Liu, W.; Wang, T.; Borthwick, A. G. L.; Wang, Y.; Yin, X.; Li, X.; Ni, J. Adsorption of Pb2 +, Cd2 +, Cu2 + and Cr3 + onto Titanate Nanotubes: Competition and Effect of Inorganic Ions. *Sci. Total Environ.* **2013**, *456*, 171–180. https://doi.org/10.1016/j.scitotenv.2013.03.082.
(288) Huang, J.; Cao, Y.; Deng, Z.; Tong, H. Formation of Titanate Nanostructures under Different NaOH Concentration and Their Application in Wastewater Treatment. *J. Solid State Chem.* **2011**, *184* (3), 712–719. https://doi.org/10.1016/j.jssc.2011.01.023.
(289) Huang, J.; Cao, Y.; Liu, Z.; Deng, Z.; Tang, F.; Wang, W. Efficient Removal of Heavy Metal Ions from Water System by Titanate Nanoflowers. *Chem. Eng. J.* **2012**, *180*, 75–80. https://doi.org/10.1016/j.cej.2011.11.005.
(290) Ma, R.; Sasaki, T.; Bando, Y. Alkali Metal Cation Intercalation Properties of Titanate Nanotubes. *Chem. Commun.* **2005**, No. 7, 948–950.
(291) Yang, D. J.; Zheng, Z. F.; Zhu, H. Y.; Liu, H. W.; Gao, X. P. Titanate Nanofibers as Intelligent Absorbents for the Removal of Radioactive Ions from Water. *Adv. Mater.* **2008**, *20* (14), 2777–2781. https://doi.org/10.1002/adma.200702055.
(292) Perotto, G.; Cittadini, M.; Tao, H.; Kim, S.; Yang, M.; Kaplan, D. L.; Martucci, A.; Omenetto, F. G. Fabrication of Tunable, High-Refractive-Index Titanate-Silk Nanocomposites on the Micro- and Nanoscale. *Adv. Mater. Deerfield Beach Fla* **2015**, *27* (42), 6728–6732. https://doi.org/10.1002/adma.201501704.
(293) Antonello, A.; Guglielmi, M.; Bello, V.; Mattei, G.; Chiasera, A.; Ferrari, M.; Martucci, A. Titanate Nanosheets as High Refractive Layer in Vertical Microcavity Incorporating Semiconductor Quantum Dots. *J. Phys. Chem. C* **2010**, *114* (43), 18423–18428. https://doi.org/10.1021/jp106951y.
(294) Portehault, D.; Giordano, C.; Sanchez, C.; Antonietti, M. Nonaqueous Route toward a Nanostructured Hybrid Titanate. *Chem. Mater.* **2010**, *22* (6), 2125–2131. https://doi.org/10.1021/cm903709m.
(295) Li, N.; Zhang, L.; Chen, Y.; Fang, M.; Zhang, J.; Wang, H. Highly Efficient, Irreversible and Selective Ion Exchange Property of Layered Titanate Nanostructures. *Adv. Funct. Mater.* **2012**, *22* (4), 835–841. https://doi.org/10.1002/adfm.201102272.
(296) Colusso, E.; Perotto, G.; Wang, Y.; Sturaro, M.; Omenetto, F.; Martucci, A. Bioinspired Stimuli-Responsive Multilayer Film Made of Silk–Titanate Nanocomposites. *J. Mater. Chem. C* **2017**, *5* (16), 3924–3931. https://doi.org/10.1039/C7TC00149E.
(297) Moore, M. N. Do Nanoparticles Present Ecotoxicological Risks for the Health of the Aquatic Environment? *Environ. Int.* **2006**, *32* (8), 967–976. https://doi.org/10.1016/j.envint.2006.06.014.
(298) Chavan, A. A.; Li, H.; Scarpellini, A.; Marras, S.; Manna, L.; Athanassiou, A.; Fragouli, D. Elastomeric Nanocomposite Foams for the Removal of Heavy Metal Ions from Water. *ACS Appl. Mater. Interfaces* **2015**, *7* (27), 14778–14784. https://doi.org/10.1021/acsami.5b03003.
(299) Morsi, R. E.; Alsabagh, A. M.; Nasr, S. A.; Zaki, M. M. Multifunctional Nanocomposites of Chitosan, Silver Nanoparticles, Copper Nanoparticles and Carbon Nanotubes for Water Treatment: Antimicrobial Characteristics. *Int. J. Biol. Macromol.* **2017**, *97*, 264–269. https://doi.org/10.1016/j.ijbiomac.2017.01.032.
(300) Yin, J.; Deng, B. Polymer-Matrix Nanocomposite Membranes for Water Treatment. *J. Membr. Sci.* **2015**, *479*, 256–275. https://doi.org/10.1016/j.memsci.2014.11.019.
(301) Bordes, P.; Pollet, E.; Avérous, L. Nano-Biocomposites: Biodegradable Polyester/Nanoclay Systems. *Prog. Polym. Sci.* **2009**, *2* (34), 125–155. https://doi.org/10.1016/j.progpolymsci.2008.10.002.
(302) Pereira, F. A.; Sousa, K. S.; Cavalcanti, G. R.; Fonseca, M. G.; De, A. S.; Alves, A. P. Chitosan-Montmorillonite Biocomposite as an Adsorbent for Copper (II) Cations from Aqueous Solutions. *Int. J. Biol. Macromol.* **2013**, *61*, 471–478. https://doi.org/10.1016/j.ijbiomac.2013.08.017.
(303) Banerjee, S. S.; Chen, D.-H. Fast Removal of Copper Ions by Gum Arabic Modified Magnetic Nano-Adsorbent. *J. Hazard. Mater.* **2007**, *147* (3), 792–799. https://doi.org/10.1016/j.jhazmat.2007.01.079.

(304) Zhao, G.; Huang, X.; Tang, Z.; Huang, Q.; Niu, F.; Wang, X. Polymer-Based Nanocomposites for Heavy Metal Ions Removal from Aqueous Solution: A Review. *Polym. Chem.* **2018**, *9* (26), 3562–3582. https://doi.org/10.1039/C8PY00484F.

(305) Kundu, B.; Rajkhowa, R.; Kundu, S. C.; Wang, X. Silk Fibroin Biomaterials for Tissue Regenerations. *Adv. Drug Deliv. Rev.* **2013**, *65* (4), 457–470. https://doi.org/10.1016/j.addr.2012.09.043.

(306) Lee, Y.-W.; Nations, F. and A. O. of the U. *Silk Reeling and Testing Manual*; Food & Agriculture Org., 1999.

(307) Qi, Y.; Wang, H.; Wei, K.; Yang, Y.; Zheng, R.-Y.; Kim, I. S.; Zhang, K.-Q. A Review of Structure Construction of Silk Fibroin Biomaterials from Single Structures to Multi-Level Structures. *Int. J. Mol. Sci.* **2017**, *18* (3). https://doi.org/10.3390/ijms18030237.

(308) Altman, G. H.; Diaz, F.; Jakuba, C.; Calabro, T.; Horan, R. L.; Chen, J.; Lu, H.; Richmond, J.; Kaplan, D. L. Silk-Based Biomaterials. *Biomaterials* **2003**, *24* (3), 401–416.

(309) Shimura, K. Chemical Composition and Biosynthesis of Silk Proteins. *Experientia* **1983**.

(310) Lotz, B.; Colonna Cesari, F. The Chemical Structure and the Crystalline Structures of Bombyx Mori Silk Fibroin. *Biochimie* **1979**, *61* (2), 205–214.

(311) Ho, M. P.; Wang, H.; Lau, K. T. Effect of Degumming Time on Silkworm Silk Fibre for Biodegradable Polymer Composites. **2012**. https://doi.org/10.1016/j.apsusc.2011.12.068.

(312) Vepari, C.; Kaplan, D. L. Silk as a Biomaterial. *Prog. Polym. Sci.* **2007**, *32* (8–9), 991–1007. https://doi.org/10.1016/j.progpolymsci.2007.05.013.

(313) Hu, X.; Shmelev, K.; Sun, L.; Gil, E.-S.; Park, S.-H.; Cebe, P.; Kaplan, D. L. Regulation of Silk Material Structure by Temperature-Controlled Water Vapor Annealing. *Biomacromolecules* **2011**, *12* (5), 1686–1696. https://doi.org/10.1021/bm200062a.

(314) Rockwood, D. N.; Preda, R. C.; Yücel, T.; Wang, X.; Lovett, M. L.; Kaplan, D. L. Materials Fabrication from Bombyx Mori Silk Fibroin. *Nat. Protoc.* **2011**, *6* (10), 1612–1631. https://doi.org/10.1038/nprot.2011.379.

(315) Seib, F. P.; Jones, G. T.; Rnjak-Kovacina, J.; Lin, Y.; Kaplan, D. L. PH-Dependent Anticancer Drug Release from Silk Nanoparticles. *Adv. Healthc. Mater.* **2013**, *2* (12), 1606–1611. https://doi.org/10.1002/adhm.201300034.

(316) Mitropoulos, A. N.; Perotto, G.; Kim, S.; Marelli, B.; Kaplan, D. L.; Omenetto, F. G. Synthesis of Silk Fibroin Micro- and Submicron Spheres Using a Co-Flow Capillary Device. *Adv. Mater. Deerfield Beach Fla* **2014**, *26* (7), 1105–1110. https://doi.org/10.1002/adma.201304244.

(317) Wenk, E.; Merkle, H. P.; Meinel, L. Silk Fibroin as a Vehicle for Drug Delivery Applications. *J. Control. Release Off. J. Control. Release Soc.* **2011**, *150* (2), 128–141. https://doi.org/10.1016/j.jconrel.2010.11.007.

(318) Campagnolo, L.; Morselli, D.; Magrì, D.; Scarpellini, A.; Demirci, C.; Colombo, M.; Athanassiou, A.; Fragouli, D. Silk Fibroin/Orange Peel Foam: An Efficient Biocomposite for Water Remediation. *Adv. Sustain. Syst. 0* (0), 1800097. https://doi.org/10.1002/adsu.201800097.

(319) Wang, Y.; Rudym, D. D.; Walsh, A.; Abrahamsen, L.; Kim, H.-J.; Kim, H. S.; Kirker-Head, C.; Kaplan, D. L. In Vivo Degradation of Three-Dimensional Silk Fibroin Scaffolds. *Biomaterials* **2008**, *29* (24–25), 3415–3428. https://doi.org/10.1016/j.biomaterials.2008.05.002.

(320) Kim, J. H.; Park, C. H.; Lee, O.-J.; Lee, J.-M.; Kim, J. W.; Park, Y. H.; Ki, C. S. Preparation and in Vivo Degradation of Controlled Biodegradability of Electrospun Silk Fibroin Nanofiber Mats. *J. Biomed. Mater. Res. A* **2012**, *100A* (12), 3287–3295. https://doi.org/10.1002/jbm.a.34274.

(321) Pant, H. C.; Patra, M. K.; Verma, A.; Vadera, S. R.; Kumar, N. Study of the Dielectric Properties of Barium Titanate–Polymer Composites. *Acta Mater.* **2006**, *54* (12), 3163–3169. https://doi.org/10.1016/j.actamat.2006.02.031.

(322) Perotto, G.; Antonello, A.; Ferraro, D.; Mattei, G.; Martucci, A. Patterned TiO2 Nanostructures Fabricated with a Novel Inorganic Resist. *Mater. Chem. Phys.* **2013**, *142* (2–3), 712–716. https://doi.org/10.1016/j.matchemphys.2013.08.029.

(323) Jin, H.-J.; Park, J.; Karageorgiou, V.; Kim, U.-J.; Valluzzi, R.; Cebe, P.; Kaplan, D. L. Water-Stable Silk Films with Reduced β-Sheet Content. *Adv. Funct. Mater.* **2005**, *15* (8), 1241–1247. https://doi.org/10.1002/adfm.200400405.

(324) Caputo, G.; Nobile, C.; Kipp, T.; Blasi, L.; Grillo, V.; Carlino, E.; Manna, L.; Cingolani, R.; Cozzoli, P. D.; Athanassiou, A. Reversible Wettability Changes in Colloidal TiO2 Nanorod Thin-Film Coatings under Selective UV Laser Irradiation. *J. Phys. Chem. C* **2008**, *112* (3), 701–714. https://doi.org/10.1021/jp0777061.

(325) Dokmanić, I.; Sikić, M.; Tomić, S. Metals in Proteins: Correlation between the Metal-Ion Type, Coordination Number and the Amino-Acid Residues Involved in the Coordination. *Acta Crystallogr. D Biol. Crystallogr.* **2008**, *64* (Pt 3), 257–263. https://doi.org/10.1107/S090744490706595X.

(326) Zhou, C.-Z.; Confalonieri, F.; Jacquet, M.; Perasso, R.; Li, Z.-G.; Janin, J. Silk Fibroin: Structural Implications of a Remarkable Amino Acid Sequence. *Proteins Struct. Funct. Bioinforma.* **2001**, *44* (2), 119–122. https://doi.org/10.1002/prot.1078.

(327) Liu, W.; Zhao, X.; Wang, T.; Fu, J.; Ni, J. Selective and Irreversible Adsorption of Mercury(II) from Aqueous Solution by a Flower-like Titanate Nanomaterial. *J. Mater. Chem. A* **2015**, *3* (34), 17676–17684. https://doi.org/10.1039/C5TA04521E.

(328) Shao, J.; Liu, J.; Zheng, J.; Carr, C. M. X-Ray Photoelectron Spectroscopic Study of Silk Fibroin Surface. *Polym. Int.* **2002**, *51* (12), 1479–1483. https://doi.org/10.1002/pi.1092.

(329) Bureau, C.; Chong, D. P. Density Functional Calculations of Core-Electron Binding Energies of Amines. Application to (CH3)3N-Ni and (CH3)4N+-Ni. *Chem. Phys. Lett.* **1997**, *264* (1), 186–192. https://doi.org/10.1016/S0009-2614(96)01282-1.

(330) Li, N.; Zhang, L.; Chen, Y.; Tian, Y.; Wang, H. Adsorption Behavior of Cu(II) onto Titanate Nanofibers Prepared by Alkali Treatment. *J. Hazard. Mater.* **2011**, *189* (1–2), 265–272. https://doi.org/10.1016/j.jhazmat.2011.02.031.

(331) Yang, D.; Zheng, Z.; Liu, H.; Zhu, H.; Ke, X.; Xu, Y.; Wu, D.; Sun, Y. Layered Titanate Nanofibers as Efficient Adsorbents for Removal of Toxic Radioactive and Heavy Metal Ions from Water. *J. Phys. Chem. C* **2008**, *112* (42), 16275–16280. https://doi.org/10.1021/jp803826g.

(332) Wang, S.; Ariyanto, E. Competitive Adsorption of Malachite Green and Pb Ions on Natural Zeolite. *J. Colloid Interface Sci.* **2007**, *314* (1), 25–31. https://doi.org/10.1016/j.jcis.2007.05.032.

(333) Hammond, J. S.; Holubka, J. W.; deVries, J. E.; Dickie, R. A. The Application of X-Ray Photo-Electron Spectroscopy to a Study of Interfacial Composition in Corrosion-Induced Paint de-Adhesion. *Corros. Sci.* **1981**, *21* (3), 239–253. https://doi.org/10.1016/0010-938X(81)90033-0.

(334) Pederson, L. R. Two-Dimensional Chemical-State Plot for Lead Using XPS. *J. Electron Spectrosc. Relat. Phenom.* **1982**, *28* (2), 203–209. https://doi.org/10.1016/0368-2048(82)85043-3.

(335) Ki, C. S.; Gang, E. H.; Um, I. C.; Park, Y. H. Nanofibrous Membrane of Wool Keratose/Silk Fibroin Blend for Heavy Metal Ion Adsorption. *J. Membr. Sci.* **2007**, *302* (1–2), 20–26. https://doi.org/10.1016/j.memsci.2007.06.003.

(336) Llavona, R.; Suarez, M.; Garcia, J. R.; Rodriguez, J. Lamellar Inorganic Ion Exchangers. Alkali Metal Ion Exchange on .Alpha.- and .Gamma.-Titanium Phosphate. *Inorg. Chem.* **1989**, *28* (14), 2863–2868. https://doi.org/10.1021/ic00313a033.

(337) Lv, L.; Tsoi, G.; Zhao, X. S. Uptake Equilibria and Mechanisms of Heavy Metal Ions on Microporous Titanosilicate ETS-10. *Ind. Eng. Chem. Res.* **2004**, *43* (24), 7900–7906. https://doi.org/10.1021/ie0498044.

(338) Shannon, R. D. Revised Effective Ionic Radii and Systematic Studies of Interatomic Distances in Halides and Chalcogenides. *Acta Crystallogr. A* **1976**, *32* (5), 751–767. https://doi.org/10.1107/S0567739476001551.

(339) Marcus, Y. Thermodynamics of Solvation of Ions. Part 5.—Gibbs Free Energy of Hydration at 298.15 K. *J. Chem. Soc. Faraday Trans.* **1991**, *87* (18), 2995–2999. https://doi.org/10.1039/FT9918702995.

(340) Pearson, R. G. Hard and Soft Acids and Bases. *J. Am. Chem. Soc.* **1963**, *85* (22), 3533–3539. https://doi.org/10.1021/ja00905a001.

(341) Parr, R. G.; Pearson, R. G. Absolute Hardness: Companion Parameter to Absolute Electronegativity. *J. Am. Chem. Soc.* **1983**, *105* (26), 7512–7516. https://doi.org/10.1021/ja00364a005.